NASA Contractor Report -178172

(NASA-CR-178172) DEVELOPMENT OF ROTORCRAFT INTERIOR NOISE CONTROL CONCEPTS. PHASE 3: DEVELOPMENT OF NOISE CONTROL CONCEPTS Final Report (United Technologies Corp.) 148 p CSCL 20A G3/71

N88-14762

Unclas 0103572

Development of Rotorcraft Interior Noise Control Concepts

Phase III : Development of Noise Control Concepts

C.A. Yoerkie

P.J. Gintoli

S.T. Ingraham

United Technologies Corporation

SIKORSKY AIRCRAFT DIVISION
STRATFORD, CT 06601

J.A.Moore

Cambridge Collaborative, Inc.
CAMBRIDGE, MA 02138

Contract NAS1-16932

July 1987

National Aeronautics and
Space Administration

Langley Research Center
Hampton, Virginia 23665-5225

NASA Contractor Report -178172

Development of Rotorcraft Interior Noise Control Concepts

Phase III : Development of Noise Control Concepts

C.A. Yoerkie

P.J. Gintoli

S.T. Ingraham

United Technologies Corporation

SIKORSKY AIRCRAFT DIVISION
STRATFORD, CT 06601

J.A.Moore

Cambridge Collaborative, Inc.
CAMBRIDGE, MA 02138

Contract NAS1-16932

July 1987

National Aeronautics and
Space Administration

Langley Research Center
Hampton, Virginia 23665-5225

TABLE OF CONTENTS

DESCRIPTION	PAGE
LIST OF FIGURES	iv
LIST OF PHOTOS	viii
LIST OF TABLES	x
FOREWORD	1
PHASE III OBJECTIVES	2
INTERIOR CABIN NOISE CONTROL CONCEPTS	12
Conventional Treatment approaches	14
Advanced Treatment Approaches	18
Introduction to Modeling Concepts	21
Dissipative Type Treatments	24
Free extensional damping layers	24
Constrained layer damping	27
Acoustic absorption (cabin)	29
Transmission Type Treatments	35
Trim panel acoustic cavities	35
2-D acoustic modes	36
Effect of cavity absorption treatments	36
Trim panel isolation mounts	41
Interior Configurations of the S-76 Aircraft	43
Utility interior	56
Executive (VIP) interior	57
Advanced interior	57
SEA Model of the Treated Interior	57
SEA models of trim panel transmission loss	58
Utility interior	63
Executive interior	73
Advanced interior	77
SEA Predictions for the Treated S-76 Cabin	84
Power flow description of transmission paths	84
ISOLATION AS AN ALTERNATE NOISE CONTROL CONCEPT	92
Gearbox Isolation Mounts	92
Preliminary Design Definition	95
Physical constraints	95
Shape and size effects	96
Predicted isolation characteristics	98
Isolation effectiveness	110
Plan for Validation	114
Isolation	114

TABLE OF CONTENTS (Cont'd)

DESCRIPTION	PAGE
CONCLUDING COMMENTS	118
RECOMMENDATIONS	119
REFERENCES	120
APPENDIX A	121
STANDARD BIBLIOGRAPHIC PAGE	138

LIST OF FIGURES

FIGURE		PAGE
1.	Flow of Activities for the Development of Rotorcraft Interior Noise Control Concepts	4
2.	Laboratory Experiment Schematic for Evaluation of Acoustic Treatment	8
3.	Typical Constrained Layer Damping Cross Section	15
4.	Typical Free Extensional Damping Layer Cross Section	15
5.	Typical Trim Panel, Cavity, Airframe Cross Section	16
6.	Typical Trim Panel Isolation Cross Section	17
7.	Trim Panel Isolation Mount Nomenclature	17
8.	Main Gearbox/Airframe Isolation Schematic	18
9.	Main Gearbox/Airframe Isolation Mount Nomenclature	18
10.	Typical Composite Panel Sandwich Construction Cross Section	19
11.	Typical Constrained Layer Damping Composite Panel Cross Section	20
12.	Typical Double Honeycomb Constrained Layer Damping Composite Panel Cross Section	20
13.	Loss Factor for Free Extensional Damping Treatment	26
14.	Carpet Absorption	32
15.	Carpet and Pad Absorption	33
16.	Flow Resistivity of Glass Fiber Products	37
17.	Compressibility of Air Within a Porous Material	39
18.	Transmission Loss for a Utility Type Interior Panel.	60
19.	Transmission Loss for an Executive Type Interior Panel	61

LIST OF FIGURES (Cont'd)

FIGURE		PAGE
20a.	S-76 Overhead Panel Vibration Levels for Utility Type Interior	64
20b.	S-76 Overhead Panel Vibration Levels for Executive Type Interior	65
20c.	S-76 Overhead Panel Vibration Levels for Advanced Type Interior	66
21a.	S-76 Overhead Cavity Levels for Utility Type Interior	67
21b.	S-76 Overhead Cavity Levels for Executive Type Interior	68
21c.	S-76 Overhead Cavity Levels for Advanced Type Interior	69
22.	Utility Treatment Effectiveness Relative to Overhead Cavity Levels and Untreated Cabin Levels	70
23.	SEA Predictions for the Relative Distribution of Overhead Skin, Panel and Cavity Levels at 1000 Hz	71
24.	Coupling Loss Factors for Cavities to Cabin Through Panels and Holes (Leakage) for a Utility Type Interior	72
25.	Effect of Air Conditioning Openings and Panel Leakage on the SEA Predictions of a Utility Type Interior	74
26.	Influence of Cavity Loss Factor on the SEA Predictions of a Utility Type Interior	75
27.	Comparison of the SEA Predictions for a Utility Type Interior With S-76 Flight Data at the Standard Cruise Condition	76
28.	Coupling Loss Factors for Cavities to Cabin Through Panels and Holes (Leakage) for an Executive Type Interior	78

LIST OF FIGURES (Cont'd)

FIGURE		PAGE
29.	Effect of Air Conditioning Openings and Panel Leakage on the SEA Predictions of an Executive Type Interior	79
30.	Comparison of the SEA Prediction, for an Executive Type Interior With S-76 Flight Data at the Standard Cruise Condition	80
31.	S-76 Frame Transfer Function Levels	85
32.	S-76 Skin Panel Transfer Function Levels	86
33.	S-76 Overhead Cavity Noise Levels	87
34.	S-76 Cabin Noise Levels	89
35.	Typical Isolator Installation	101
36.	Single Isolator Geometry	102
37.	Gearbox Attachment Points and Sign Conventions	103
38.	Airframe Attachment Points and Sign Conventions	103
39.	Block Diagram of Analytic Model	104
40.	Main Gearbox Driving Point Frequency Response - Port Forward - Vertical	105
41.	Airframe Driving Point Frequency Response - Port Forward - Vertical	106
42.	Main Gearbox Driving Point Frequency Response - Port Forward - Lateral	107
43.	Airframe Driving Point Frequency Response - Port Forward - Lateral	108
44.	Isolator Bench Test Results	109
45.	Variation of Material Properties at Constant Frequencies	111

LIST OF FIGURES (Cont'd)

FIGURE		PAGE
46.	Influence of Temperature on the Predicted Isolation Effectiveness with Two Isolators in the Vertical Direction	112
47.	Influence of Preload on the Predicted Transmissibility with Two Isolators at 80°C in the Vertical Direction	113
48.	Predicted Isolation Effectiveness for Two vs. Four Isolators at 80°C in the Vertical Direction	115
49.	Predicted One-Third Octave Band Attenuation vs. Isolator Stiffness	116
50	Relative Comparison of Bare Cabin Levels to the Utility, Executive and Advanced Overhead Cavities and Cabin Levels	124
51.	Effect of Increased Leakage Area on Panel TL	125
52.	Absorption Provided by Several Typical Cabin Furnishings	126
53.	Typical Total Absorption of Cabin Furnishings	126
54a.	Measured Intensity Contours for a Utility Type Panel at 0.5 kHz	127
54b.	Measured Intensity Contours for a Utility Type Panel at 1 kHz	128
54c.	Measured Intensity Contours for a Utility Type Panel at 2 kHz	129
54d.	Measured Intensity Contours for a Utility Type Panel at 4 kHz	130
55a.	Measured Intensity Contours for an Executive Type Panel at 0.5 kHz	131
55b.	Measured Intensity Contours for an Executive Type Panel at 1 kHz	132
55c.	Measured Intensity Contours for an Executive Type Panel at 2 kHz	133
55d.	Measured Intensity Contours for an Executive Type Panel at 4 kHz	134

LIST OF PHOTOS

PHOTO		PAGE
1	Sikorsky S-76A	3
2	Typical Utility Interior, Aft Passenger Cabin	6
3	Typical Executive Interior, Aft Passenger Cabin	7
4	Panel Testing - Reference Specimen, Reverberant Room Side	9
5	Panel Testing - Reference Specimen, Anechoic Room Side	16
6	Typical Utility Interior Seating	44
7	Typical Utlity Interior Sidewall, Ceiling, and Aft Bench Seat	45
8	Typical Executive Interior with Soft VIP Seats, Forward Curtains, Hard Ceiling and Sidewalls	46
9	Executive Interior Aft Divan Section, Hard Surface Sidewall and Duct Covers	47
10	Executive Interior with Table and Credenza	48
11	Executive Interior with Short Credenza. Curtains Provide Forward View for Passengers	49
12	Executive Interior with Soft Sidewalls and Duct Covers, Hard Center Celing	50
13	Totally Soft Surface Executive Interior with High Back Seats and Extra Thick Padded Headrest	51
14	Totally Hard Surface Executive Interior, Aft Section	52
15	Totally Hard Surface Executive Interior with Full Forward Bulkhead Containing Sliding Windows	53

LIST OF PHOTOS (Cont'd)

PHOTO		PAGE
16	Executive Interior with Soft Surface Full Forward Bulkhead Containing Sliding Windows	54
17	Executive Aircraft Cockpit Treatment	55
18	Isolation Test Rig	99
19	Typical Isolator	100
20	Typical Utility Type Panel Being Tested for TL in the Test Chambers from Anechoic Side, Sound Intensity Probe Shown	135
21	Typical View of Panel TL Testing - Anechoic Side	136
22	Typical View of Panel TL Testing - Reverberant Side	137

LIST OF TABLES

TABLE		PAGE
1	Noise Control Treatments: Extensions to the SEA Model of the S-76	23
2	Major Contributors to Power Flow into the Cabin	73
3	Major Contributors to Advanced Cabin Model at 1000 Hz	81
4a	Summary of S-76 SEA Model: Bare Interior	83
4b	Summary of S-76 SEA Model: Utility Interior	83
5	Power Flow Description for an Overhead Cavity (OC56L)	90
6	Power Flow Description of the Utility Interior Cabin Noise Environment for LF14LO Vibratory Input	91

FOREWORD

The goal of this NASA contract in broad terms is the understanding of helicopter internal noise mechanisms and the development, design, and testing of noise control concepts which will produce significant reductions in the acoustic environment to which the passengers and pilots are exposed. The Phase I and Phase II efforts [1, 2]* have produced much progress toward this goal. Phase I provided a basic understanding of the complex helicopter cabin noise environment and also produced an analytic method for prediction of the relatively high-frequency structure-borne vibrations which lead to the generation of bare cabin acoustic energy levels. The success of any large-scale analytic method clearly depends on validation of its accuracy. The Phase II effort provided the full-scale validation required to build confidence in the application of Statistical Energy Analysis (SEA) technology to helicopter cabin noise and structure-borne energy predictions in a bare aircraft configuration.

The Phase III effort described herein involved the identification and evaluation of current and advanced treatment concepts, including isolation of structure-borne paths. In addition, a plan was devised for the full-scale test and evaluation of an isolation concept during Phase IV: Validation of Concepts.

*Numbers in brackets refer to the Reference list.

PHASE III OBJECTIVES

The Phase III development program general objectives are: 1) incorporation of various noise control treatment concepts into the analytic SEA model developed for the S-76A (see Photo 1) in Phase I [1] of this contracted effort and validated in Phase II [2], 2) prediction of the relative effectiveness of these noise control concepts, 3) definition and evaluation of a preliminary acoustic isolator design, and 4) formulation of a full-scale validation plan for the Phase IV effort. Specific items which will allow these objectives to be met are as follows:

a) identification and characterization of various noise control concepts,

b) implementation of noise control concepts within the S-76 SEA model,

c) experimentation involving some aspects of these noise control concepts,

d) definition and evaluation of a preliminary acoustic isolation design to reduce structure-borne transmission of acoustic frequency main gearbox gear clash vibrations into the airframe,

e) formulation of a plan (to be implemented in Phase IV) for the full-scale validation of the isolation concept, and

f) prediction of the cabin noise environment with various noise control concepts installed.

Completion of these objectives allows comparisons to be made showing the relative effectiveness of various noise control concepts on a dB per pound or dB per dollar basis. The Phase III effort and an overview of its place in the total program is shown in the Flow of Activities (Figure 1). Phase III provides a framework for the follow-on, full-scale evaluation of the most effective noise control concepts. Isolation of the airframe from acoustic frequency gear mesh loading tones and harmonics still appears to rank first in effectiveness, followed by various skin damping techniques, acoustic isolation of panels, and airframe modification. As such, the Phase IV activities shown in Figure 1 anticipate validation of an isolation concept as the primary effort, with airframe modification effects as an interesting approach for future aircraft.

ORIGINAL PAGE IS
OF POOR QUALITY

Photo 1. Sikorsky S-76A.

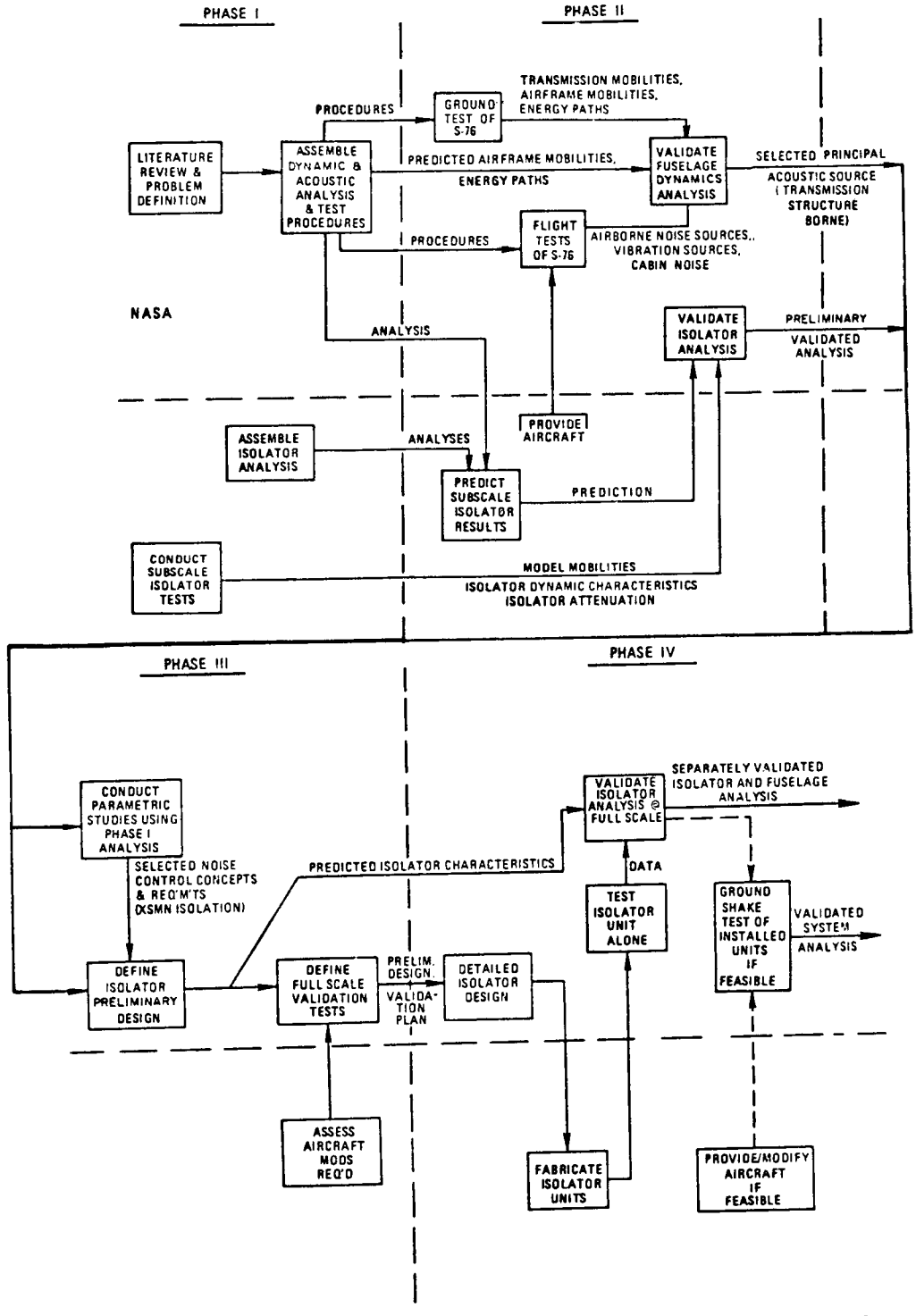

Figure 1. Flow of Activities for the Development of Rotorcraft Interior Noise Control Concepts.

ORIGINAL PAGE IS OF POOR QUALITY

These various tasks are described as:

Task 1: Identification of noise control concepts

In this task the practical considerations taken into account during the design, fabrication, and installation of an interior cabin treatment will be outlined. Included will be concerns for cost, weight, producibility, installation, accessibility, flammability and toxicity. These considerations place certain constraints on the treatment types. Current treatment approaches, including trim panels, panel isolators, skin and web damping, and absorption, will be identified. Advanced concepts which have attractive acoustic and weight benefits will also be identified. A mini case study will aid in these identifications by depicting real-world applications.

Task 2: Characterization of the Task 1 noise control concepts

The next step in the process is to characterize the acoustic and dynamic behavior associated with the various noise control concepts outlined in Task 1. These models incorporate any experimental/empirical information appropriate for the situation. Based on the relative confidence levels for these models, a small scale experiment was conducted to test the model validity.

Task 3: Implementation of noise control concepts

Once the noise control concepts have been identified and characterized, they must then be incorporated within the S-76 analytic model. This involves the transformation of information generated under Task 2 into a SEA format consistent with the S-76 SEA model [1]. In particular, the model was modified to include the standard interior shown in Photo 2 (light weight, hard surface trim panels), the executive (VIP) interior shown in Photo 3 (higher surface density, generally with soft surface trim panels), and an advanced noise control concepts interior variation. These additions transform the Phase II bare aircraft model into a model capable of predicting and evaluating the complete aircraft including the relative merits of acoustic treatment concepts.

Task 4: Experimentation to support development of SEA noise control treatment models

During the identification and characterization of various noise control concepts, limited laboratory experiments are required to support this development work. Mounting characteristics for both trim panel isolation and gearbox isolation present two areas where experimental work is useful. These experiments involve shake test measurements to characterize the frequency response of the isolator material. In addition, experimentation on the sound blocking characteristics of the various trim panel types was performed. This was done in a special side by side chamber arrangement shown schematically in Figure 2 and in Photos 4 and 5. Information gained in this task is used to enhance the S-76 SEA model developed in Task 3.

Task 5: Prediction of the effect various noise control concepts have on S-76 cabin noise levels

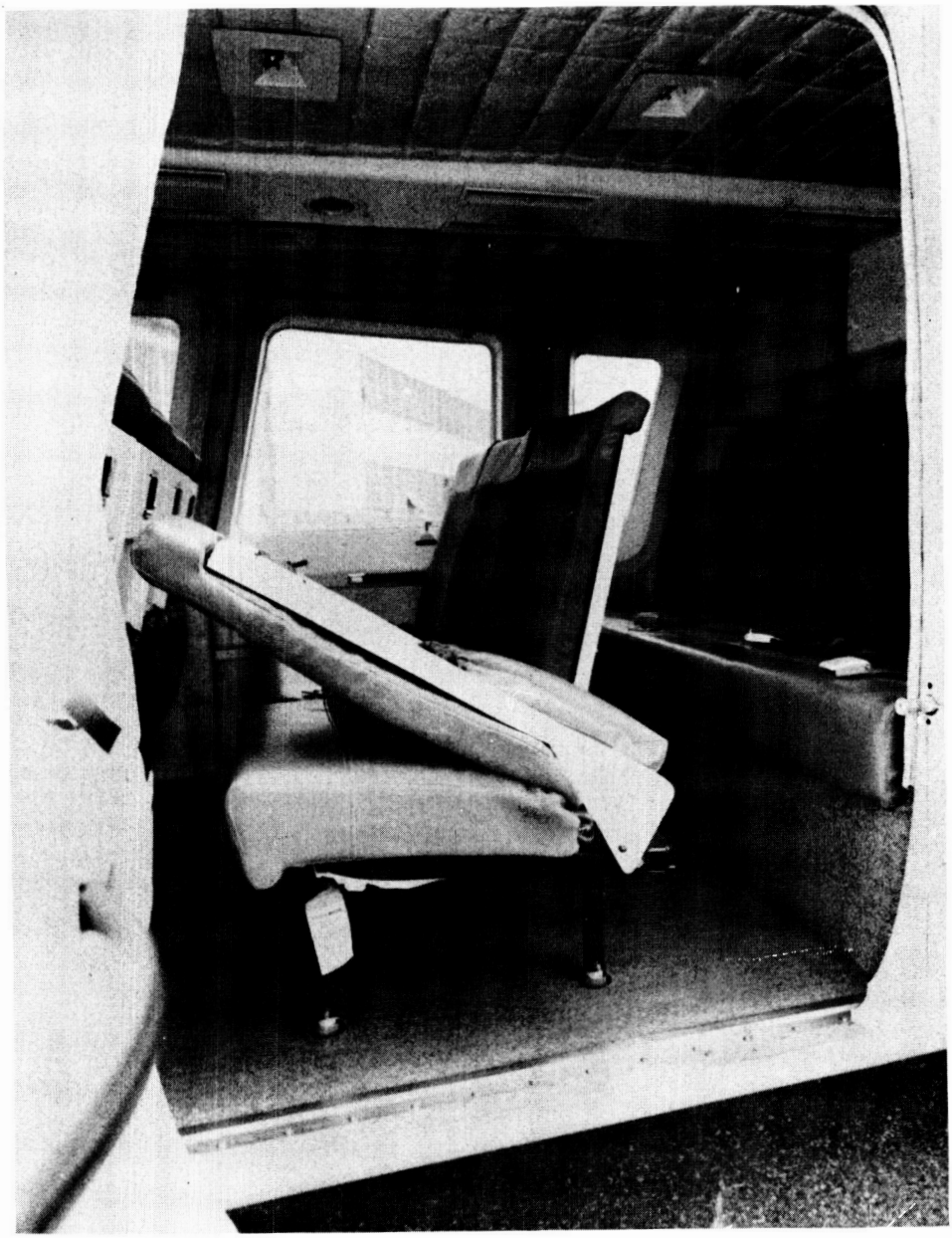

Photo 2. Typical Utility Interior, Aft Passenger Cabin.

ORIGINAL PAGE IS
OF POOR QUALITY

ORIGINAL PAGE IS
OF POOR QUALITY

Photo 3. Typical Executive Interior, Aft Passenger Cabin.

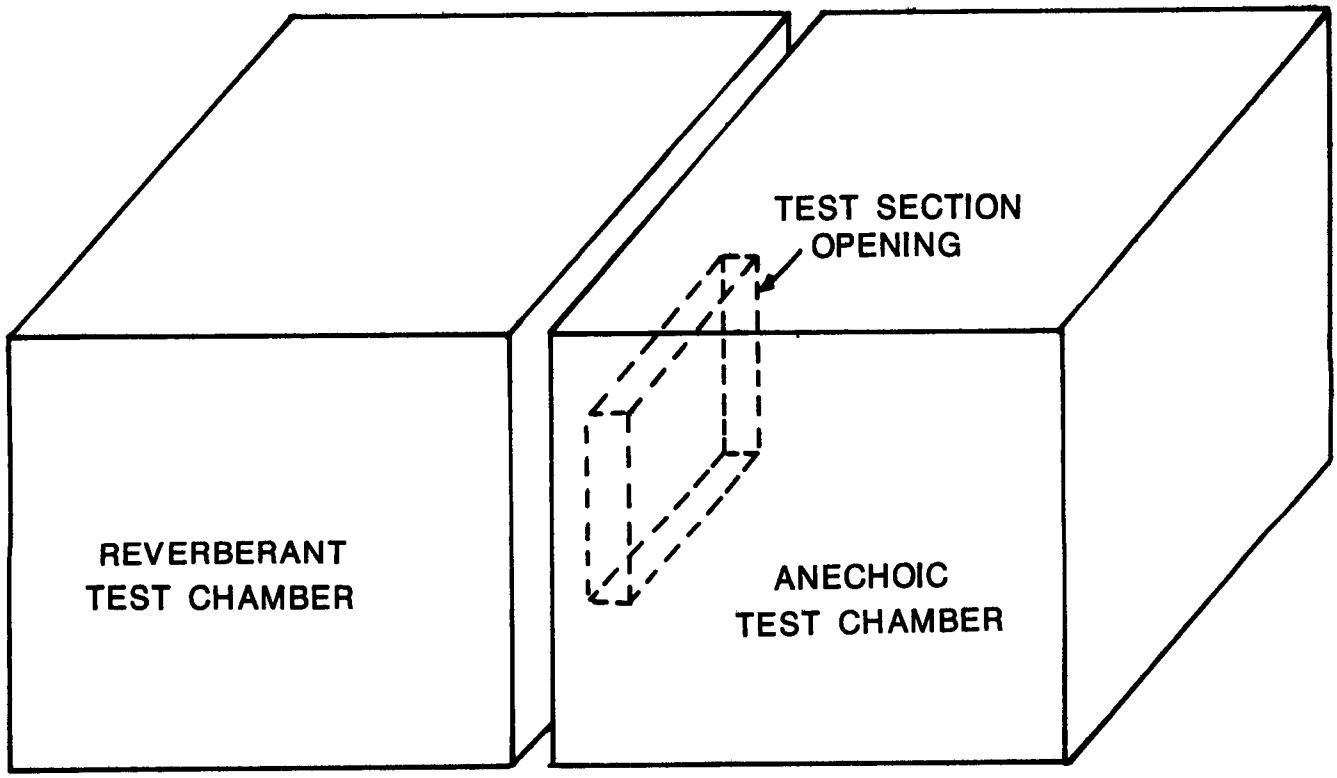

Figure 2. Laboratory Experiment Schematic for Evaluation of Acoustic Treatment.

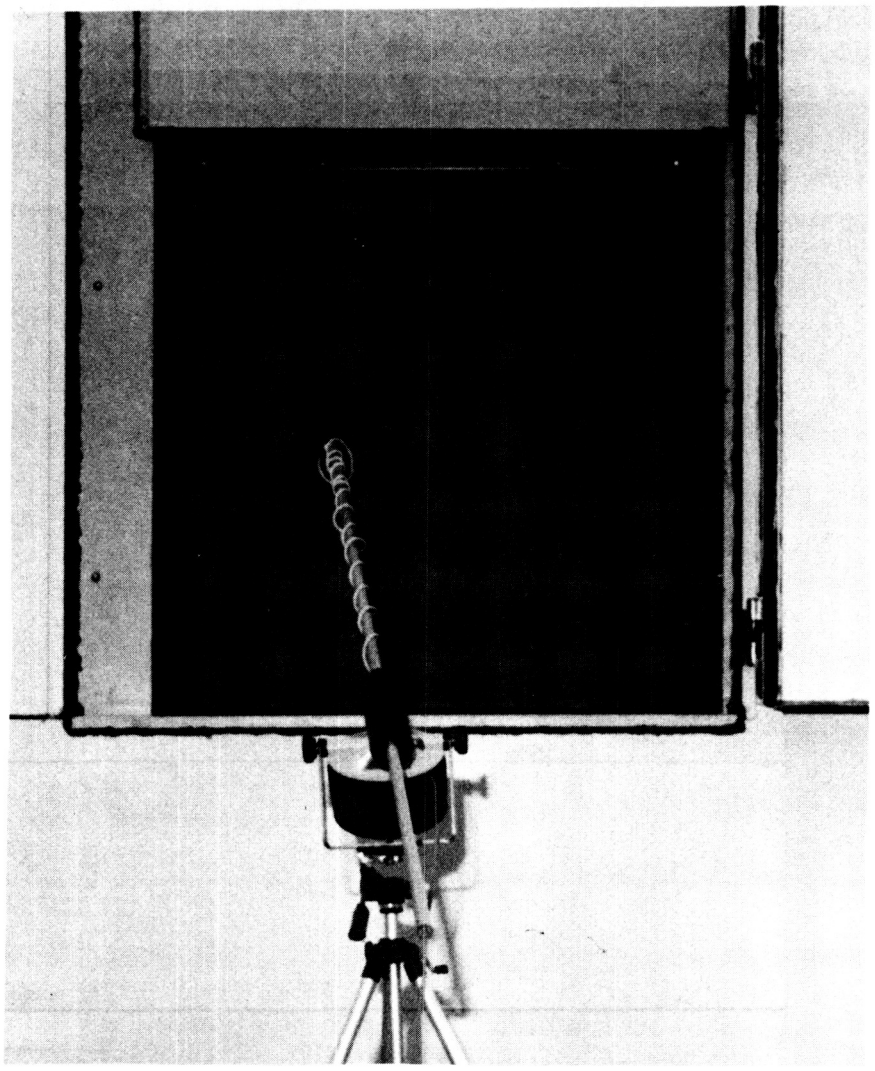

Photo 4. Panel Testing - Reference Specimen, Reverberant Room Side.

ORIGINAL PAGE IS
OF POOR QUALITY

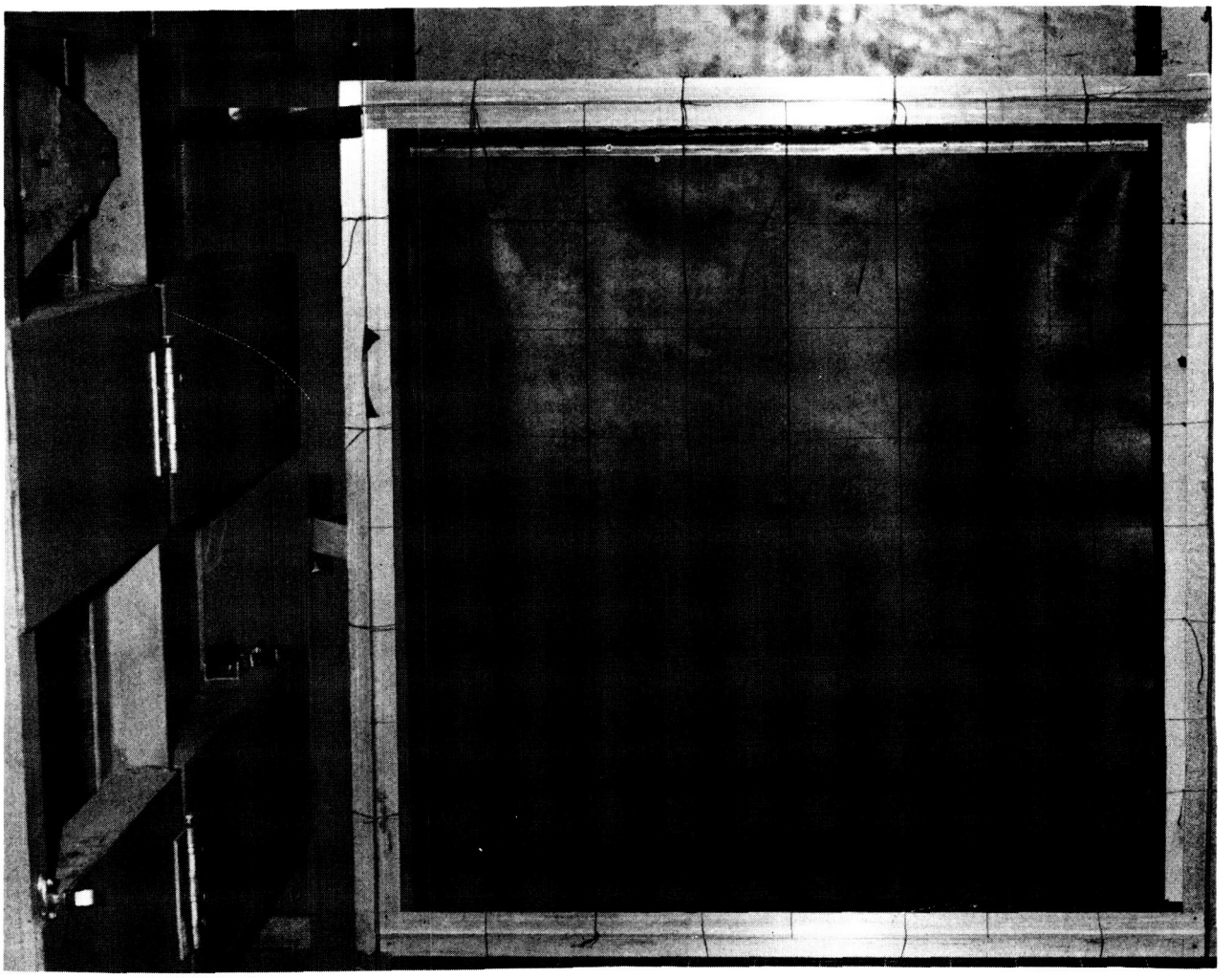

Photo 5. Panel Testing - Reference Specimen, Anechoic Room Side.

ORIGINAL PAGE IS
OF POOR QUALITY

The SEA model, as modified to include these noise control concepts outlined in Tasks 1 through 4, is now ready to be exercised. This task includes the generation of additional parameters related to specific noise control treatments incorporated within the model by the Task 3 improvements. Parameters required for the basic bare aircraft were developed under Phase II and, where possible, are retained for this task. Predictions are generated for various noise control configurations. These predictions are compared with available measured aircraft data. The performance of these noise control concepts are then interpreted and evaluated relative to a benefit parameter such as cost and/or weight.

Task 6: Definition of a preliminary isolation design and validation plan

In this task the preliminary design definition of an isolator is accomplished. This involves the physical constraints present in the helicopter, such as: attachment point geometry and size limitations, static and dynamic shaft alignment (engine and tail drive shaft) for various flight maneuvers, control linkage motion and system sensitivity, airframe dynamic effects, main rotor loads transfer, and environmental integrity.

The isolation design/prediction procedure is exercised to determine candidate designs consistent with the above constraints and material characteristics. The shape and size of an isolator is then defined to achieve these desired characteristics. The final portion of this effort involves the formulation of a practical plan, which would form the basis of the Phase IV program, to establish, on a full-scale basis, the validity of this isolation design. The general intent is to ground test the isolator on a modified aircraft.

INTERIOR CABIN NOISE CONTROL CONCEPTS

Damping as a treatment type is being modeled in several distinct configurations, including: (1) constrained layer damping where a viscoelastic material is sandwiched between a base structure and a stiff non-structural member to provide a shearing action within the elastomer, (2) free extensional damping which is just a free damping layer applied to a surface, and (3) a damping layer within a built-up panel. The modeling of these three damping types involves changes to the mass and stiffness properties of the particular subsection as well as the energy propagation within that subsection. In some construction types, the coupling loss factors to other subsections may also be modified.

Acoustic panel treatments are initially being subdivided by their conceptual impact on cabin acoustics. One type is the relatively thin trim panel, closely mounted to an adjoining panel (e.g.: an airframe outer skin panel). In this configuration there is a very small acoustic space created between the skin and treatment panel. Essentially the treatment can be considered as a septum which modifies the radiation efficiency of the skin panel while assuming that the trim panel response is of a non-resonant nature. The difficulty with this approach is that batting material stuffed in the bay between these two panels would not be properly modeled, since a change in radiation efficiency alone would not account for the energy dissipation mechanism of the intervening batting. The damping loss factor effects of batting material in larger bays is taken into consideration because the larger bays are considered to be acoustic spaces in the model (i.e.: an additional subsection/degree of freedom). A larger space between the trim panel and the outer skin has several distinct differences: (1) the acoustic space will have resonant modes in the frequencies of interest, (2) the trim panel cannot be modeled as a radiation efficiency modification, and (3) the batting material can be treated as a modification to the acoustic space loss factor.

An interesting, albeit subtle, modeling change involves the acoustic radiation from the beam webs and flanges. In the bare cabin configuration these web and flange surfaces exhibit an unbaffled radiation into the cabin acoustic space. This is a very inefficient mode of radiation and, in the bare configuration, has negligible impact on cabin sound pressure levels. However, when trim panels are attached to the inboard side of the beam flanges, the web and flange radiation changes to a baffled configuration. Not only does the web and flange now become a more efficient radiator, but it also now radiates into the acoustic cavity created between the aircraft outer skin and the trim panel rather than into the cabin. When modeled in this manner, the influence of add-on beam damping will be seen not only as an energy loss mechanism for that particular subsystem, but also as a reduction in radiated energy contributing to the reverberent build-up in the acoustic cavity.

Another type of modeling consideration is the isolation of panels where the frames are coupled through point stiffnesses to panels which have their own resonances. Point impedance models are used at the attachment points looking into each subsystem. Consideration is given to the beam attachment and whether the energy transfer is from out-of-plane modes or the combined in-plane/torsion modes.

Included are typical conventional approaches, such as: 1) cabin acoustic absorption, 2) panel damping treatments, 3) trim panel and cavity absorption, and 4) trim panel isolation, as well as advanced treatment approaches, such as: 1) gearbox isolation mounts, and 2) advanced composite material designs.

The following sections summarize these approaches and indicate areas of concern:

Conventional Treatment Approaches

1. Cabin Acoustic Absorption

   a) Use of absorbing "carpet" materials

      walls, floors, ceilings, furnishings (seating, credenzas, etc.), bulkheads

   b) Effect on total wall absorption in the cabin (absorption coefficient)

   c) Cabin acoustic loss factor for SEA acoustic subsystem

   d) Effect on pressure level distribution within the cabin:

      - direct field levels near radiating panels
      - reverberant levels in central region of cabin
      - non-uniform distribution of absorbing materials

   e) Information inputs from:

      carpet manufacturers, product suppliers, reverberant room absorption testing, sample testing, impedance tube measurements.

2. Panel Damping Treatments

   a) Constrained layer shear treatment

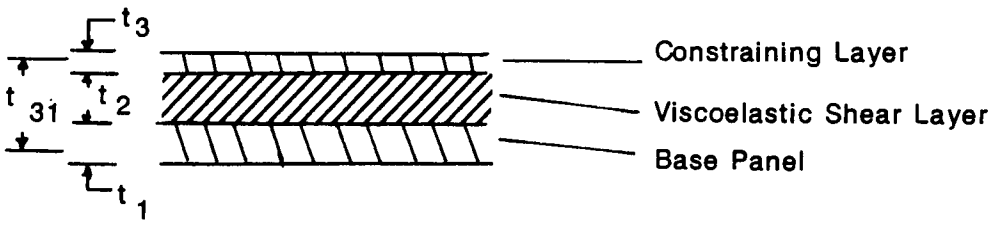

Figure 3. Typical Constrained Layer Damping Cross Section

b) Free extensional treatment

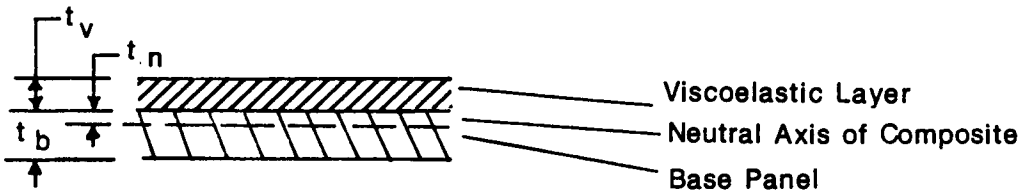

Figure 4. Typical Free Extensional Damping Layer Cross Section

c) Modeling to include:

- increase in panel damping
- effects on propagation behavior

  changes in bending rigidity of base panel and increase in total mass [3]

d) Inputs to the model:

- material properties of the viscoelastic layers

  mass, shear and Young's moduli, loss factor, frequency dependence of properties

- geometries

3. Trim Panel and Cavity Absorption (Acoustic Path)

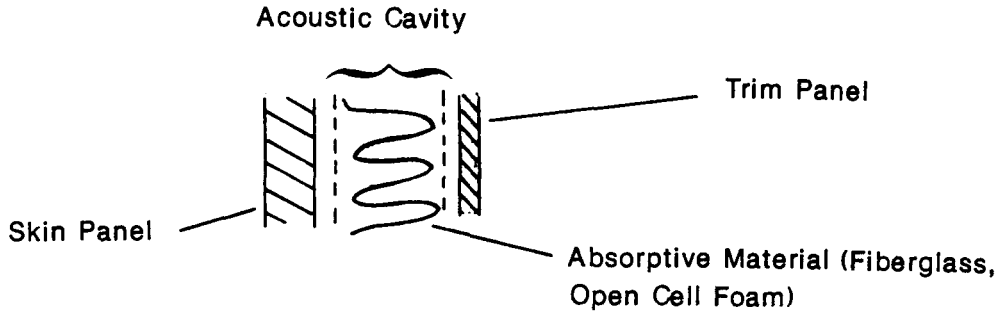

Figure 5. Typical Trim Panel, Cavity, Airframe Cross Section

Acoustic transmission into the cabin

Acoustic resonances in the cavity

a) Absorbing cavity fill material

- flow resistivity of blanket material
- effect on sound propagation
  isothermal compression of air,
  porosity, flow resistivity,
  determination of propagation phase speed,
  attenuation [4]
- damping of acoustic cavity resonances
- typical cavity dimensions: 0.1 to 0.2 m

b) Trim panel

- mass law transmission
  slowly propagating bending waves - non-coincident acoustic radiation
  coupling of acoustic cavity modes to the cabin acoustic modes
- resonant response of trim panel
  coupling to acoustic cavity modes

d) Flanking transmission path due to gaps in trim panel junctions and penetrations (e.g.: lights, vents, etc.)

4. Trim Panel Isolation (Structureborne Path)

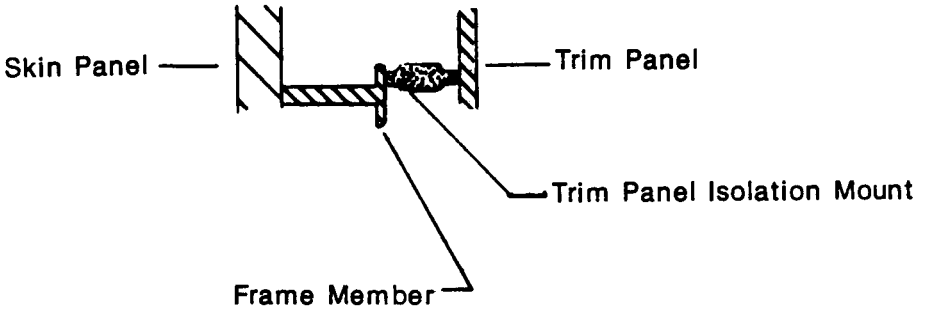

Figure 6. Typical Trim Panel Isolation Cross Section

Acoustic radiation due to point excitation of trim panel at mount support (radiation from flexural near field)

a) Radiated power (P) due to point excitation [5]

b) Trim panel point impedance (Z_p)

c) Trim panel mount point velocity

Related to mount impedance characteristics and support frame velocity

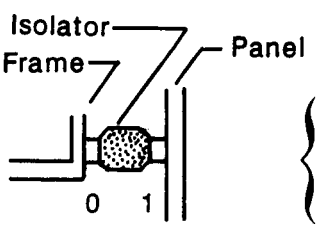

Mount Impedance Matrix

$$\begin{Bmatrix} F_0 \\ F_1 \end{Bmatrix} = \begin{bmatrix} Z_{11} & -Z_{12} \\ Z_{12} & -Z_{22} \end{bmatrix} \begin{Bmatrix} \tilde{V}_0 \\ \tilde{V}_1 \end{Bmatrix}$$

Figure 7. Trim Panel Isolation Mount Nomenclature

Required inputs to the model:

d) Mount characteristics

impedance measurements
low frequency simple stiffness model
SEA model of mount at higher frequency

e) Final result is in the form of a coupling loss factor between the frame (or skin panel) subsystem, to which the mount attaches, and the cabin acoustic subsystem. Power is radiated by nearfield flexural vibrations of the trim panel.

Advanced Treatment Approaches

1. Gearbox Isolation Mounts

a) Mount reduces power inflow to the airframe - (reduced velocity at attachment point on the airframe)

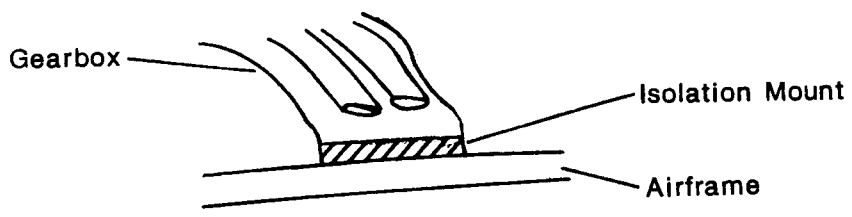

Figure 8. Main Gearbox/Airframe Isolation Schematic

b) Impedance description at attachment point assuming uncorrelated motions/forces in the different directions.

- Gearbox velocity in the i-th direction
- Airframe velocity
- Mount impedance matrix

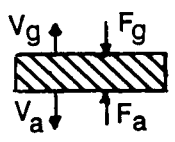

$$\begin{Bmatrix} F_g \\ F_a \end{Bmatrix} = \begin{bmatrix} Z_{11} & -Z_{12} \\ Z_{12} & -Z_{22} \end{bmatrix} \begin{Bmatrix} V_g \\ V_a \end{Bmatrix}$$

Figure 9. Main Gearbox/Airframe Isolation Mount Nomenclature

- Ratio of airframe velocities with mount, V_a^*, to case with no mount, V_a

c) Change in input power into airframe:
power is proportional to: $|V_a|^2$

d) Modeling of attached components

- Airframe: already in SEA Model

  SEA description of airframe impedance
  Measured mobility on actual airframe

- Gearbox: not currently modeled

  Measured mobility on actual gearbox
  Further consideration required in deciding approach

- Isolation mount:

  Low frequency simple stiffness model
  Higher frequency - SEA model of propagation resonances within mount
  Measured impedances on actual mount
  Transmission line modeling of mount impedances

2. Advanced Composite Material Designs

a) Composite panel sandwich construction

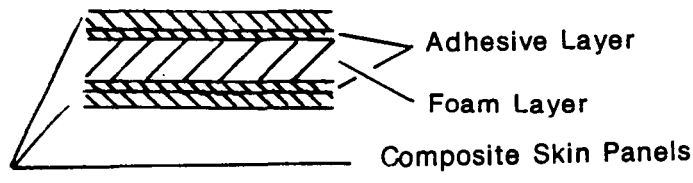

Figure 10. Typical Composite Panel Sandwich Construction Cross Section

b) Composite panel constructions with constrained shear layers

- Four layer construction

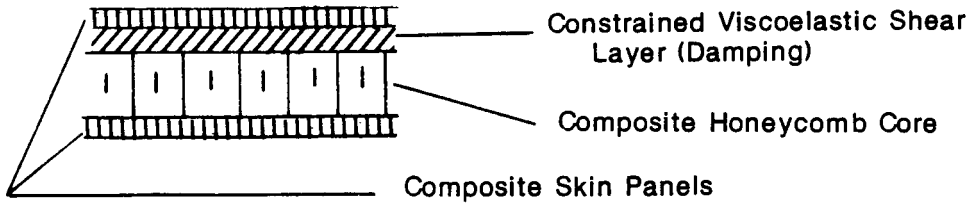

Figure 11. Typical Constrained Layer Damping Composite Panel Cross Section

- Five layer construction

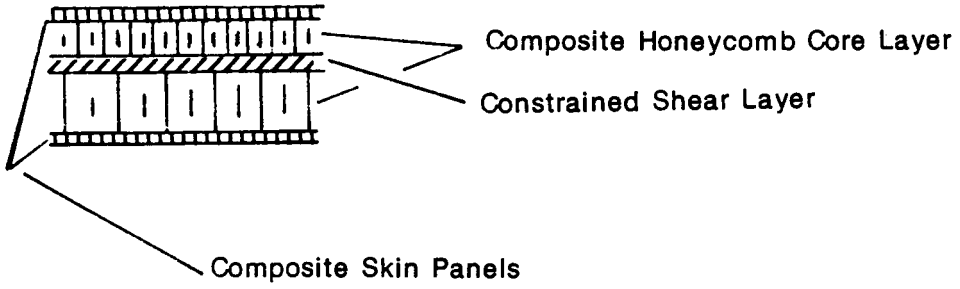

Figure 12. Typical Double Honeycomb Constrained Layer Damping Composite Panel Cross Section

Introduction to Modeling Concepts

The previous section described conventional and advanced noise control treatments applicable for use in helicopter airframes to reduce cabin noise. This section addresses the development of models of their behavior for inclusion within the overall SEA model of the S-76 airframe and cabin noise environment. The cabin noise control treatments fall within two general categories based on their primary intended effect: 1) those effecting the dissipation of vibratory and acoustic energy; and 2) those that alter the transmission of energy from the source to receiver, in this case from the gearbox to the bounding panel and frame surfaces which radiate into the cabin.

Dissipative treatments include add-on free extensional (Figure 4) and constrained layer (Figure 3) damping treatments on skin panels and frame webbing. Dissipative treatments within acoustic spaces include the surface absorption provided due to added fiberglass or open cell foam materials within the different cavities (Figure 5) other than the cabin that, in part, are created by the addition of trim and ceiling panels.

Transmission type treatments have the primary effect of reflecting energy back towards the source, with the intent of reducing the energy which reaches the receiving subsystems. An important consideration is whether source levels increase as a result of the treatments, thereby negating their effects. It is often important to incorporate additional damping at the source in order to minimize the tendency for increased source levels.

The primary transmission type treatments for the helicopter cabin are the side and ceiling trim panels that cover the structural skin panel and frame surfaces (Figure 5). Acoustically, their overall effect is to reduce the radiation into the cabin due to panel and frame vibration (Figure 6). They define additional acoustic spaces that are coupled to the skin and trim panels and which are coupled directly to the cabin through non-resonant mass controlled response of the trim panels. While not a treatment, per se, the presence of leaks or gaps in the trim panel coverage must be accounted for in describing the coupling across the trim panel between the cavity and the cabin.

The isolation mounts, shown schematically in Figure 6, used to suspend the trim panels are transmission type treatments that affect the direct coupling of skin panel or frame vibratory energy into the trim panels. Isolation mounts at the gearbox attachment to the airframe (Figure 8) are a potentially important application of a transmission treatment directly affecting the dominant source of power flow into the airframe. Other types of treatment, including the dissipation treatments, affect individual connections or response levels often in parallel with many other paths having comparable contributions, so that significant reductions in cabin noise levels will require extensive application of such treatments.

Dissipative type treatments can also affect the propagation behavior in the subsystems to which they are applied. Added panel damping treatments will effect the bending rigidity and surface mass of the panel. Fiberglass and foam treatments within the acoustic cavities created by the trim panels provide dissipation and in addition alter the propagation characteristics in the air within the cavity due to the porosity, thermal capacity and flow resistivity of the fill material.

Noise control treatments potentially effect all of the parameters of an SEA model of the cabin noise environment. Treated subsystems will have altered damping levels, mode densities and also coupling loss factors to other subsystems due to the effects of the treatments on propagation characteristics. In addition, modifications to the existing S-76 SEA model need to include the additional subsystems associated with particular treatments. Table 1 summarizes the specific items to be discussed in this section.

Table 1. Noise Control Treatments: Extensions to the SEA Model of the S-76

1. Dissipative Type Treatments
   - 1.1 Free extensional damping layers
   - 1.2 Constrained layer damping
   - 1.3 Acoustic absorption

2. Transmission Type Treatments
   - 2.1 Trim panels
     - Resonant response
     - Mass law response
   - 2.2 Trim panel acoustic cavities
     - Resonant acoustic modes
     - Cavity absorption
     - Gaps or holes
   - 2.3 Trim panel isolation mounts
   - 2.4 Gearbox isolation mounts

Dissipative Type Treatments

Free extensional damping layers. - The addition of viscoelastic layers to panel surfaces increases the overall damping level as a result of flexural and extensional deformation in the added layers. The amount of damping increase is dependent on the relative energy storage within the viscoelastic material and base panel during bending. The greater the relative energy storage within the viscoelastic material, the greater will be the increase in overall loss factor. In addition to the material loss factor of the viscoelastic material, the stiffness properties and thicknesses of both layers are important in scaling the effectiveness of the damping treatment.

The SEA model of a panel subsystem relies on a description of bending wave propagation characteristics in order to determine coupling loss factors between the panel and adjacent frames and panels, and also to adjacent acoustic spaces as a result of panel radiation. Bending propagation behavior also determines the mode density of the panel. Panel damping loss factors are important, explicit parameters in the model. The added viscoelastic layer potentially effects the SEA model in each of these areas.

The evaluation of bending rigidity of the composite, Figure 4, presumes that cross-sections remain plane during deformation. The neutral axis for bending is shifted as a result of flexural and extensional stiffness of the viscoelastic layer:

$$t_n = \frac{1}{2} \left[\frac{E_b \; t_b^2 \; - \; E_v \; t_v^2}{E_b \; t_b + E_v \; t_v}\right] \tag{1}$$

where E_b, t_b and E_v, t_v are the elastic modulus and thickness of the base panel and viscoelastic treatment, respectively. The overall bending rigidity, B_c, is as follows:

$$B_c = \frac{E_b \; t_b^3}{12} + \frac{E_v \; t_v^3}{12} + E_b \; t_b \left(\frac{t_b}{2} - t_n\right)^2 + E_v \; t_v \left(\frac{t_v}{2} + t_n\right)^2 \tag{2}$$

where t_n is the distance between the viscoelastic layer/base panel interface and the neutral axis of the combined composite structure. The surface mass of the treatment must also be accounted for in determining the bending wave speed:

$$M_c = \rho_b t_b + \rho_v t_v \tag{3}$$

and

$$c_b = \left(\frac{B_c}{M_c}\right)^{\frac{1}{4}} \sqrt{\omega} \tag{4}$$

where M_c is the surface mass per unit area and c_b the bending wave speed of the panel.

The expression for the loss factor of the composite is taken from work by Ungar and Ross [3].

$$\eta_c = \frac{\beta_v}{1 + \dfrac{h^2 (1+\beta_v^2) + (r_b/t_{bv})^2 [(1+h)^2 + (\beta_v h)^2]}{h \{ 1 + (r_v/t_{bv})^2 [(1+h)^2 + (\beta_v h)^2]\}}} \tag{5}$$

where

β_v	-	loss factor of viscoelastic material
$h = \dfrac{E_v t_v}{E_b t_b}$	-	ratio of extensional stiffnesses
$r_b = t_b/12$, $r_v = t_v/12$	-	radii of gyration of base panel, viscoelastic layer
$t_{bv} = (t_b + t_v)/2$	-	distance between vertical planes of the layers

The dependence of the composite loss factor on relative thicknesses and stiffnesses is illustrated in Figure 13 [4]. Increasing thickness or stiffness modulus of the viscoelastic material relative to the value for the base panel increases the energy storage within it resulting in a greater loss factor for the composite.

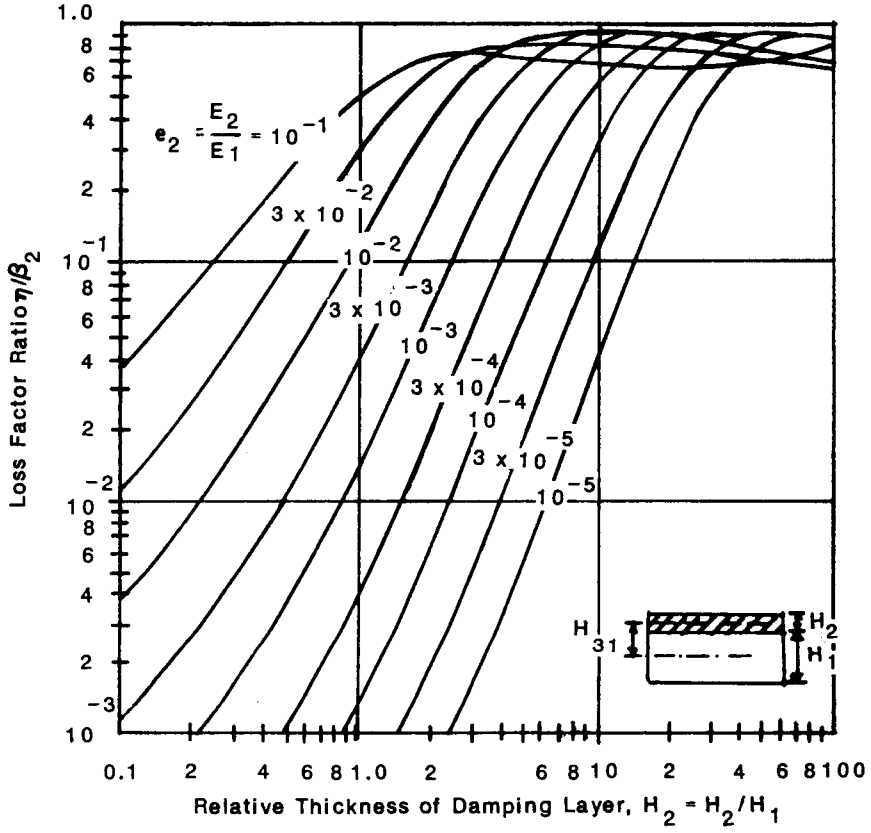

Figure 13. Loss Factor for Free Extensional Damping Treatment.

The above description does not include the effects of temperature and frequency on the material properties of the viscoelastic material layer. If material loss factor and modulus are known for individual frequencies and temperatures, the above analytic expressions can be used to estimate propagation and damping behavior for the composite.

Material property data can be obtained to varying degrees of completeness from the manufacturers and suppliers of viscoelastic material layers for damping purposes. Empirical damping loss factor data for specific treated panels may also be available from the manufacturers. Damping measurements on actual sample panels is an alternative source of loss factor data for input to the SEA subsystem model.

Empirical data characterizing propagation behavior is relatively rare so that the above expressions would be needed to determine bending wave speed. The principle effect of the treatment is often due to the mass it adds to the base panel as stiffness moduli of typical viscoelastic materials are relatively small compared to those for base materials and do not significantly increase the bending rigidity. Also, the required composite damping level, while significantly greater than for the base panel material, is not typically on the order of that for the viscoelastic material but at least a factor of ten less. Treatments requiring larger composite loss factors often involve composite constructions with constraining layers or internal shear layers where the design focus is to induce more strongly damped shear deformation in the constrained shear layer, as will be discussed in the next section.

Constrained layer damping. - Constraining layers are used in conjunction with lossy viscoelastic material layers, as shown in Figure 3, to induce greater shear deformation, thereby taking advantage of the inherently larger damping of such materials in shear. The relative proportion of potential energy stored in shear deformation of the constrained layer is again important in determining the effective damping level of the composite. The degree of shear deformation that occurs is dependent on the curvature or wavelength of the panel bending deformation.

At very long bending wavelengths little shear deformation occurs within the constrained layer resulting in reduced composite loss factor. The energy associated with shear deformation for very short wavelengths decreases relative to the energy in bending of the base panel, also resulting in a loss of effective damping. Constrained layer treatments exhibit a broadly defined optimum effective loss factor, as a function of frequency, related to the wavelength for bending wave propagation in the composite panel.

The analysis of constrained layer damping treatments is also adapted from the work of Ungar and Ross [3] and which is described in Reference [4]. The composite panel loss factor is given by:

$$\eta_c = \frac{\eta_2 \, YX}{1 + (2+Y)X + (1+Y)\,(1+\beta_2^2)X^2} \tag{6}$$

where Y is a stiffness parameter given by:

$$\frac{1}{Y} = [\frac{E_1 \, t_1^3 + E_3 \, t_3^3}{12 \, t_{31}^2} \, (\frac{1}{E_1 t_1} + \frac{1}{E_3 t_3})] \tag{7}$$

and E_1, E_3, and t_1, t_3 are the elastic moduli and thicknesses of the base panel and the constraining layer, and t_{31} is the distance between neutral planes of these individual layers. The quantity X is referred to as the shear parameter defined as:

$$X = \frac{G_2}{k^2 t_2} \, (\frac{1}{E_1 t_1} + \frac{1}{E_3 t_3}) \tag{8}$$

where G_2 and t_2 are the storage modulus in shear and thickness of the visco-elastic constrained layer. The wavenumber for bending wave propagation in the composite, k, is given by:

$$k = \frac{\omega}{c_b} \tag{8}$$

where c_b is the bending wavespeed:

$$c_b = (\frac{B}{\rho_c})^{\frac{1}{4}} \sqrt{\omega} \tag{9}$$

ρ_c is the surface mass density of the composite:

$$\rho_c = \rho_1 t_2 + \rho_2 t_2 + \rho_3 t_3 \tag{10}$$

and B is its' bending rigidity, equal to the real part of the complex bending rigidity, B*, which is given by:

$$B^* = (B_1 + B_3)\left(1 + \frac{X^* Y}{1 + X^*}\right) \tag{11}$$

the complex shear parameter X* equals

$$X^* = X(1 + i\eta_2) \tag{12}$$

B_1 and B_3 are the bending rigidities of the base panel and constraining layer, respectively.

The process of determining the effective loss factor requires an iterative approach to evaluating the shear parameter. The shear parameter depends on the bending wavenumber, k, which at a particular frequency, depends on the bending rigidity of the composite panel. Iteration is required because the bending rigidity depends on the shear parameter whose value we are seeking. A useful starting point for the iteration is to assume a long wavelength limit characterized by rigid shear coupling between the base panel and constraining layer. This yields an initial value for the bending rigidity of:

$$B' = (B_1+B_3)(1+Y) \tag{13}$$

which is then used to determine a value for k and subsequently, X. Using this value of X determine B* and compare its real part with B. If it is close in value the iteration is complete, otherwise continue using the real part to determine a new value for k, etc.

As was the case for free extensional damping treatments, the effects of a constrained layer treatment on both the damping level and bending wave propagation are required for the SEA model of the treated panel subsystem.

Acoustic absorption (cabin). - This treatment refers to materials that are added to an acoustic space which result in the dissipation of acoustic energy within the space. The treatments include both materials placed against a bounding surface of the space, such as floor or wall carpeting and overhead panels, and also materials that behave as space absorbers. The latter refers primarily to porous seat upholstery which acoustically is characterized by its flow resistance. Porous materials within the cavities defined by trim panels are discussed in the section dealing with transmission treatments in that they occupy a larger volume fraction with potentially significant effect on acoustic propagation within the cavity.

Absorbing surface treatments are most straightforwardly accounted for using standard approaches from room acoustics. The loss factor for acoustic resonances within a space is related to the absorption of energy at the wall surfaces according to the following:

$$\eta = \frac{c\ S}{8\pi\ V\ f}\ \bar{\alpha} \tag{14}$$

where

- c - sound speed
- S - total wall surface area
- V - volume of space
- f - frequency, Hz

and $\bar{\alpha}$ is the area weighted average absorption coefficient for all bounding surfaces of the space defined by:

$$\bar{\alpha} = \frac{1}{S}\ \Sigma_i\ S_i\ \alpha_i \tag{15}$$

where S_i, α_i are the individual wall surface areas and corresponding absorption coefficients.

The absorption coefficients, α_i, should account for the energy dissipated upon reflection from the surface and not include the transmitted energy which is accounted for in the SEA model in coupling to resonant panel response or direct coupling to adjacent spaces through non-resonant response of interviewing panels, or holes. When transmission of this type is not otherwise accounted for within the SEA model then it should be included in α_i in addition to the dissipation at that surface.

The most common source of absorption data is reverberation time measurements where the decay of acoustic pressure levels is recorded when the sound source is abruptly turned off. The reverberation time, T_R, the extrapolated time required for the pressure levels to decay 60 dB, is related to the average absorption coefficient according to the Sabine equation:

$$T_R = \frac{60V}{1.086\ cS\bar{\alpha}} \tag{16}$$

Reverberation time measurements are utilized to determine $\bar{\alpha}$ which then gives η according to Equation (14). The loss factor for the treated cabin configuration may be directly estimated from reverberation time data, if available, according to the following:

$$\eta = \frac{2.2}{f_o T_R} \tag{17}$$

If treated space data is unavailable then an independent evaluation for the absorption coefficient of the treatment, α_a, is required along with Equations (14) and (15). Presuming also that information exists for $\bar{\alpha}_{ut}$, the average absorption coefficient in the untreated case, then α_t in the treated case is based on α_a and the treated area, S_t, according to the following:

$$\bar{\alpha}_t = \frac{(S-S_t)\ \bar{\alpha}_{ut} + S_t\ \alpha_a}{S} \tag{18}$$

Absorption coefficient data is generally obtained from reverberant room measurements in specially designed test chambers. Representative data for two carpet materials are shown in Figures 14 and 15. The test materials are placed on an acoustically rigid floor in the chamber. It is presumed that effects due to potential differences in backing impedance between the reverberant room measurements and the actual cabin installation can be neglected in the above evaluation for $\bar{\alpha}_t$.

While primarily intended for other functions, porous seating upholstery is also a source of acoustic dissipation in the cabin. Sound waves impinging on the relatively thin porous material layers will undergo dissipation within the pores of the material. Depending on the configuration of the seating both faces or sides of the material may be accessible to sound waves in the cabin.

The modeling of a free standing porous absorbing layer accounts for the flow resistance, porosity and mass per unit area of the material. As sound propagates through the material, viscous dissipation occurs as a result of the motion of the air particles relative to the fibers making up the material. The viscous forces that are generated by the relative motion tend to accelerate the fibers along with the air particles. The fiber motion is inhibited by its mass reactance, presuming a limp structure. At lower frequencies the mass reactance may be insufficient to prohibit fiber motion resulting in a loss of relative motion between fiber and air, and an associated reduction in absorption provided.

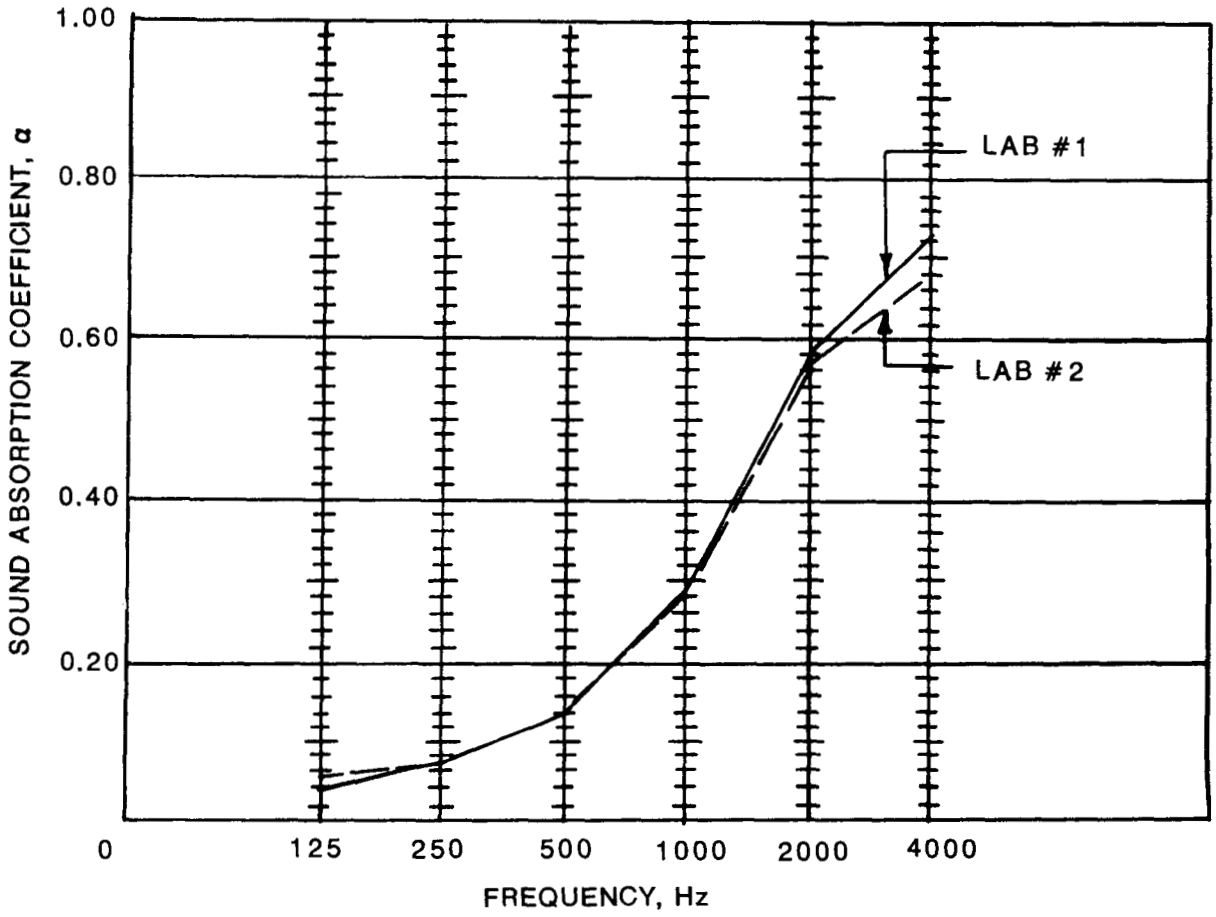

Figure 14. Carpet Absorption.

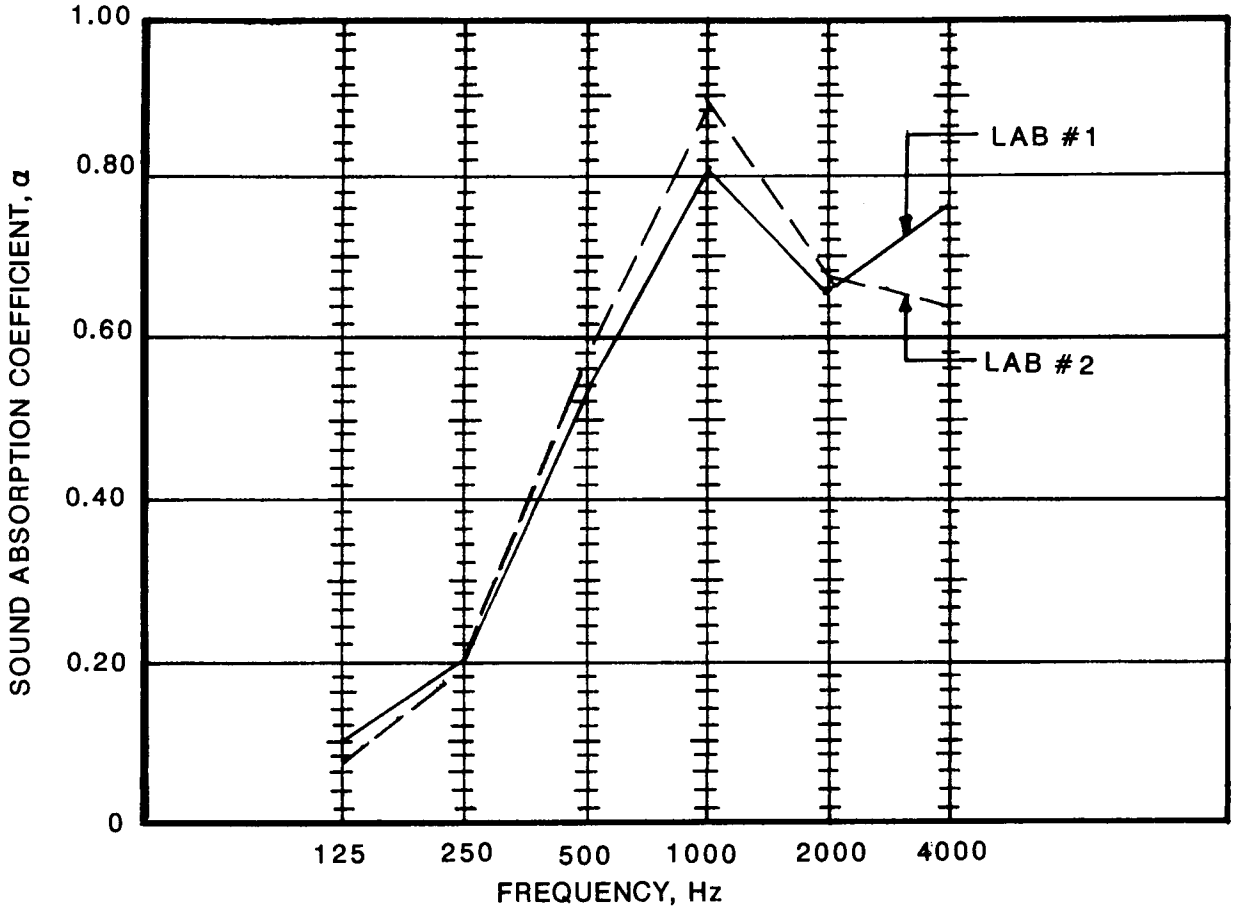

Figure 15. Carpet and Pad Absorption.

The absorption coefficient is given by the following expression:

$$\alpha = \frac{2\, Z_a \left[\frac{(\omega M_f)^2 R_m}{R_m^2 + (\omega M_f)^2}\right]}{|Z_a + Z_m|^2} = \frac{2\left(\frac{R_m}{Z_a}\right)\left[\frac{(\omega M_f/R_m)^2}{1 + (\omega M_f/R_m)^2}\right]}{\left|1 + \frac{Z_m}{Z_a}\right|^2} \tag{19}$$

where:

R_m - flow resistance of material

M_f - surface mass per unit area

and $$Z_a = \frac{2\rho c}{\cos\theta} \tag{20}$$

Z_a is an acoustic radiation impedance including the air on both sides of the layer, and

$$Z_m = \frac{(-i\omega M_f)R_m}{R_m - i\omega M_f} = \frac{-i\omega M_f}{1 - i\omega M_f/R_m} \tag{21}$$

is the acoustic impedance of the material. It is the parallel combination of surface mass reactance and flow resistance. To characterize the absorption occurring in a diffuse or reverberant acoustic environment,an average over θ, the angle of incidence of the plane wave, is required to use the expression for α.

The loss of absorption at low frequencies or for very light layers is readily identified in the above expressions. When the surface mass reactance is small compared to the flow resistance, i.e., when

$$\frac{\omega M_f^2}{R_m} \ll 1 \tag{22}$$

then α is also small. At higher frequencies or for heavier absorbing blankets Z_m approaches R_m in value, and:

$$\alpha \cong \frac{2\,\frac{R_m}{Z_a}}{\left(1 + \frac{R_m}{Z_a}\right)^2} \tag{23}$$

At normal incidence, $Z_a = 2\rho c$ and

$$\alpha \cong \frac{\frac{R_m}{\rho c}}{\left(1 + \frac{R_m}{2\rho c}\right)^2} \tag{24}$$

which exhibits a maximum value for α equal to .5 when $R_m = 2\rho c$.

The effects of free standing absorbing layers on the acoustic loss factor of the cabin are accounted for according to the previously described approach based on the above expression for α. Where sound waves in the cabin impinge on the material from both sides the appropriate area is twice the area of the material. Reverberation time measurements in the cabin with such materials in place provide a direct measure of their effect.

Transmission Type Treatments

Trim panel acoustic cavities. - The addition of trim panel treatments creates acoustic cavities between the trim and skin panels, which are segmented by frame members. Additional acoustic subsystems are straightforwardly included within the SEA model to describe the acoustic levels within these spaces. At lower frequencies the thickness dimension of the cavities becomes small compared to an acoustic wavelength and the resonances are those of flat two dimensional acoustic spaces.

The acoustic cavities are coupled to the frame, outer skin, and trim panel structures that form the bounding surfaces. There is a direct coupling between adjacent cavities through holes in intervening frames and non-resonant mass controlled response of the frame webs. The cavities also couple directly into the cabin through non-resonant trim panel response and as a result of gaps in

the trim panel treatment. At higher frequencies and for the larger cavities in the cabin overhead, a transition occurs to three dimensional acoustic spaces for which all of the above coupling types are described in the current SEA model.

2-D acoustic modes. - At low frequencies, the two dimensional nature of the acoustic field in cavities created by trim panels effects the evaluation of the mode density. The mode density for a flat thin space, where S is the surface area and P is the perimeter around that area, becomes:

$$n(\omega) = \frac{S\omega}{2\pi c_o^2} + \frac{P}{2\pi c_o} \tag{25}$$

This expression is valid when the thickness dimension is less than one-half the acoustic wavelength.

Effect of cavity absorption treatments. - Acoustic treatments in the form of fiberglass or open cell foam materials are often added to control noise levels in cavities. In such cases the volume may be substantially filled with the absorptive material. Its effect is more than the absorption due to a simple surface treatment, and must be assessed in terms of its affect on acoustic propagation within the space. Although sound propagation in porous materials has been studied extensively by numerous investigators, a practical engineering description of the cabin noise environment for use within the SEA model is desired. The following approach is based on the discussion given in Reference [4] and accounts for the thermal capacity, porosity, and flow resistivity of the material in evaluating a complex propagation constant.

The flow resistivity of common porous materials is dependent on the cross dimension of the filaments or fibers and the bulk density of the material, a description of the fiber content. This dependence is shown for common glass-fiber materials in Figure 16. The relationship is described by the following algebraic expression:

$$r = 3.18\text{x}10^3 \, \rho_b^{1.53}/d_f^2 \tag{26}$$

where r is the flow resistivity in mks rayls/m, ρ_b is the density of the bulk material in kg/m^3, and d_f is the fiber diameter in microns (10^{-6}m). The bulk density is related to the density of the material making up the fibers, ρ_f, and the porosity of the bulk material, h_o, according to:

$$\rho_b = \rho_f \, (1-h_o) \tag{27}$$

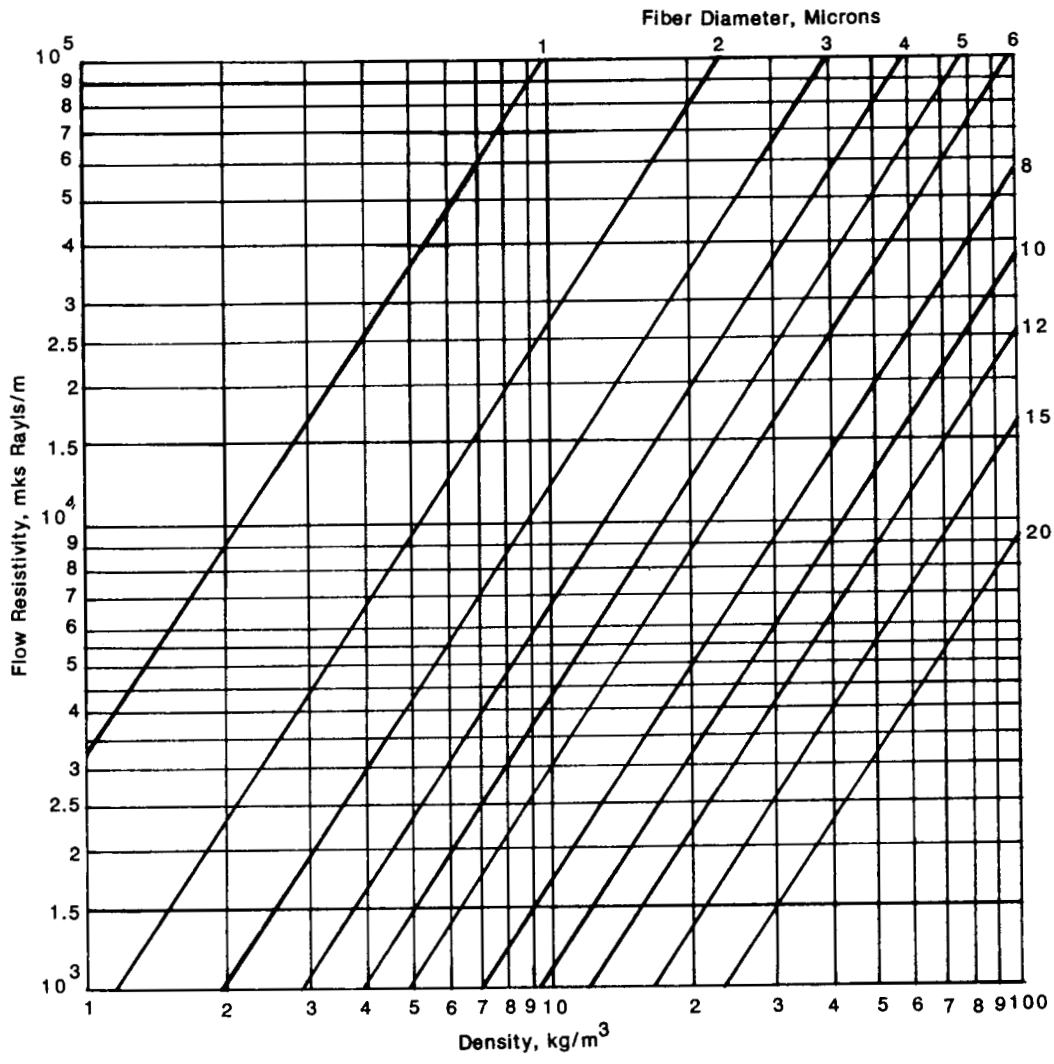

Figure 16. Flow Resistivity of Glass Fiber Products.

Thermal conduction between the air and the solid material can significantly influence the compression of the air as sound propagates through the material. At sufficiently low frequency the sound propagation occurs isothermally as heat transfer to and from the solid compensates for the temperature rise and fall which would otherwise occur during compression and rarefaction of the air. At high frequency the fluctuation occurs too rapidly for heat transfer to have a significant effect and the process is adiabatic.

The gas compressibility relates pressure and volume changes according to the following expression:

$$K' = \frac{K}{h_o} = V \frac{dp}{dV} \tag{28}$$

where K is the compressibility of the air and K' the compressibility of the porous material. K' accounts for the reduced volume of air available to be compressed as a result of the presence of the material. The volume, V, and associated volume change, dV, refer to the bulk porous material. The solid portion of the material is assumed to be volumetrically incompressible in comparison with the air. The variation of K with frequency due to thermal effects is shown in Figure 17.

Flow resistivity directly affects the propagation by introducing dissipation due to viscous losses. Its effects are conveniently accounted for in terms of a complex density, ρ^*, for propagation within the porous material:

$$\rho^* = \frac{\rho}{f_1} \left(f_2 + \frac{i\ 1.2\ r}{\rho\ \omega}\right) \tag{29}$$

where ρ is the density of air and

$$f_1 = 1 + \left(\frac{1.2\ r}{\rho\omega}\right)^2 \tag{30}$$

and

$$f_2 = 1 + \left(h_o + \frac{\rho_m}{\rho}\right) \left(\frac{1.2\ r}{\rho_m \omega}\right)^2 \tag{31}$$

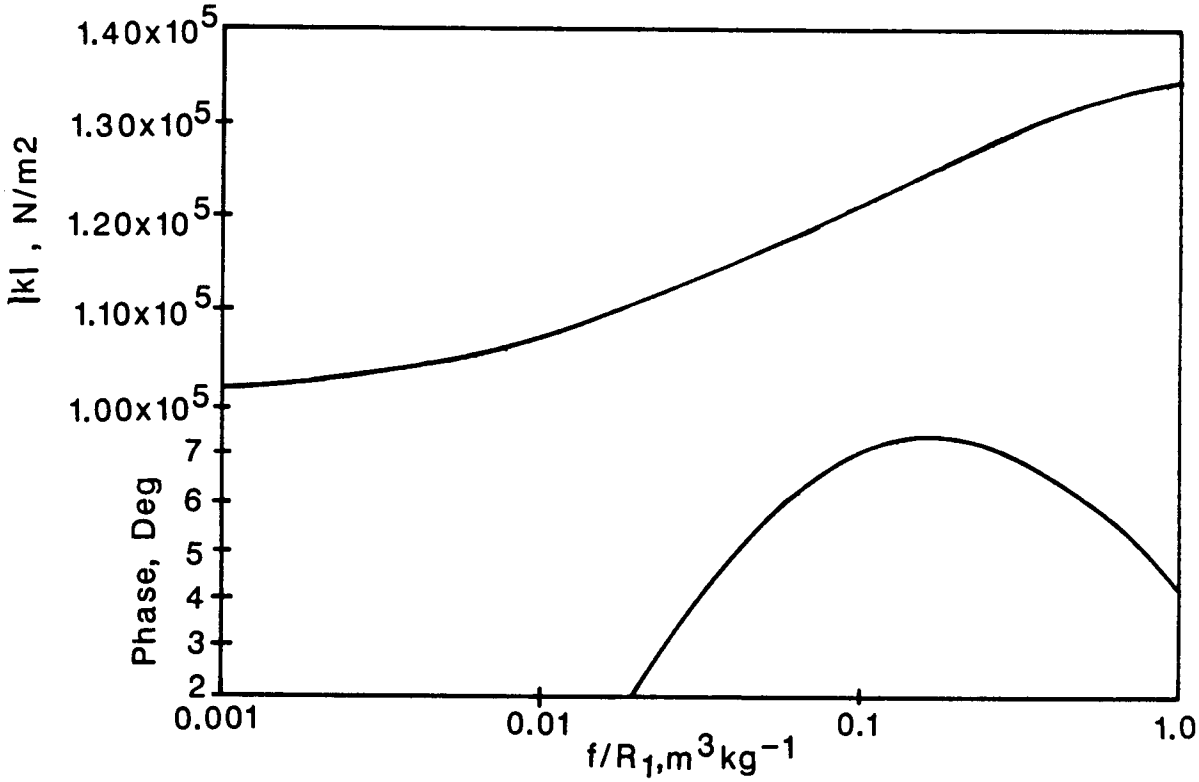

Figure 17. Compressibility of Air Within a Porous Material.

For materials with rigid frames:

$$f_1 = f_2 = 1 \tag{32}$$

The expressions, when applied to soft or semi-rigid materials, show an increase in effective air mass, i.e., the real part of the complex density, which is dependent on flow resistivity. The effective mass is that of the air alone for low flow resistivity. As flow resistivity increases the viscous forces accelerate the mass of the frame material along with the mass of the air particles resulting in an increase in effective air mass.

A complex propagation constant or wavenumber for the porous material, for $e^{-i\omega t}$ time dependence, is defined by:

$$b = \omega\sqrt{\rho^*/K^*} \tag{33}$$

where

$$p(x,t) \;\; \alpha \;\; e^{i(bx-\omega t)} \tag{34}$$

In terms of real and imaginary components:

$$b = id + \frac{\omega}{c_m} = id + \frac{2\pi}{\lambda_m} \tag{35}$$

where c_m, λ_m are sound phase speed and wavelength in the porous material, and d is the attenuation constant in nepers/m.

The attenuation constant, d, can then be related to the loss factor for acoustic resonances within the porous material filled cavity by modifying the total sabine absorption to account for propagation loss in addition to wall absorption:

$$(S\bar{\alpha})_t = S\bar{\alpha} + 8dV \tag{36}$$

Combining Equation (36) with Equation (14), replacing $S\bar{\alpha}$ in Equation (14) with $(S\bar{\alpha})_t$ from Equation (36), gives the desired loss factor.

Alternatively, the component of loss factor associated with propagation losses can be obtained directly from the complex propagation constant by recognizing that the complex phase speed is related to the loss factor according to:

$$c^* = c_m(1 - i\frac{\eta}{2}) = \sqrt{K'/\rho^*} \tag{37}$$

and that

$$b = \frac{\omega}{c^*} = \frac{\omega}{c_m}(1 + i\frac{\eta}{2}) \tag{38}$$

by comparison with Equation (35), it can be seen that,

$$\eta = \frac{2c_m}{\omega} d \tag{39}$$

The loss factor, given by Equation (39), associated with propagation attenuation is added to the value for η corresponding to wall absorption to account for both dissipation mechanisms. This approach is preferred to that indicated by Equation (36) in that it does not depend on details as to whether the cavity is a two dimensional or three dimensional acoustic space. Equation (36) is based on a three dimensional diffuse field representation of the acoustic space.

Trim panel isolation mounts. - Trim panel mounts are important to the SEA model in that they are a potential flanking transmission path to the airborne transmission loss provided by the trim panels themselves. They constitute a flanking transmission path in two respects, firstly power flow through the mount transmits into resonant motion of the trim panels with subsequent radiation into the cabin. Secondly, the point attachment of the mount to the trim panel generates a flexural near field that radiates directly into the cabin. This section describes the modeling of the mount dynamic behavior and calculation of coupling loss factors for both mechanisms.

Commonly, mounts attach to frame members making up the cabin airframe structure as shown schematically in Figure 6. The desired coupling loss factors are between the frame and trim panel subsystems in one case and directly between the frame and cabin acoustic subsystems for the mechanism involving radiation from the flexural nearfield. Coupling loss factors are evaluated for out-of-plane motion of the frame and compressional motion through the mount.

The acoustic power radiated by the flexural nearfield of a point excited plate is given by the following [4]:

$$\Pi_{rad} = \frac{8}{\pi^3} \rho c \lambda_c^2 \tilde{V}_1^2 \tag{40}$$

Where: λ_c - bending wavelength of trim panel at coincidence frequency

$\tilde{V}_1^2$ - mean square velocity of the trim panel at the point where it attaches to the frame through the isolation mount.

The trim panel velocity is related to the mean square velocity of the frame at the mount attachment, $\tilde{V}_o^2$, by the following expression which depends on impedances characterizing the dynamic behavior of the mount and the trim panel:

$$\tilde{V}_1^2 = \left|\frac{Z_{12}}{Z_p + Z_{22}}\right|^2 V_o^2 \tag{41}$$

where Z_p is the point impedance of the trim panel:

$$Z_p = 8\sqrt{D_p M_p} \tag{42}$$

where D_p, M_p are the flexural rigidity and surface mass density of the trim panel and Z_{12}, Z_{22} are transfer and input impedances for the mount.

$$\begin{matrix} F_o \\ F_1 \end{matrix} = \begin{matrix} Z_{11} & -Z_{12} \\ Z_{12} & -Z_{22} \end{matrix} \begin{matrix} V_o \\ V_1 \end{matrix} \tag{43}$$

When the mount is modeled as a simple spring stiffness, these impedances become:

$$Z_{12} = Z_{22} = \frac{K}{i\omega} \tag{44}$$

The mount behaves as a simple spring stiffness until high frequencies relative to its dimensions where wave propagation and resonance effects occur within the mount.

The coupling loss factor between frame out-of-plane motion and the cabin acoustic space is obtained by combining Equations (40) and (41) with the additional relation that:

$$E_f = M_f \ \tilde{V}_o^2 \tag{45}$$

where M_f is the total mass of the frame subsystem, to then obtain:

$$\Pi_{rad} = \omega \eta_{f,a} E_f \tag{46}$$

$$\eta_{f,a} = \frac{1}{\omega} \frac{8\rho c \lambda_c^2}{\pi^3} \left| \frac{Z_{12}}{Z_p + Z_{22}} \right|^2 \frac{1}{M_f} \tag{47}$$

The coupling loss factor between frame motion and resonant trim panel motion $\eta_{f,t}$, describes the power input to the trim panel as a result of frame motion. The trim panel point impedance is purely resistive (i.e., $Z_p = R_p$) so that:

$$\Pi_{rad} = R_p \ \tilde{V}_1^2 = \omega \ \eta_{f,t} \ E_f \tag{48}$$

$$\eta_{f,t} = \frac{1}{\omega} R_p \left| \frac{Z_{12}}{R_p + Z_{12}} \right|^2 \frac{1}{M_f} \tag{49}$$

For mount attachments to skin panels the coupling loss factor expressions in Equations (47) and (49) are used where the frame subsystem mass is replaced by the skin panel mass. For mount attachments to both frames and panels the SEA mean square response velocity is presumed to adequately represent the velocity at the mount attachment location. The isolation mount is presumed not to significantly load the airframe structure to which it is attached.

Interior Configurations of the S-76 Aircraft

General: As discussed earlier, typical conventional approaches for noise control that we intend to focus on are: 1) cabin acoustic absorption, 2) panel damping treatments, 3) trim panel and cavity absorption, and 4) trim panel isolation mounts. These concepts are incorporated into the S-76 aircraft interior design to the greatest degree by the construction and installation of

Photo 6. Typical Utility Interior Seating.

ORIGINAL PAGE IS
OF POOR QUALITY

ORIGINAL PAGE IS
OF POOR QUALITY

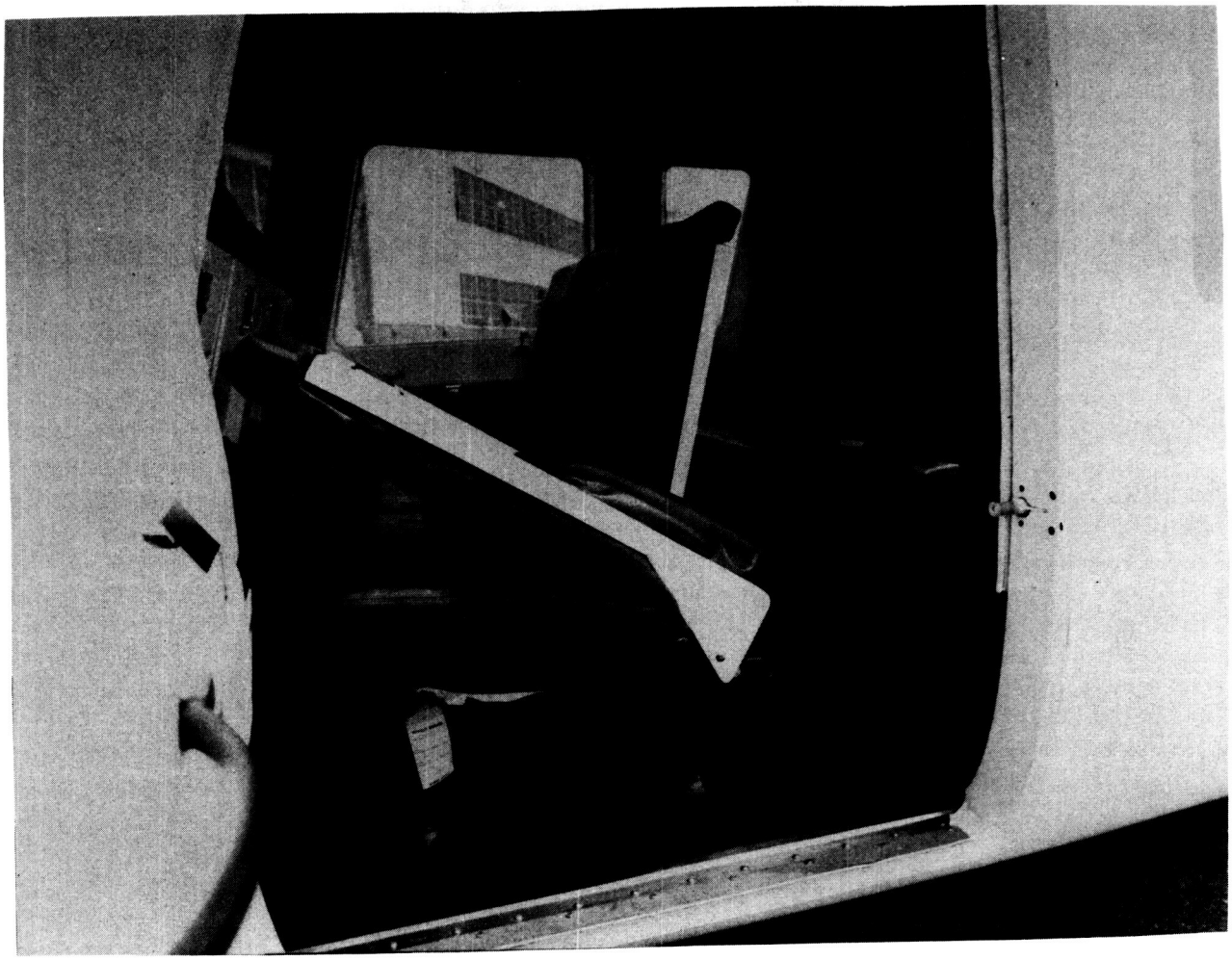

Photo 7. Typical Utlity Interior Sidewall, Ceiling, and Aft Bench Seat.

Photo 8. Typical Executive Interior with Soft VIP Seats, Forward Curtains, Hard Ceiling and Sidewalls.

ORIGINAL PAGE IS
OF POOR QUALITY

ORIGINAL PAGE IS
OF POOR QUALITY

Photo 9. Executive Interior Aft Divan Section, Hard Surface Sidewall and Duct Covers.

ORIGINAL PAGE IS
OF POOR QUALITY

Photo 10. Executive Interior with Table and Credenza.

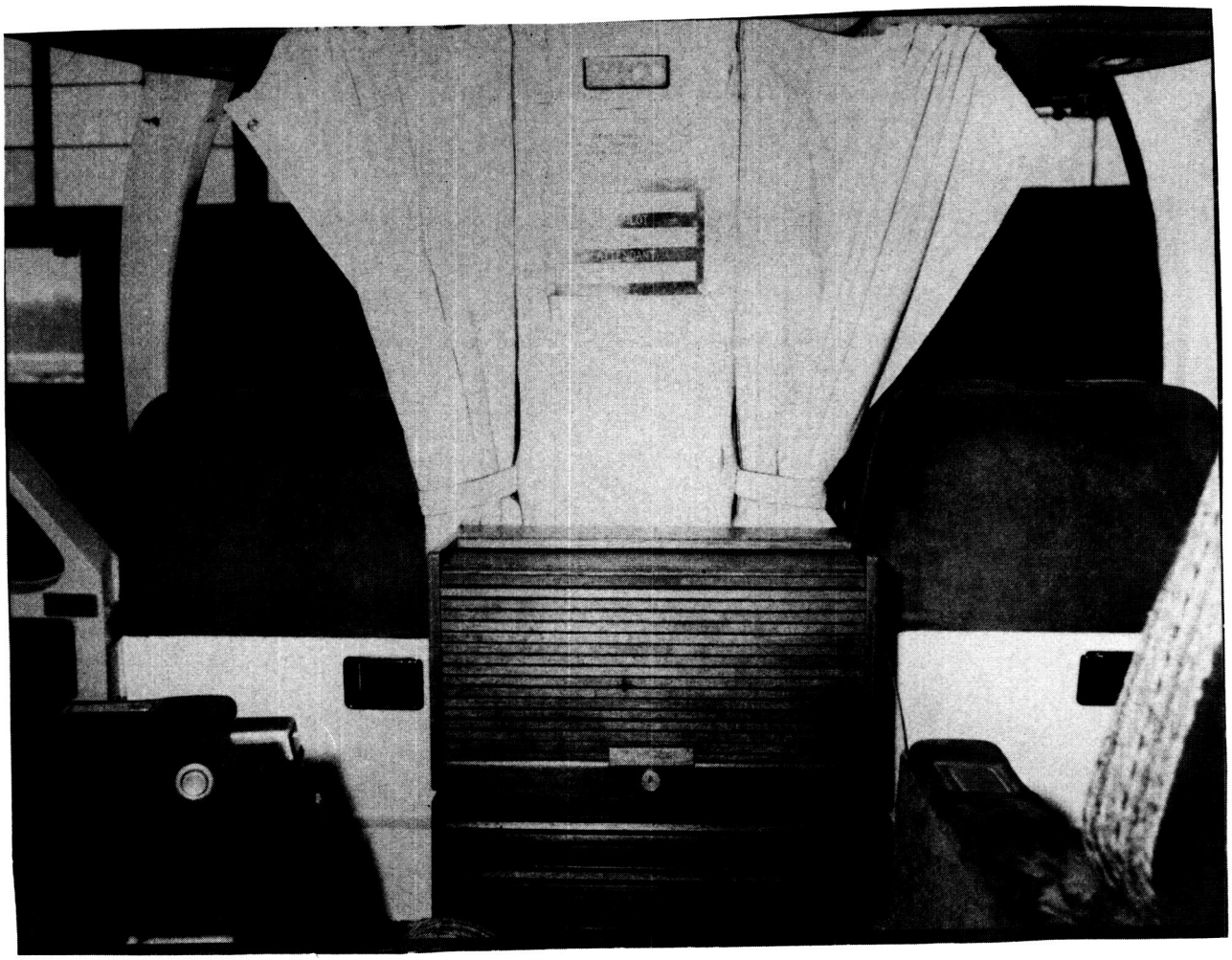

Photo 11. Executive Interior with Short Credenza. Curtains Provide Forward View for Passengers.

ORIGINAL PAGE IS
OF POOR QUALITY

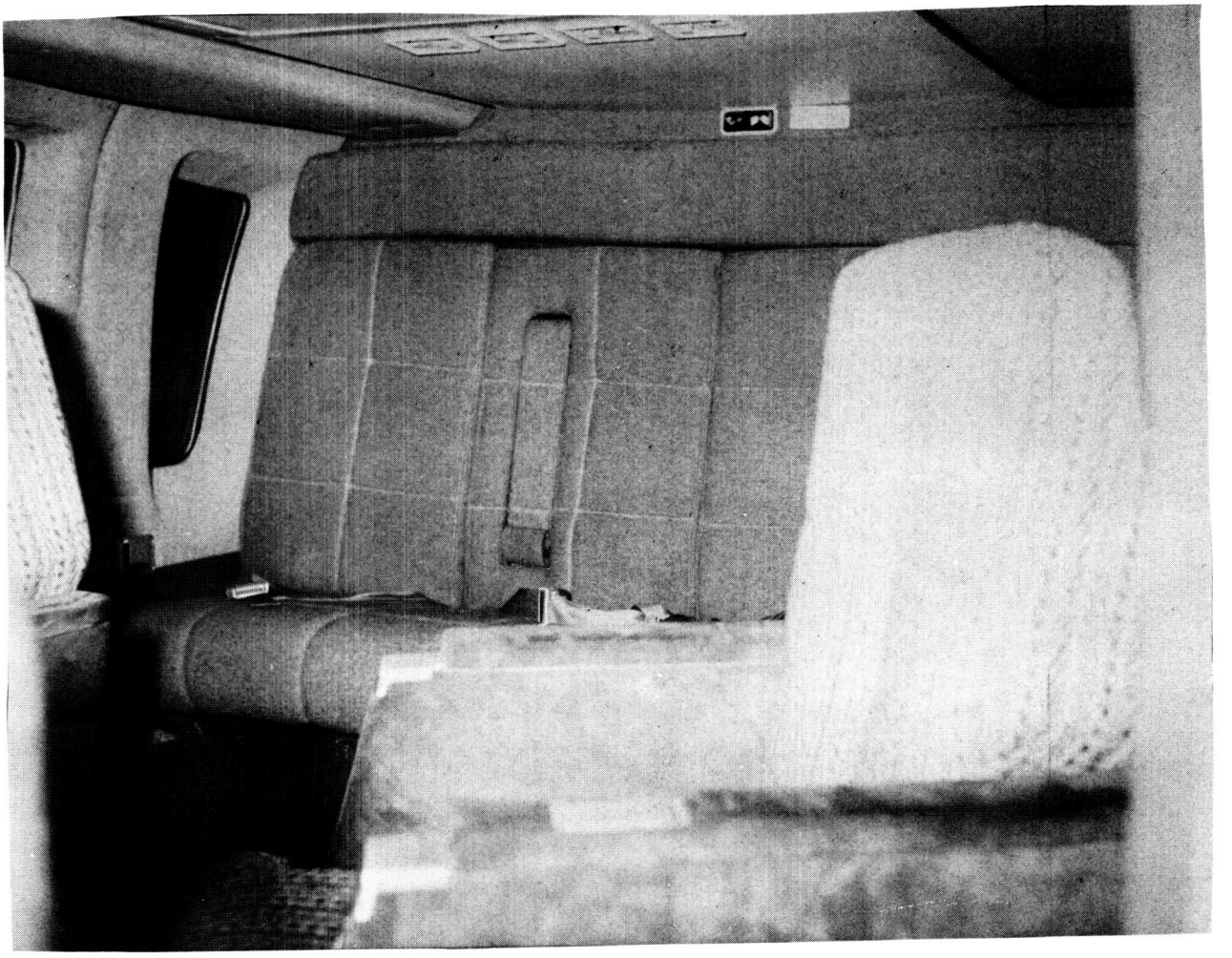

Photo 12. Executive Interior with Soft Sidewalls and Duct Covers, Hard Center Celing.

ORIGINAL PAGE IS
OF POOR QUALITY

ORIGINAL PAGE IS
OF POOR QUALITY

Photo 13. Totally Soft Surface Executive Interior with High Back Seats and Extra Thick Padded Headrest.

Photo 14. Totally Hard Surface Executive Interior, Aft Section.

ORIGINAL PAGE IS
OF POOR QUALITY

Photo 15. Totally Hard Surface Executive Interior with Full Forward Bulkhead Containing Sliding Windows.

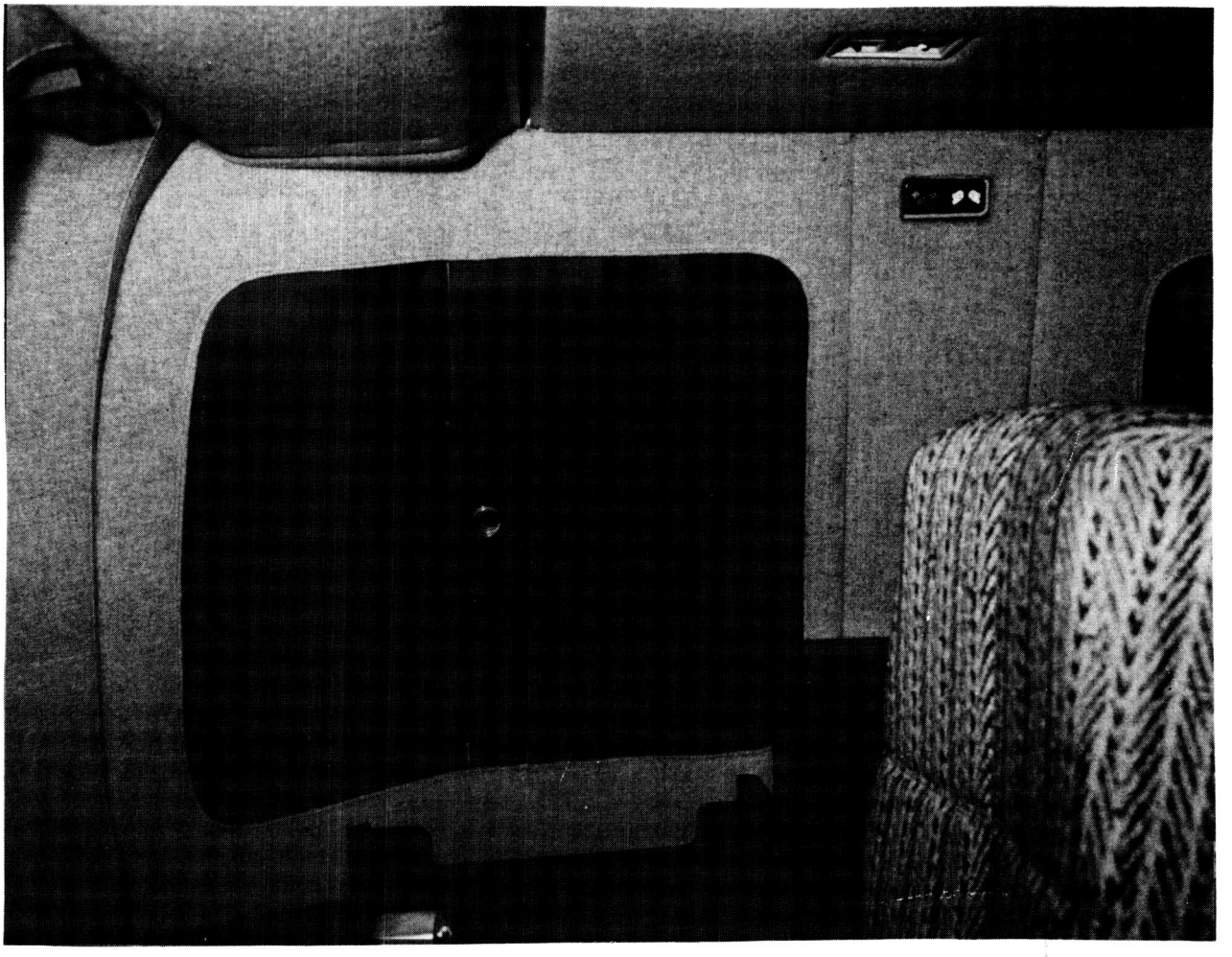

Photo 16. Executive Interior with Soft Surface Full Forward Bulkhead Containing Sliding Windows.

ORIGINAL PAGE IS
OF POOR QUALITY

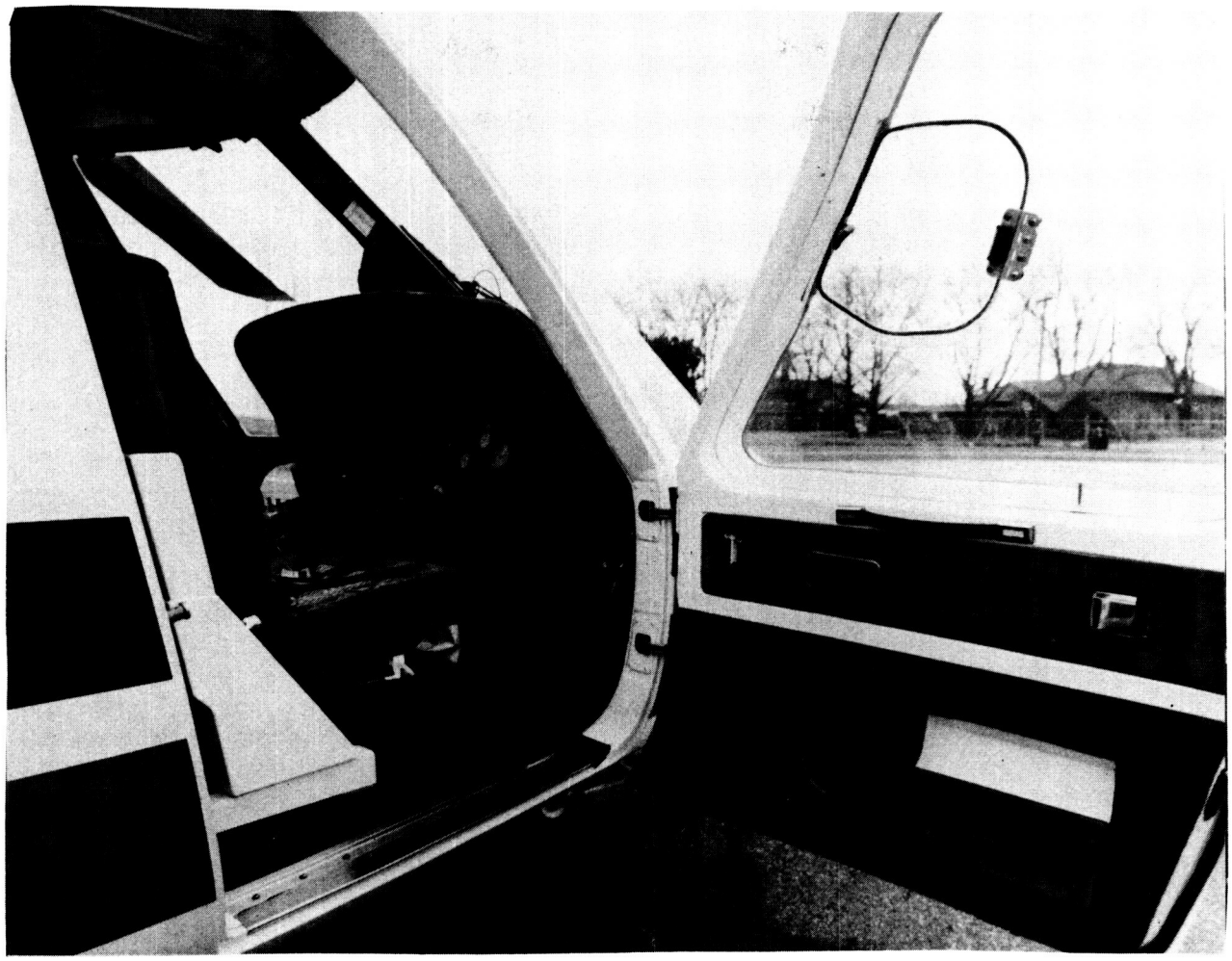

Photo 17. Executive Aircraft Cockpit Treatment.

the trim panel system. The panel is basically an isolated mass barrier with absorptive materials added. The absorptive material is added to both sides of the panel to face into both the cabin and outer cavities. Additional absorption in the cabin comes from material selection of the seats and carpeting on the deck.

The basic construction of an Interior system as modeled in this report consists of three overhead panels and four side panels (two on each side). The panels and seats are all upholstered with material best suited for their mission, i.e. durability and ease of maintenance in the Utility type and visually aesthetic plus highly noise absorptive for the quieter Executive type.

The overhead panels are inserted into H-channels (designated as Edge Panels in the model) which are supported from the overhead frames again through isolators. The H-channels also support on their outboard side the overhead air conditioning ducts. Overhead lighting and further ventilation is built into these panels with loaded vinyl boots behind them to prevent acoustic leakage.

The air conditioning ducts supply air from the Environmental Control Unit (ECU) located in the luggage compartment forward to the cabin and cockpit. The ducting splits after going through the rear bulkhead and runs up across the overhead outboard of the new overhead trim panels. Venting of the air takes place along the length of the overhead duct and is then brought into the cockpit overhead and down the sides behind the forward side trim panels. Return air is drawn from the junction area of the cockpit and cabin. The ducts are supported by the H-channels on one side and by isolators attached to the overhead frames on the other. The rest of the interior layout consists of a wool rug covering all deck space and upholstered bench seats for a seating capacity of up to 15 persons.

The side panels are attached directly to the airframe through isolators (four for the rear panels, six for the forward panels). Built into the side panel is an interior window which is isolated from the outer window. This creates a double pane effect for further noise attenuation.

Utility interior. The S-76 Utility aircraft is intended to be a low cost aircraft for general transportation such as shuttling of crews to and from off-shore oil drilling platforms. The interiors are designed for quick and efficient removal and maximum payload capacity (see Photos 2, 6 and 7, typical). Therefore, the panels and treatments are of basic construction and lightweight. Accordingly, attenuation of noise levels is nominal, roughly 10 to 15 db down from bare aircraft levels.

The structural member of the interior panels used both for the overhead and down the sides is made of 1/4" ABS plastic with a cover of 1/4" foam and vinyl trim cloth. The outboard side of the panels have an acoustic treatment of 1/2" fibrous glass batting (see Figure 5).

Executive (VIP) interior. The Executive Interior is designed for comfort of the passengers. Person capacity is limited to generally six passengers. Seating and interior layout is plush with many amenities for passenger comfort. Low noise levels in this type of aircraft is of prime importance and accordingly much attention to detail to prevent acoustic leakage is made. Noise levels in an Executive Interior equipped aircraft are generally 25 to 30 dB down from bare aircraft levels.

The interior trim panels are laid out as described above for the general interior layout. The trim cloth covering is improved both acoustically as well as visually by using fabric material (generally wool) which improves absorption characteristics. Transmission loss of the acoustic treatment is improved by using a 1 psf loaded vinyl. Leakage between panels is prevented by overlapping the loaded vinyl across panel junctions. The acoustic spaces behind all trim panels is filled with a fiberglass batting to improve absorption in those cavities. Seats are made of the same trim fabric with thick foam for comfort and increased cabin absorption.

Advanced Interior. The intent of the Advanced Interior concept was to take the lessons learned from the model about the Utility and Executive Interiors and apply treatment improvements to the model that could be again compared with equivalent treatments on a physical aircraft. Hopefully, the treatments in the aircraft would show positive results similar to the model prediction as a demonstration of the diagnostic capabilities of this method and as further varification of the model.

The improvements attempted in the model incorporated: 1) increased damping due to a constrained layer damping package applied on eight frames and four skin panels located near the two forward foot attachments; 2) increased absorption in available exterior cavities using fibrous glass material, and 3) increased absorption on outer material of the trim panels due to improved absorption capability of materials used.

Sea Model of the Treated Interior

The SEA model of the bare interior consists of 130 SEA subsystems connected to each other at 245 junctions [Ref. 1,2]. The subsystems include frame sections, skin panels, and acoustic spaces (principally the cabin). The subsystems for the treated interior include those for the bare aircraft plus additional panel subsystems that make up the trim panel treatments of the cabin overhead and sidewalls, as well as additional acoustical spaces for the cavities formed between the trim panels and outer skin panels. The trim panels are supported by soft rubber isolators which are modeled by a stiffness connection between the airframe structure and trim panel. Resonant transmission through the mount is also included, adding a subsystem for each isolation mount. Panel and space subsystems are added to describe the air conditioning ducting and duct cavities. The subsystem total increases to 307 for the treated interior with a total of 945 junctions.

Verification of the model predictions on an overall basis is done by comparison of the cabin subsystem predictions to actual interior noise levels from flight aircraft. This has been done in Reference 2 for bare interiors. Comparisons within this report are done relative to those bare levels - actual and predicted.

The SEA program takes individual subsystems in the aircraft and models them using standard subsystem types, such as cavities, panels, and frames with specific junction types defined at a subsystem end or middle. This report concerns itself with how close this comes to real world response by comparison with the laboratory experimentation and measured aircraft data.

The predicted response of frames and skin panels as part of the airframe has been shown to compare favorably to measured data for the bare aircraft configuration [Ref. 2] and is the basis of this model. The predicted flow of energy through the interior system as modeled by SEA techniques and how those predictions compare with the response of interior subsystems as measured through experimentation is discussed here within. Modeling of the treatment panels had not been done before and had to be compared to actual response. This was accomplished by measuring panel TL in the laboratory and then comparing with predicted SEA models. The panel was created using the SEA model for a panel and incorporating the parameters of the interior panel. These will be shown to compare favorably with actual panel responses. From this the response of the various panels could be modeled into the aircraft. This helps with the prediction of the Advanced Interior model which incorporated panels that have been laboratory tested, but not yet flight tested.

Laboratory experiments were performed generally within two test chambers designed to allow a variety of different acoustic measurements. The chambers are positioned side by side, yet isolated dynamically from each other and from surrounding structure. One room is a reverberant type chamber and the other is an anechoic type chamber. The rooms can be used individually or together by opening the test section between the rooms.

Other subsystem verification was performed either directly on the various aircraft, such as cabin absorption, or calculated, such as cavity absorption.

Sea models of trim panel transmission loss - In the SEA cabin noise model the trim panels are separate structural subsystems that couple directly to adjacent acoustic space. In addition, non-resonant panel response results in a direct coupling between adjacent spaces on either side of the trim panel, independently of the coupling to resonant panel response. An area junction between a trim panel subsystem and adjacent spaces consists of three separate coupling loss factor evaluations: resonant panel response separately coupled to each space, and space to space coupling through non-resonant panel response.

To substantiate the SEA modeling of trim panel behavior a series of laboratory experiments were carried out to evaluate the resonant and non-resonant transmission through trim panel designs for the Utility, VIP, and Advanced interiors. Leakage around the edges of trim panels also constitutes an additional direct coupling between the adjacent acoustic spaces. A series of experiments were also performed to support the modeling approach for leakage.

The experimental procedures are described in Appendix A. The measurement involves placing the test trim panel in an opening between a reverberent room and an anechoic chamber. With an acoustic source in the reverberent room the power transmitted through the panel to the anechoic chamber is measured using an acoustic intensity probe scanning over the panel surface to determine the total power.

An SEA model was developed of the experimental test setup. The room volumes and the trim panel size were identical to those for the measurement. The output of the SEA model was interpreted in terms of the transmission loss (TL) in the same manner as the data reduction that was applied to the experimental results to determine TL. The acoustic intensity incident on the test panel was determined from the space average pressure level in the reverberent room. In identical fashion the SEA model pressure response in the source space was converted to an incident acoustic intensity. The intensity probe was used to directly measure the transmitted intensity, and the SEA model directly predicts the transmitted power. The transmission loss is the ratio of transmitted to incident intensities.

The Utility trim panel design is basically a limp mass construction in that panel bending and coincidence effects do not occur until high frequencies above the band of primary interest. The measured TL results in Figure 18 following the conventional mass law behavior with a 6dB change in TL for each doubling or halving of frequency. The SEA result follows closely the measured data.

As previously described, the VIP trim panel is fundamentally a double wall construction with two mass layers separated by a compliant foam core. The outer foam and facing layers can be expected to have little influence on the TL. Their function is to provide absorption in the adjacent acoustic spaces. Such constructions can be modeled in detail with the addition of SEA subsystems to describe each mass layer, which must also include flexural stiffness effects, and the foam core.

The primary TL feature of double wall constructions is a dip in TL in the frequency region near the double wall resonance of the masses of the mass layers against the stiffness of the foam core. Above the double wall resonance the TL increases rapidly at a rate approaching a practical value of 12dB per doubling of frequency. The TL exceeds mass law based on the total mass of the panel design. This behavior is observed in the experimental results in Figure 19.

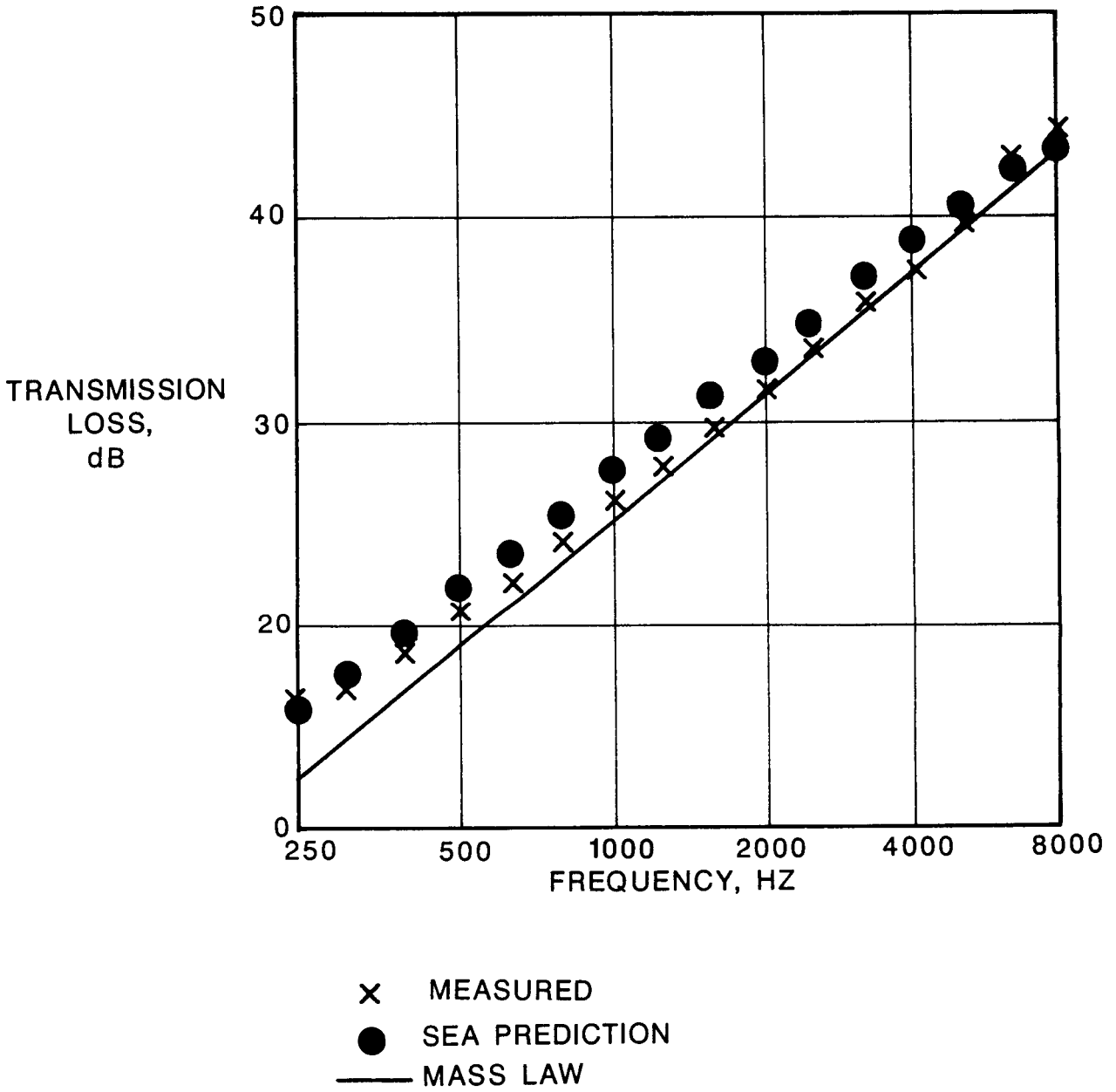

Figure 18. Transmission Loss for a Utility Type Interior Panel.

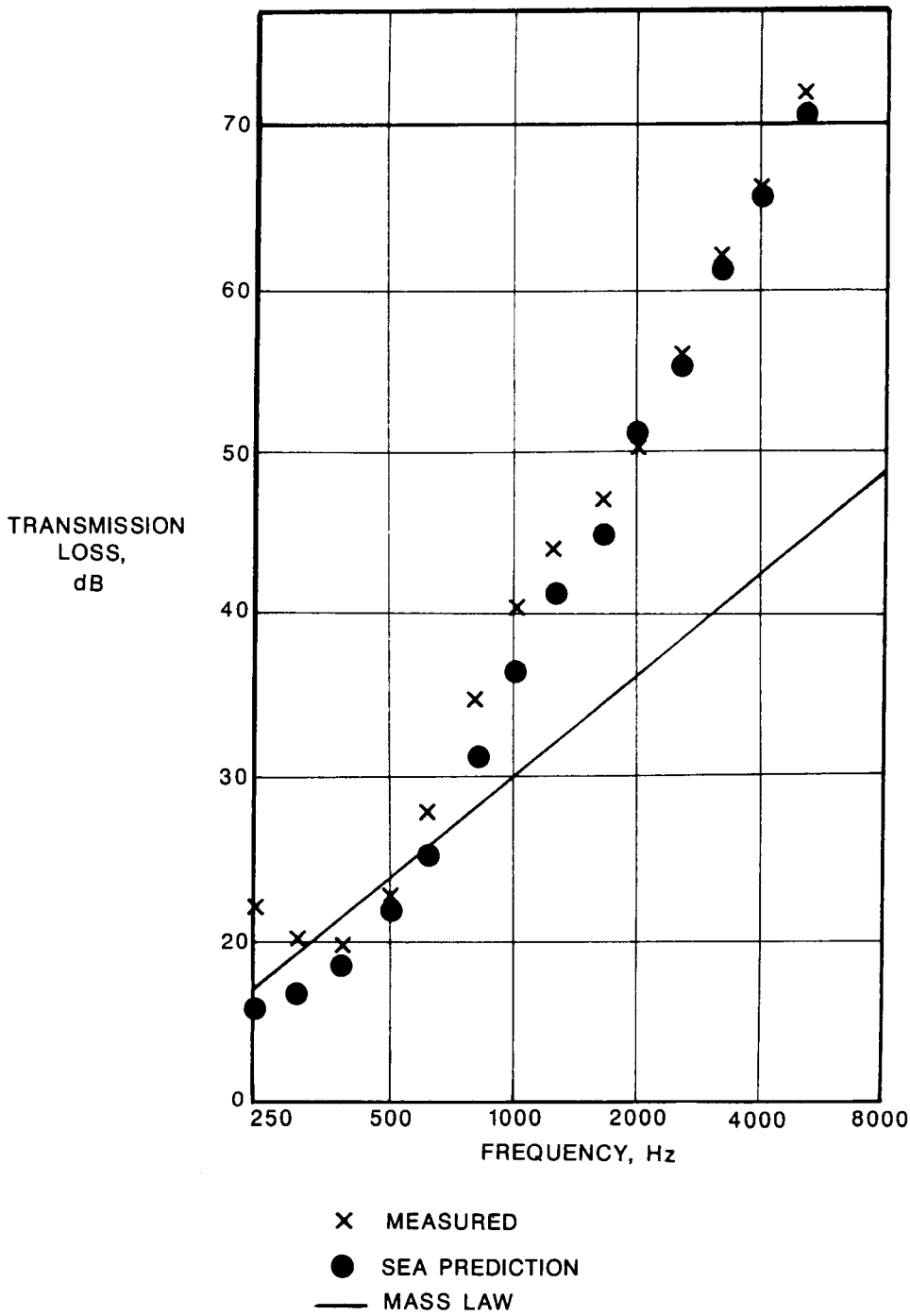

Figure 19. Transmission Loss for an Executive Type Interior Panel.

A simplified SEA model of the VIP panel was developed in order to avoid the additional complexity in modifying the cabin noise model to include the increased number of subsystems required to describe the double wall constructions. The double wall dip in TL is described by introducing panel coincidence for conventional panel bending at the frequency of the double wall resonance. The rapid increase above double wall resonance is achieved by adding a simple distributed stiffness at the area junction between the panel and the adjacent spaces. In qualitative terms the added stiffness accounts for the stiffness of the foam core. Increased panel damping levels also contribute to modeling the rapid increase. No additional SEA subsystems are required to describe the VIP panel when modeled in this fashion. The comparison of the SEA model results and the measured data is good.

A final comparison involved the effects of leakage as a flanking transmission path between adjacent spaces. For the experimental measurements holes, in the form of narrow slits, were cut in the utility trim panel construction. The results in Figure 55 show the adverse effects of leakage in reducing the TL. An otherwise negligibly small leakage area that is .06% of total panel area results in an up to 10dB decrease in TL at higher frequencies.

The SEA model of the experimental setup was augmented to include the transmission through the leakage by adding an area junction equal in area to that of the opening in the panel. In the cabin noise model the leakage area can only be estimated. The SEAM code estimates impedances characterizing the radiation at the opening into the adjacent spaces. The predicted results agree with the measured data at lower frequencies, particularly for the smaller opening. At lower frequency the panel TL is not as great so that transmission through the panel dominates and additional transmission through the opening, which is less frequency sensitive, is not as significant. At higher frequencies the panel TL is greater so that transmission through openings will be of greater consequence.

The SEA model at higher frequencies overpredicts the total transmission, with lesser TL values in comparison with the data. The predictions level out to constant TL consistent with a ray acoustics characterization of the opening where the total transmission at high frequency becomes proportional to the area ratio of the opening to the total panel area.

Sources for the discrepancy may lie with the modeling in not appropriately accounting for geometry effects in the shape of the opening, or possibly, in accounting for flow resistance as the air in the opening oscillates back and forth due to the incident acoustic wave.

Utility interior - Sea predictions of cabin and cavity levels are shown in Figure 22 along with the cabin levels for the bare aircraft. The same arbitrary input power (to the frame section that the gearbox attaches to on the left side) was used for the bare and treated cases without attempting to scale the results for actual flight input levels. An 11 to 18 dB reduction in cabin levels from 500 to 4000 Hz is predicted. This is consistent with differences in flight levels for the Bare and Utility interior aircraft.

As described above, the interior treatment is basically add-on in character and would not be expected to significantly change the vibration transmission in the airframe structure. SEA predictions of frame and skin panel levels confirm this, showing negligible changes (<1 dB) with the addition of the treatment.

However, the trim panels trap acoustic energy radiated by the skin panels and framing, thereby raising the levels in the cavities in comparison with the bare airframe cabin levels. Added acoustic absorption in the cavities is insufficient to significantly limit this buildup of acoustic energy. The overhead cavities are strongly coupled by openings in the frame webbing that allow for the passage of wiring, control cables, etc. As a result the cavity levels are more uniformly distributed throughout the cabin overhead in comparison with the skin panel vibration levels which are the primary source of radiation into the cavities, as shown in Figure 23.

Figure 20a and 21a show the predicted energy of the various cavities and associated skin panels in the overhead region. As expected levels are highest around the input source and generally decrease as the subsystems get further removed. OP14D is misleading as it is a very "thin" cavity (only 1/2").

The increase in acoustic levels in the cavities with the trim panels in place diminishes the panel effectiveness in reducing cabin noise levels. The noise reduction potential of a panel system is dependent on the panel's transmission loss (TL). An independent measurement of trim panel TL was carried out in a reverberant room/anechoic chamber facility. Power transmitted from the reverberent room through the panel was measured using an acoustic intensity probe on the anechoic chamber side of the panel.

The data is compared in Figure 18 with SEA predictions for the experimental setup of a 4.1 kg/m2 panel. The behavior is governed by mass law TL for the frequencies of interest.

In the aircraft leakage around the trim panels can significantly reduce the noise reduction actually achieved if not carefully limited by proper design and installation. Estimates of leakage area were incorporated in the SEA coupling between the cavities and the cabin. Coupling loss factors between cavity and cabin characterizing panel TL and transmission through leakage openings are shown in Figure 24. At 500 Hz transmission through the trim panel is greater than through the leakage openings. The relative contributions are nearly equal near 1000 Hz. Above 1000 Hz leakage contribution dominate due to the increase in panel TL associated with mass law behavior.

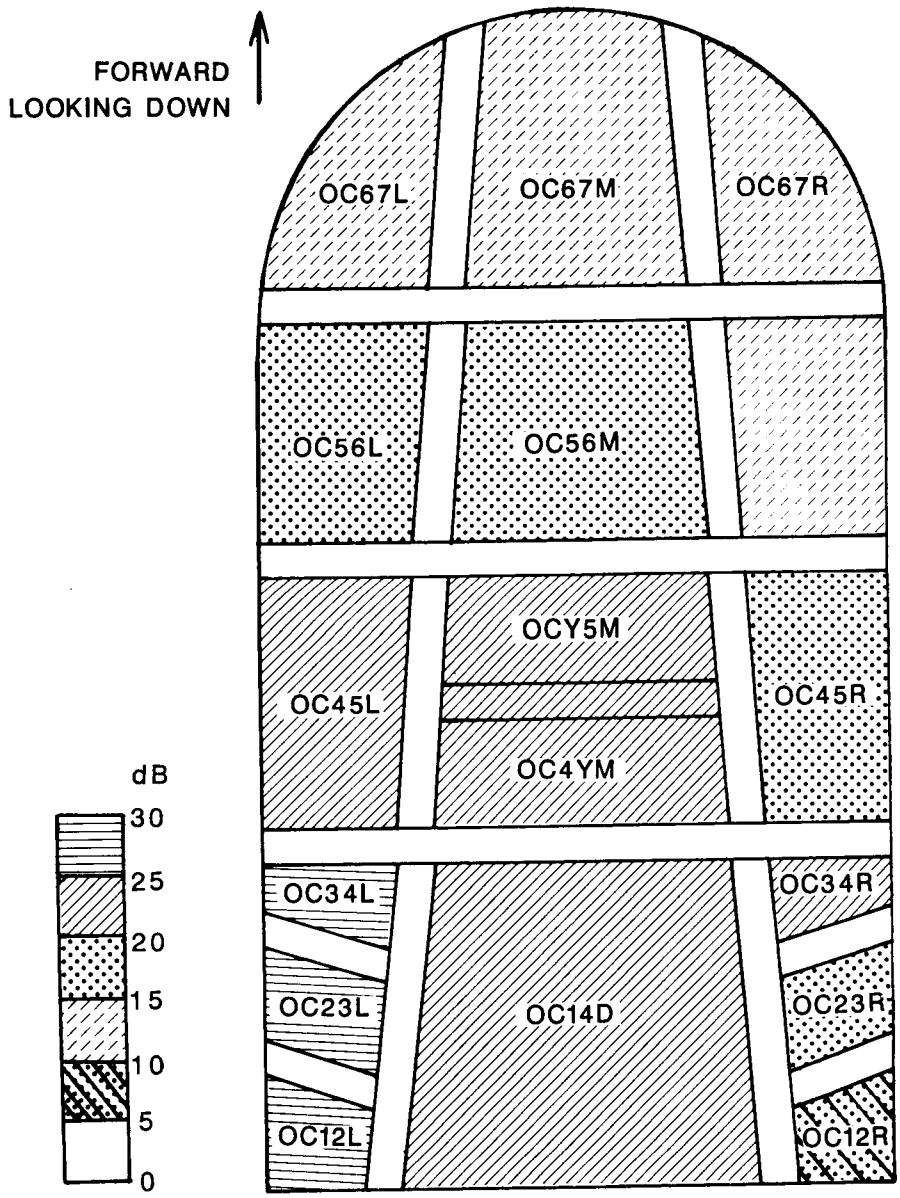

Figure 20a. S-76 Overhead Panel Vibration Levels for Utility Type Interior.

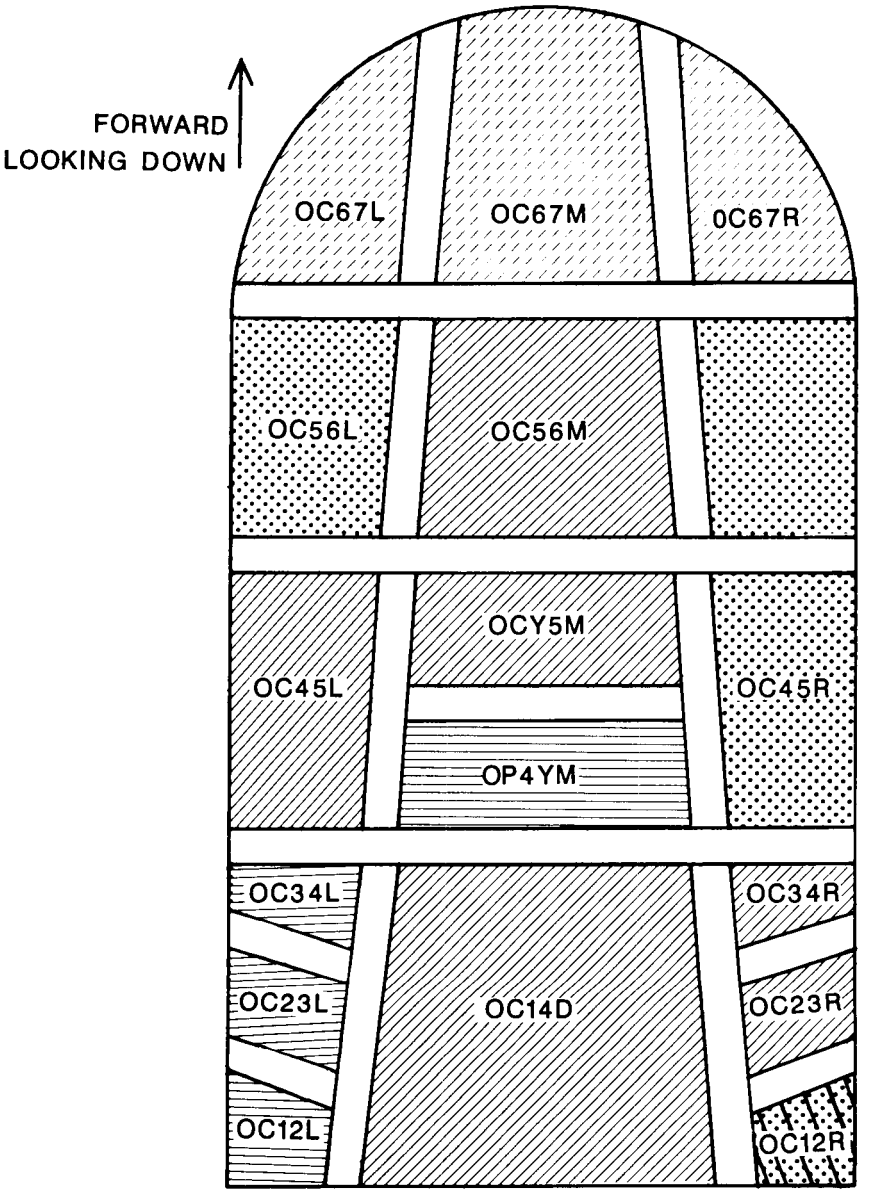

Figure 20b. S-76 Overhead Panel Vibration Levels for Executive Type Interior.

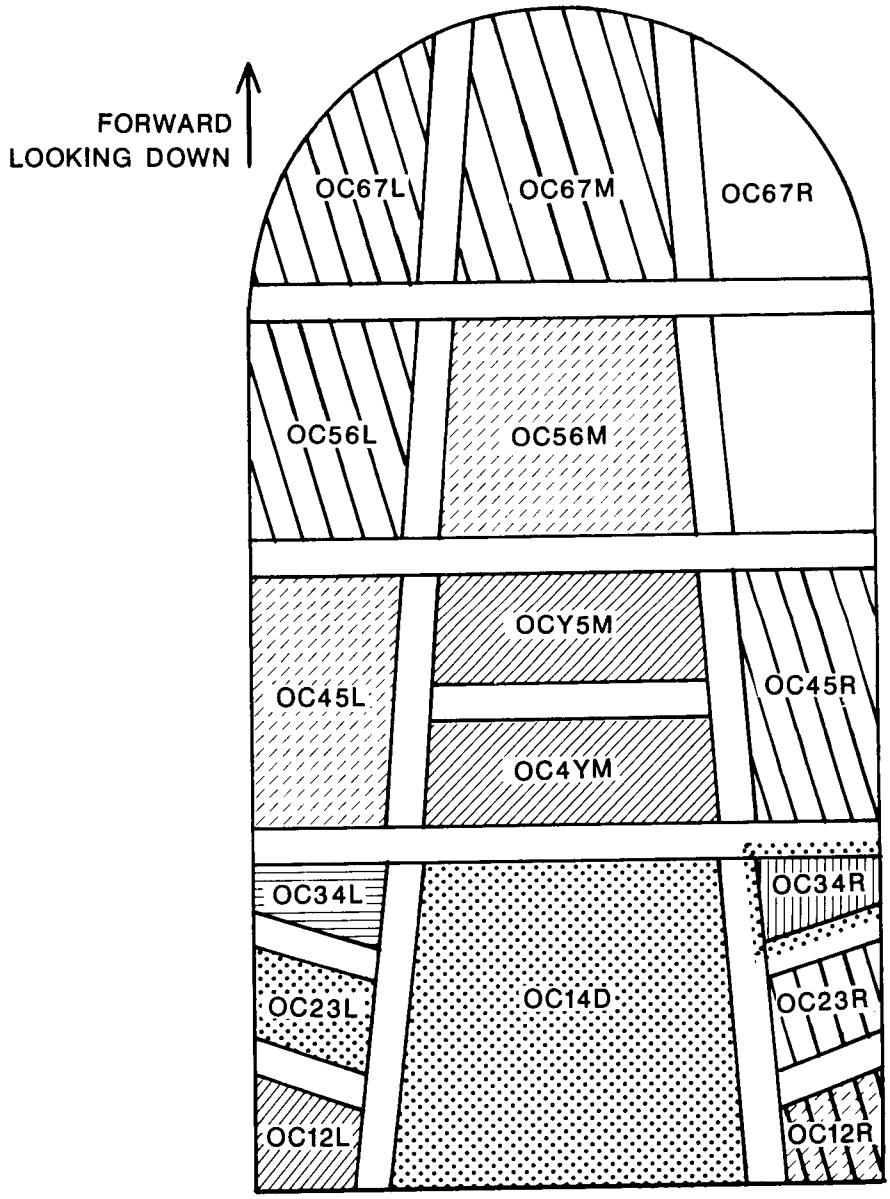

Figure 20c. S-76 Overhead Panel Vibration Levels for Advanced Type Interior.

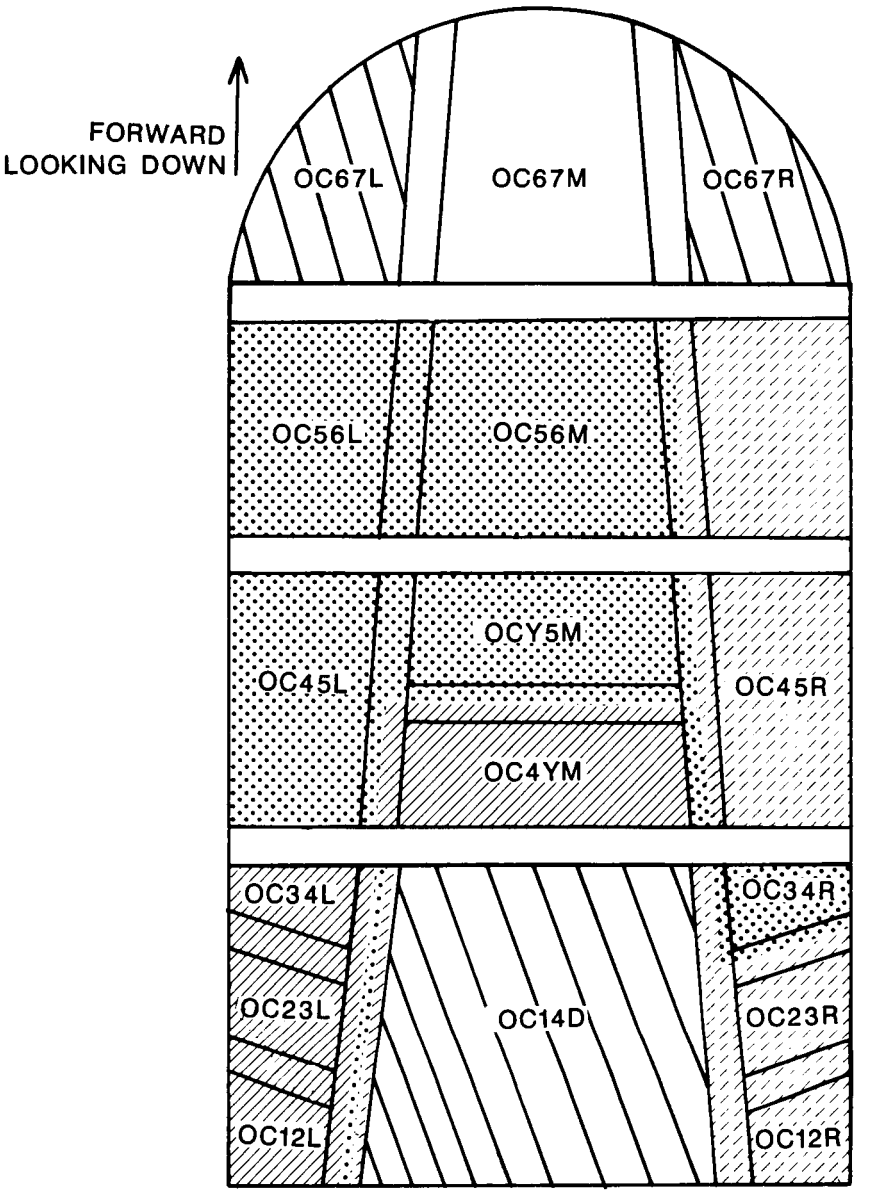

Figure 21a. S-76 Overhead Cavity Levels for Utility Type Interior.

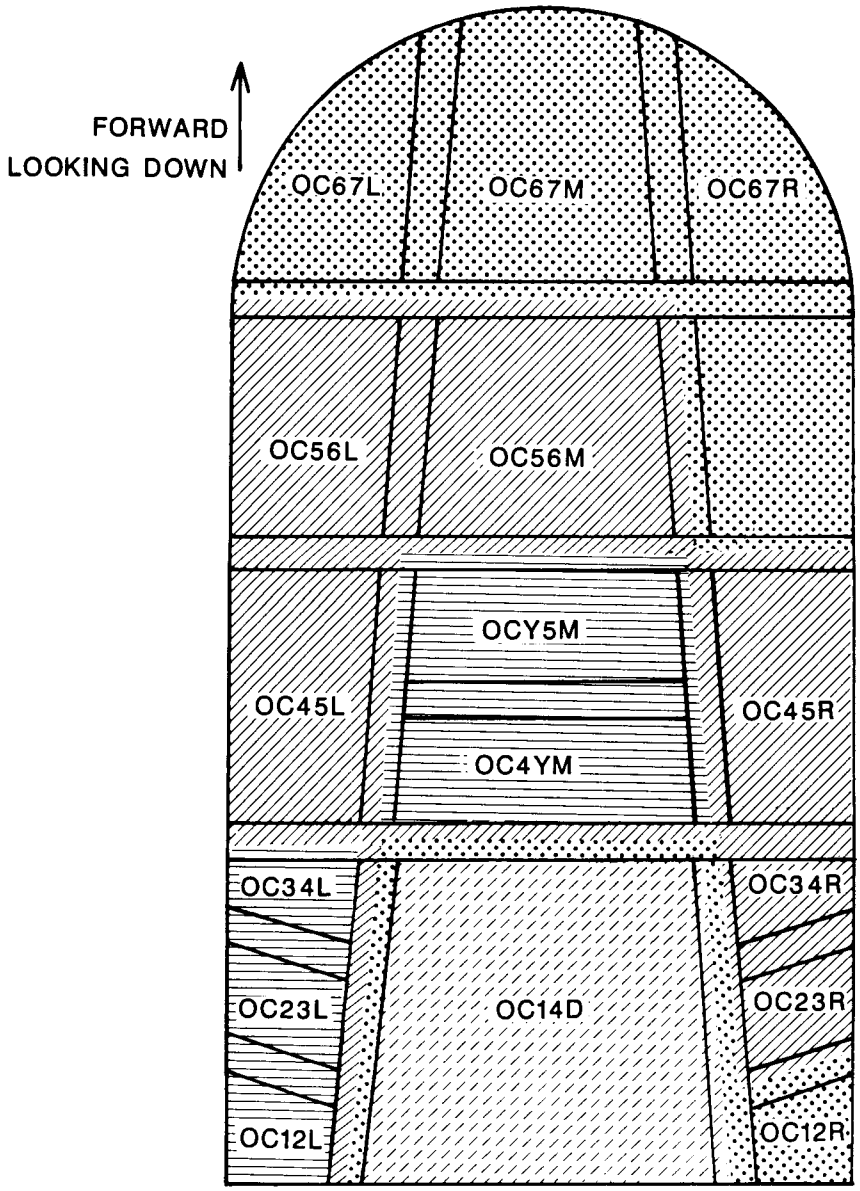

Figure 21b. S-76 Overhead Cavity Levels for Executive Type Interior.

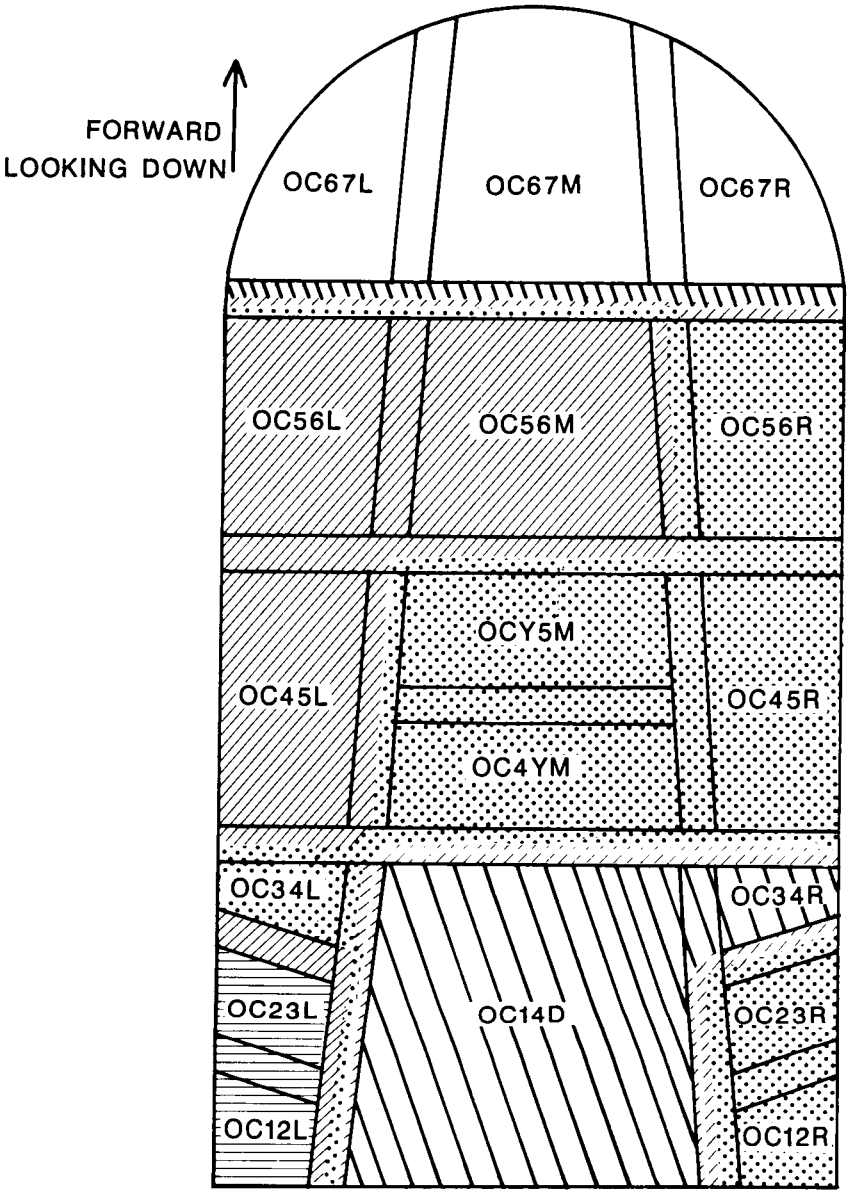

Figure 21c. S-76 Overhead Cavity Levels for Advanced Type Interior

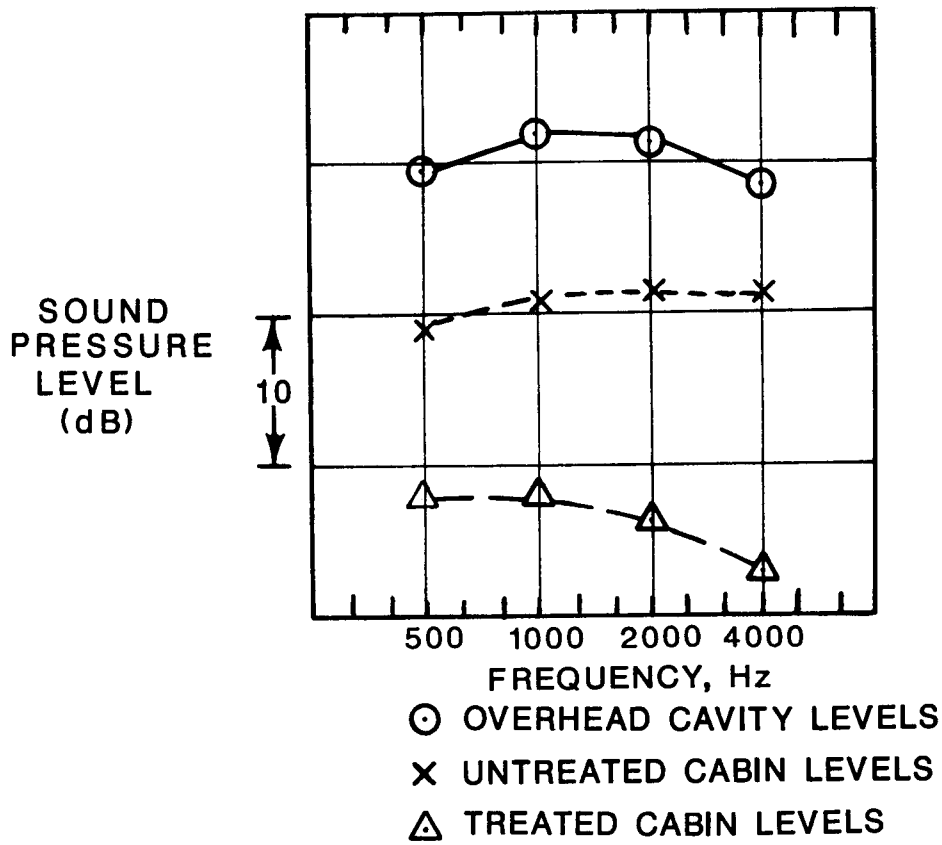

Figure 22. Utility Treatment Effectiveness Relative to Overhead Cavity Levels and Untreated Cabin Levels.

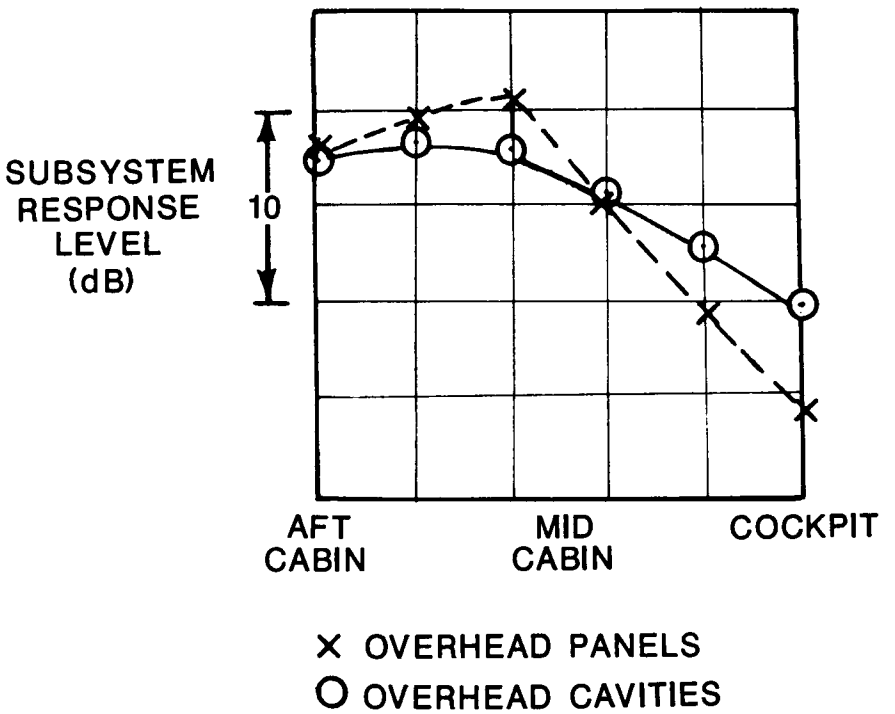

Figure 23. SEA Predictions for the Relative Distribution of Overhead Skin, Panel and Cavity Levels at 1000 Hz.

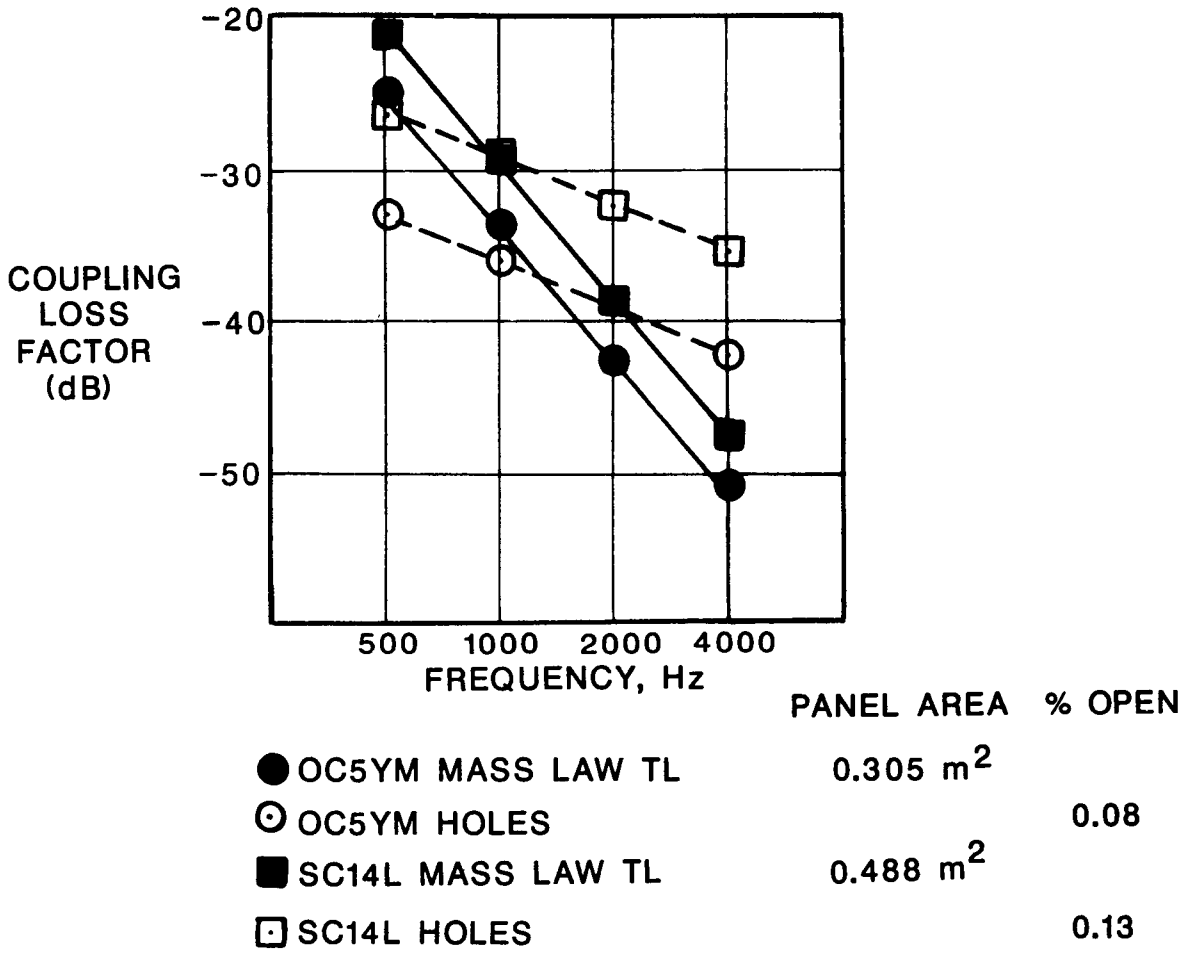

Figure 24. Coupling Loss Factors for Cavities to Cabin Through Panels and Holes (Leakage) for a Utility Type Interior.

As a result, the effects of reducing leakage would be expected to be of somewhat greater significance at higher frequency, as can be seen in Figure 25. A doubling or halving of leakage area for all trim panels produces a 2 to 3 dB change in the cabin level at high frequencies. Completely removing all of the leakage reduces the cabin levels by nearly 10 dB at 4000 Hz, with a diminishing effect at lower frequencies where panel transmission becomes of greater importance. Closing of the air conditioning duct openings into the cabin has a minimal effect for the Utility interior.

The effect of changing cavity absorption, as shown in Figure 26, are also somewhat greater at higher frequency. A factor of 2 increase in the Sabin absorbing area in either the cavities or the cabin produces the same reduction in cabin noise level. Increases in cabin acoustic absorption will not be effective in reducing cabin noise levels unless the loss factor associated with the absorption is comparable to or greater than the coupling loss factor between the cavities and the cabin. Greater coupling between the cavities and the cabin (i.e., TL plus leakage) at lower frequencies reduces the effectiveness of increased cabin absorption.

A comparison of SEA predictions with flight data is shown in Figure 27. The flight data is an average of many typical Utility interior installations (as in Photo 1) in S-76 aircraft. The SEA prediction for 0% leakage is shown only as an indication of the maximum cabin noise reduction potential since, by the nature of its usage, a Utility type interior cannot be sealed that tightly. The measured data are shown to agree well with the expected leakage of approximately 0.08%.

Table 2. Major Contributors to Power Flow into the Cabin* at 1000 Hz

Location	Bare	Utility	Executive
OC23L	13.2	5.2	6.4
OC45L	8.8	9.2	10.2
OC4YM	10.8	8.2	7.8
OCY5M	10.7	11.1	5.9
SC14L	9.9	18.0	14.4
SC56L	3.3	7.3	10.6

Executive interior - The contributors to the cabin level in the Executive model are quite similar to those of the Utility. Energy flow from the overhead cavities accounts for 47.8% of the cabin level. Again SC14L is the greatest single contributor providing 14.4% of the total. Because of the similarity of the treatment models the effect is still negligible on the overhead frames and panels.

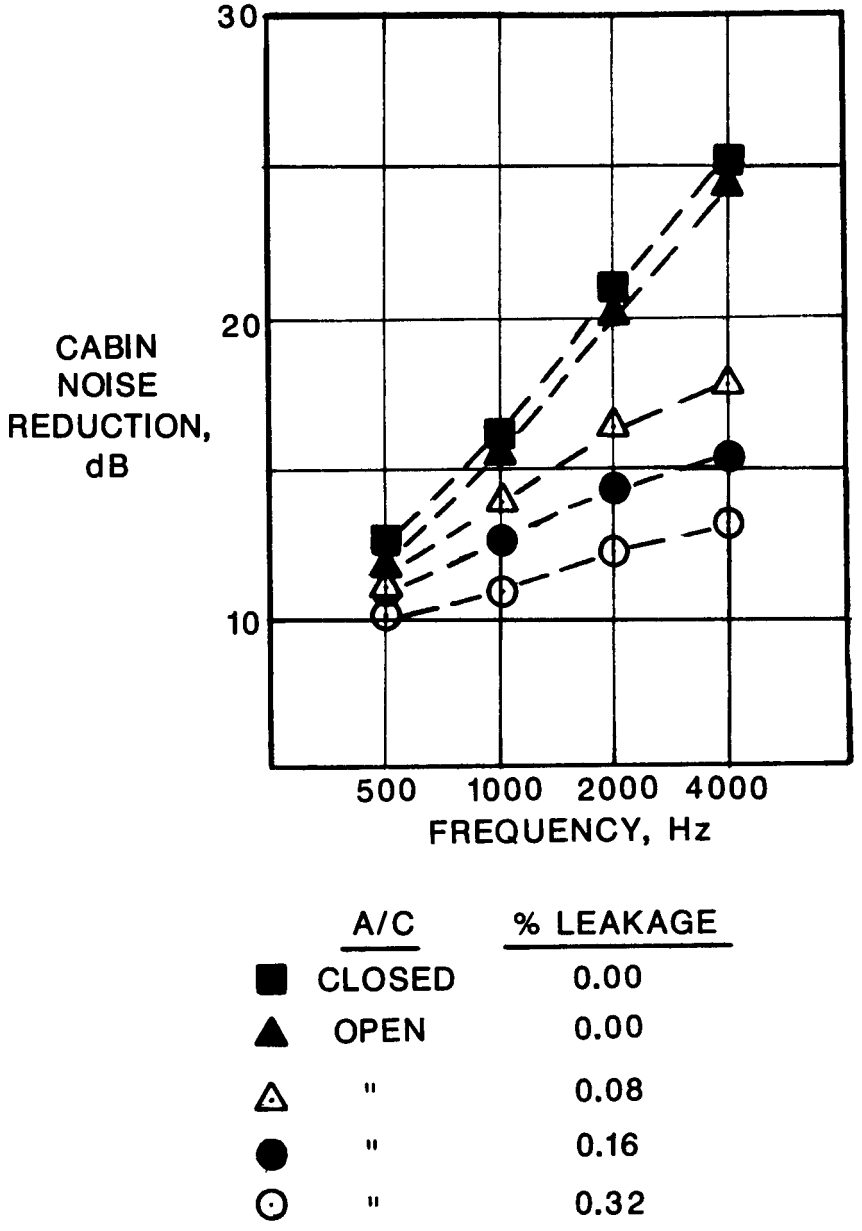

Figure 25. Effect of Air Conditioning Openings and Panel Leakage on the SEA Predictions of a Utility Type Interior.

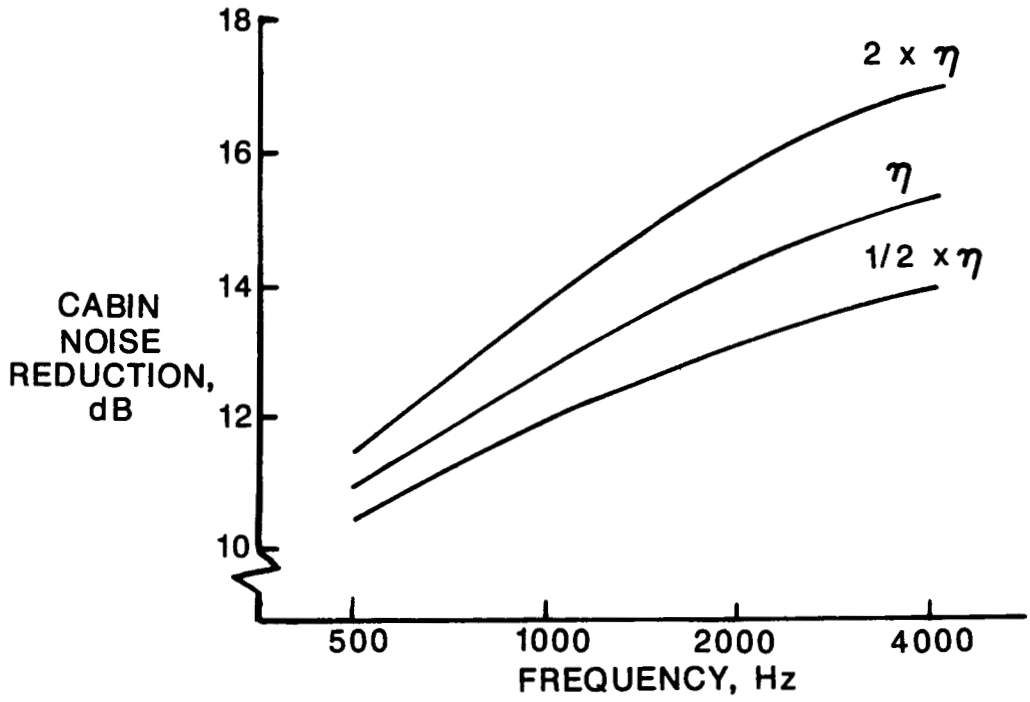

Figure 26. Influence of Cavity Loss Factor on the SEA Predictions of a Utility Type Interior.

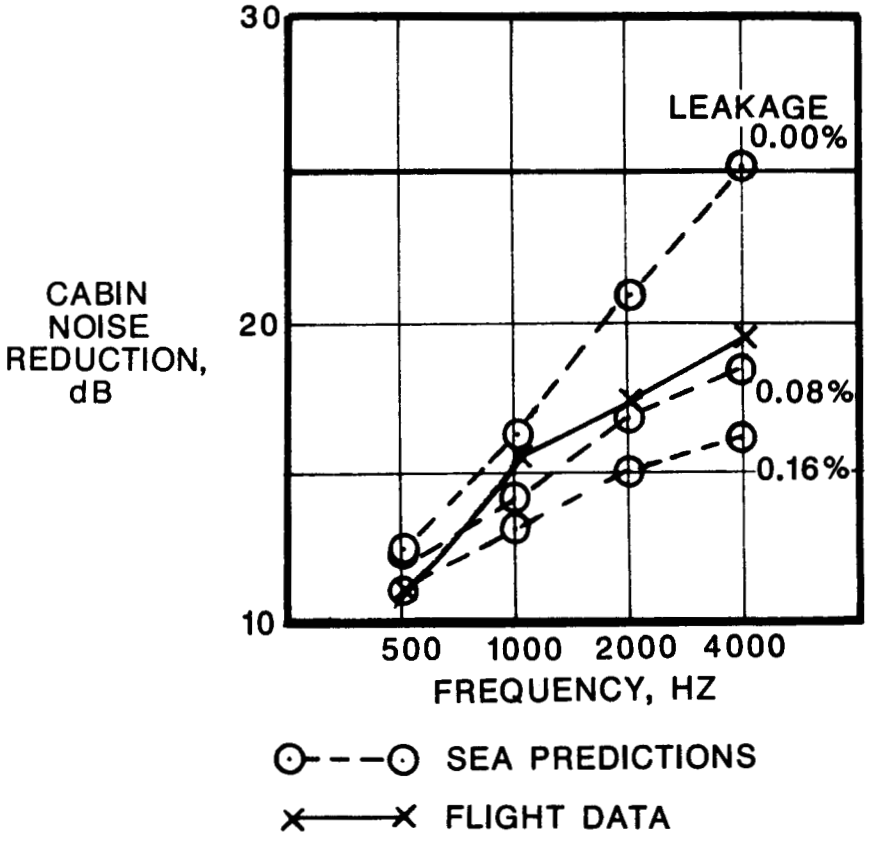

Figure 27. Comparison of the SEA Predictions for a Utility Type Interior With S-76 Flight Data at the Standard Cruise Condition.

The Executive noise control treatment package incorporates an improved trim panel design (7.3 Kg/m2) with greater TL and increased absorption levels in the cavities (up 36%) and the cabin (up 18%). Reduced leakage around the trim panels is also achieved. The distribution of power flow into the cabin is very similar to that for the Utility interior (see Table 2). The power flow from the cavities to the cabin occurs with similar relative contributions but with reduced absolute levels for the Executive interior.

TL data for a typical Executive type trim panel is shown in Figure 19, along with results from the SEA model of this panel. The panel involves a double wall construction with a foam layer between the structural panel and a (lead) vinyl septum. The TL data shows a double wall resonance dip near 315-400 Hz with rapid increases in TL at the rate of 15 dB/octave at higher frequencies.

The improved panel TL behavior results in a greater significance for transmission through leakage openings around the trim panels. Coupling loss factors for panel TL and leakage in the Executive interior are shown in Figure 28. The leakage coupling loss factors are proportional to area. Cavity to cabin coupling through panel transmission is significantly less for the Executive interior than that associated with leakage, particularly at higher frequencies. The SEA predictions show insertion loss values ranging from about 17 dB at 500 Hz to 24 dB at 4000 Hz (see Figure 29).

A comparison of SEA predictions with flight data is shown in Figure 30. Again the flight data is an average of many typical Executive interior installations (as in Photos 2 and 3) in S-76 aircraft. The measured data are in reasonable agreement with the expected leakage in this type interior.

Advanced interior - As mentioned previously, the intent of an Advanced interior was to flight test improvements discovered through use of the model. Unfortunately, aircraft availability was such that the "Advanced" concepts could not be flight tested as a complete set. Many noise control systems have been designed and tested in laboratory conditions with good success but have yet to be installed onto a flight vehicle. Using the laboratory responses, these concepts were applied to the Executive model and a prediction of their effects made.

Measurements were performed on a bare configured S-76 with and without an improved frame and panel damping package applied specifically to those subsystems located near the transmission foot mounts. Loss factors of those subsystems were derived both through rap testing while on the ground and through in-flight measurements. This damping treatment was specifically designed to work in the 1000 Hz region, as this is the critical region of input frequencies from the main gearbox. The effect of damping appears straightforward enough that it could be applied to the advanced Interior treatment with confidence in the results. Verification of this system in an SEA model could not be performed as allowances for updating of the previously used bare model [2] to include improvements in the code used for the present models had not be made.

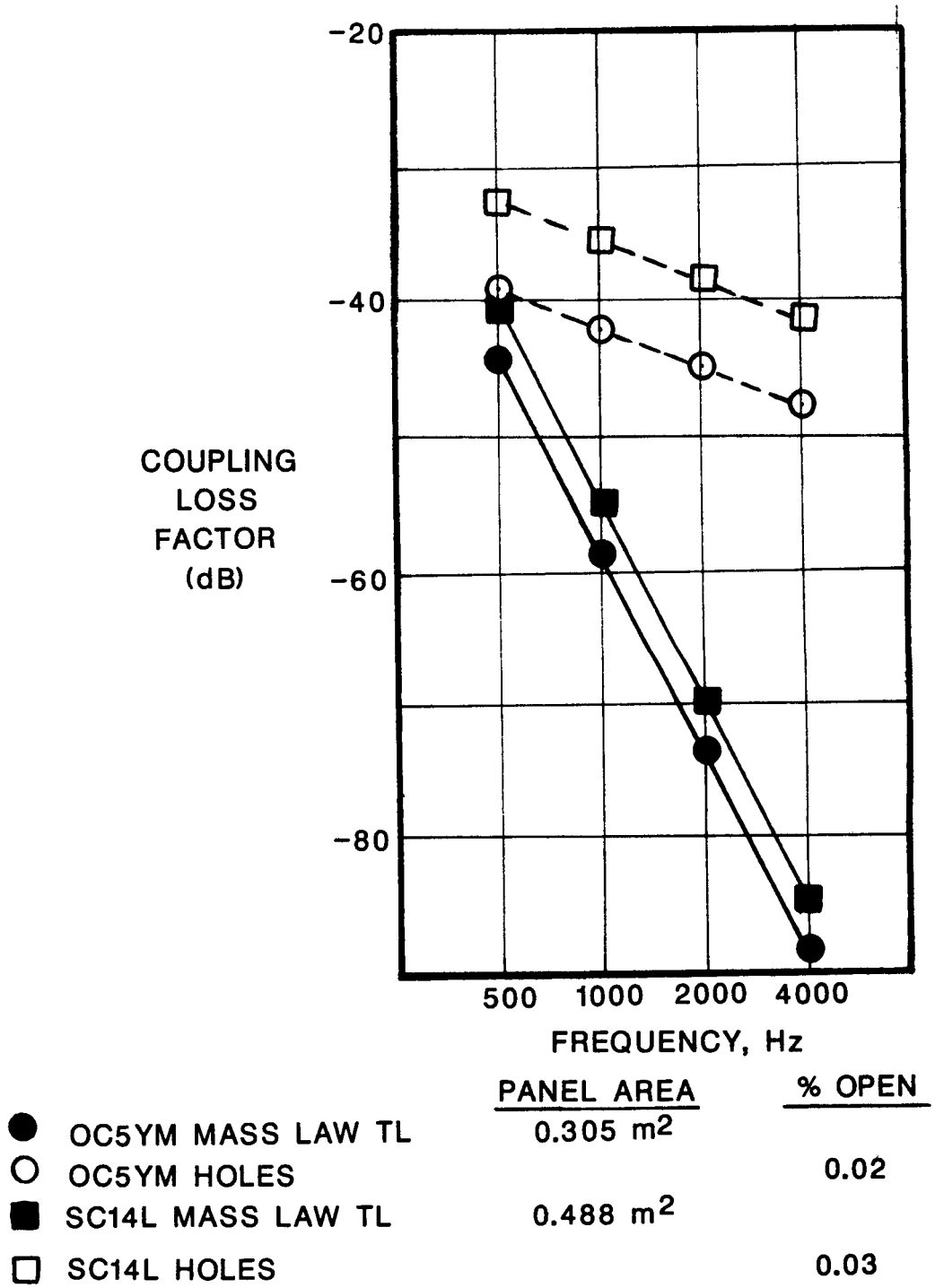

Figure 28. Coupling Loss Factors for Cavities to Cabin Through Panels and Holes (Leakage) for an Executive Type Interior.

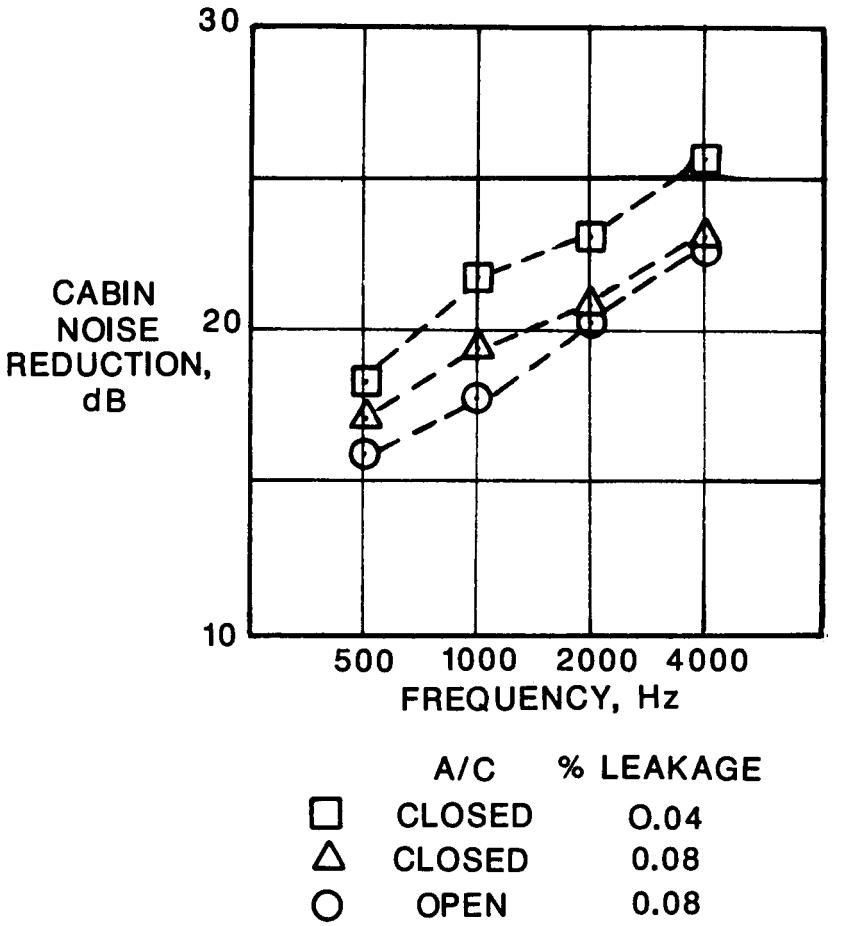

Figure 29. Effect of Air Conditioning Openings and Panel Leakage on the SEA Predictions of an Executive Type Interior.

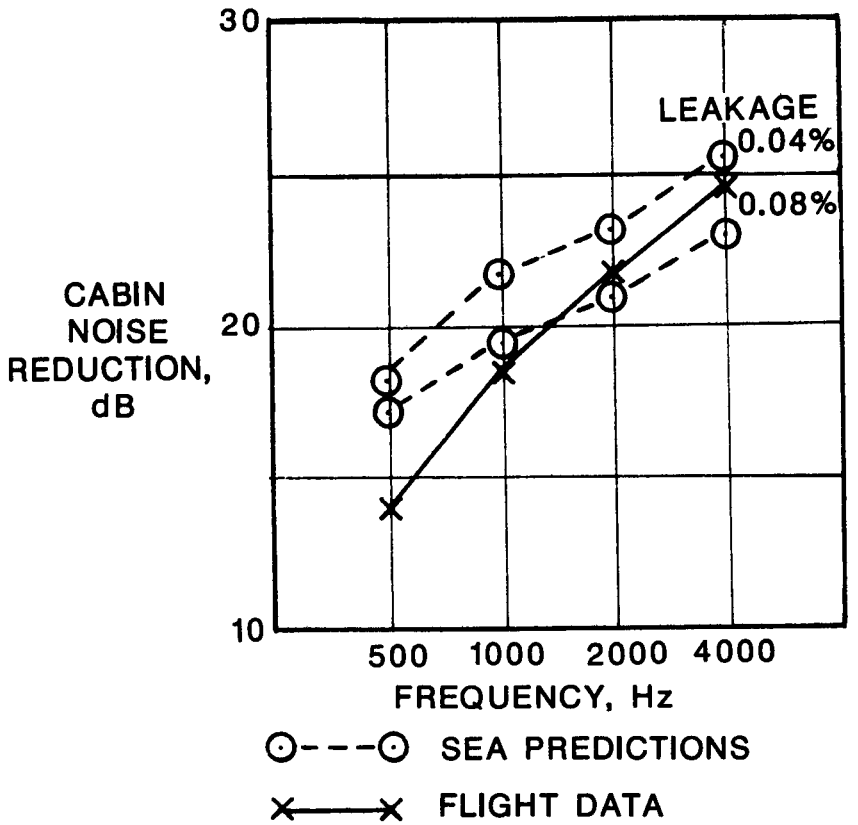

Figure 30. Comparison of the SEA Prediction, for an Executive Type Interior With S-76 Flight Data at the Standard Cruise Condition.

Table 3. Major Contributors to Advanced Cabin* Model at 1000 Hz.

Location	Advanced W/Duct Closed	Advanced W/Duct Open
OC23L	0.2	0.1
OC45L	0.2	0.1
OC4YM	14.6	8.5
OC5YM	11.1	6.4
SC14L	21.7	12.6
SC56L	14.5	8.3
FL	12.0	6.0
DCTC2L	0.0	23.6
DCTC2R	0.0	10.1

*Shown as a percentage of total power flow into the cabin.

For use in the model, those specific frames and panels that were treated when the damping was tested were assigned a new material model with an increased loss factor term as well as specific changes in the subsystem densities and wave speeds.

A low weight, cost, yet effective noise control, is the installment of fibrous glass batting into many of the overhead cavities. As was shown earlier, with the installation of trim panels, build up of noise in the overhead bays increases dramatically. With more control on leakage in the Advanced model, those levels are even greater, as can be seen in Figure 50. By placing glass batting into those bays, noise levels can be lowered, thus decreasing the amount of energy being forced through the areas of leakage.

Some of the effects of the added damping can be seen in Figures 20c and 21c. The damped panels and cavities are much lower in level than their associated utility or executive interior level. Cavities OC34L and R are both surrounded on five sides with damped frames or panel which apparently is the cause for the large decrease in energy. The damping in the frame seems to be the most effective, at least according to the model as seen in the response of cavity OC4YM as the levels here are lower than the next cavity down, OC5YM, apparently due to the frame damping in CF4M.

The results of the Advanced model shows cabin levels down an additional 6 - 8 dB over the Executive model. This would be exceptional if these concepts can be installed into an interior design for full flight testing with comparitive results. So while experimental testing of these noise control concepts and installation into the model seems to indicate positive results, they have yet to be verified as an advancement over our present interior designs.

Because of the increased absorption in the cavities and the improved leakage control, energy flow from the ducts can now be seen to be quite critical. The single largest contributor for the advanced is no longer SC14L at 12.6%, but the main supply duct DCTC2L at 33.6%. Levels from the overhead cavities are down to 16.0% total contribution. Table 3 shows that with the opening of the overhead ducts, all other contributors decrease in significance dramatically as if a dam was opened. The ducts can be shown to be an effective noise block as total cabin energy increases over 2 db by opening them.

Table 4a. Summary of S-76 SEA Model: Bare Interior

Subsection types	Number	# of D.O.F. in SEA Model
panels	53	53
frames	35	70
acoustic spaces	7	7
Totals	95	130
Junction types		
line	99	
area	86	
point	29	
frame	21	
Total	245	

Table 4b. Summary of S-76 SEA Model: Utility Interior

Subsection types	Number	# of D.O.F. in SEA Model
panels	101	101
frames	70	140
in-plane (trim panel isolators)	59	59
acoustic spaces	64	64
pipes	7	7
Totals	301	371
Junction types		
line	154	
area	330	
point	230	
frame	21	
Total	735	

SEA Predictions for the Treated S-76 Cabin

The primary interest in comparing the bare and treated interiors is in relation to the reductions in cabin noise levels that are achieved. The degree of reduction must be compared with the added weight of the total treatments package in assessing its effectiveness. Insights into the vibration and acoustic transmission processes gained from the SEA model can provide insight that are helpful in designing a weight effective treatment. Specifically, regions of high modal energy or response can be targeted for treatment, as well as the important transmission paths by which energy reaches these regions. Output from an SEA model is particularly well suited for identifying contributions to the total cabin noise environment due to particular transmission paths and the immediate panel structures that are the dominate radiators into the cabin.

An important question is the degree to which the treatments affect the transmission in the basic airframe structure, if at all. The utility treatments are primarily of the transmission type; trim panels "block" the radiation of noise from the skin panels, preventing it from reaching the cabin, directly. Connected to the airframe structure by soft isolation mounts; they are not expected to mechanically load the frames or panels from which they are supported to any significant degree. There is the possibility that by preventing the noise from radiating directly into the cabin, thereby resulting in a buildup of noise levels in the acoustic spaces between the skin and trim panels, the higher acoustic levels will mean increased panel vibration levels. Frames, which feed energy to the skin panels, would not be expected to show as noticeable an increase as the panels because they are an additional connection removed from the cavity acoustic spaces and are therefore less sensitive to the increased noise levels adjacent to the panels.

The preliminary results in Figures 31 and 32 show a trend that is counter to this argument, namely, that the frame and panel levels moving forward in the cabin away from the gearbox location are higher in the bare cabin than in the treated cabin. Panel levels adjacent to the gearbox are more closely comparable. The frames, as expected, show less of a difference between the two configurations. Acoustic levels in the cavities immediately beneath the forward skin panels, shown in Figure 33, are significantly greater than the cabin noise levels in the bare configuration consistent with expectations. Cavity levels adjacent to the gearbox are inexplicably less than the cabin levels in the bare configuration.

The apparent anomalies in the comparisons between bare and treated interior predictions are currently being investigated. The junctions describing the connections for these subsystems are currently being reviewed as to their accuracy.

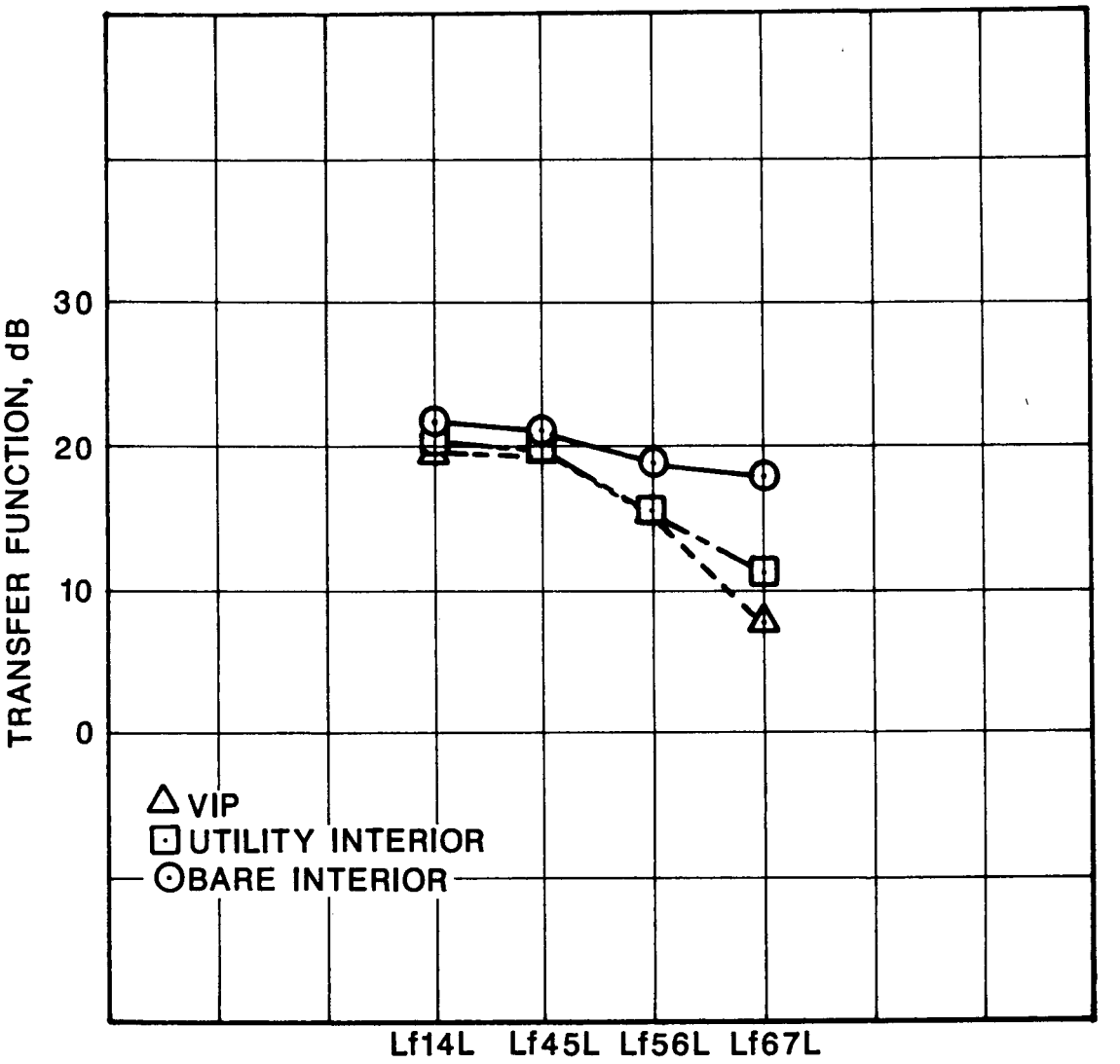

Figure 31. S-76 Frame Transfer Function Levels.

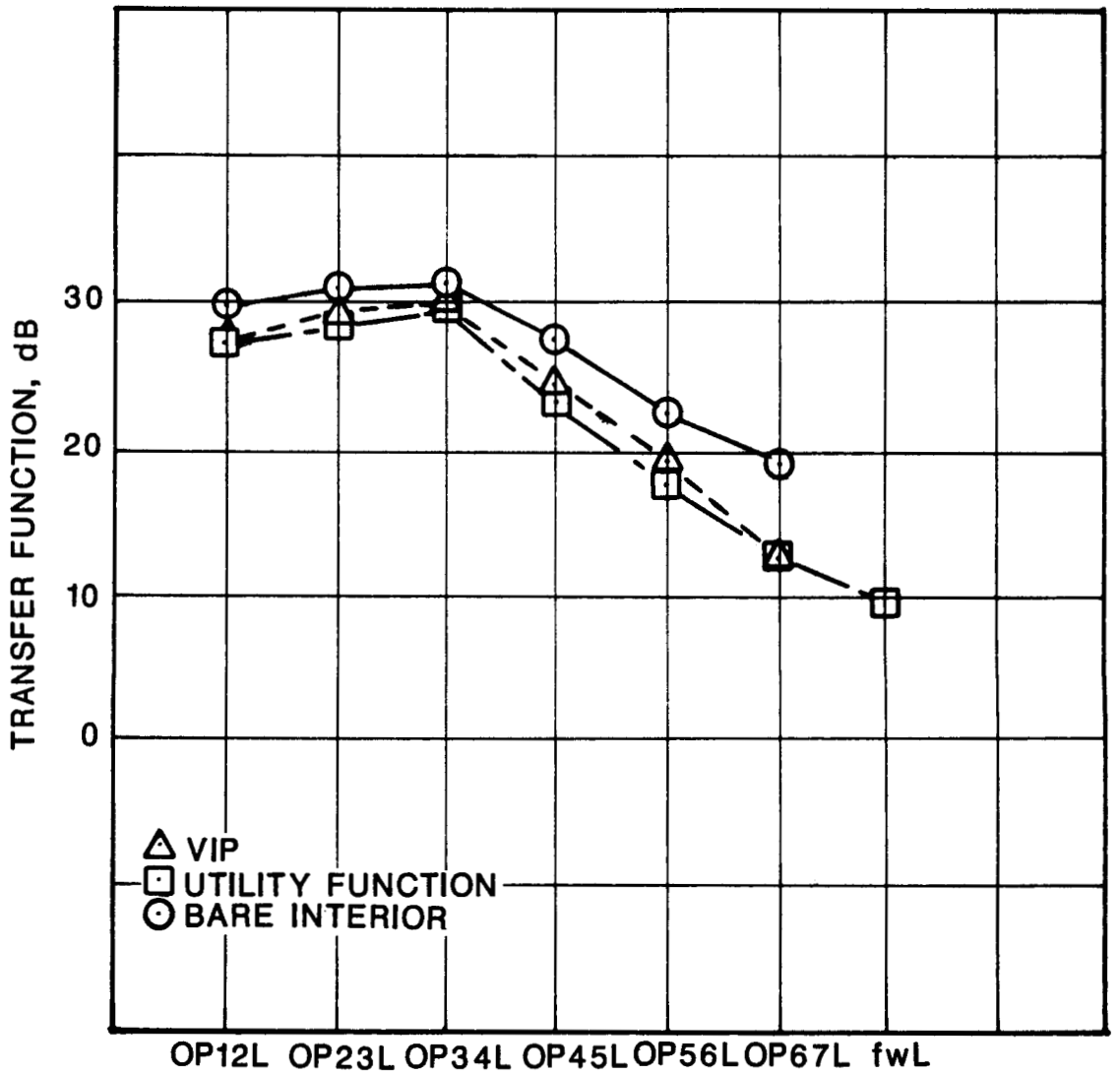

Figure 32. S-76 Skin Panel Transfer Function Levels.

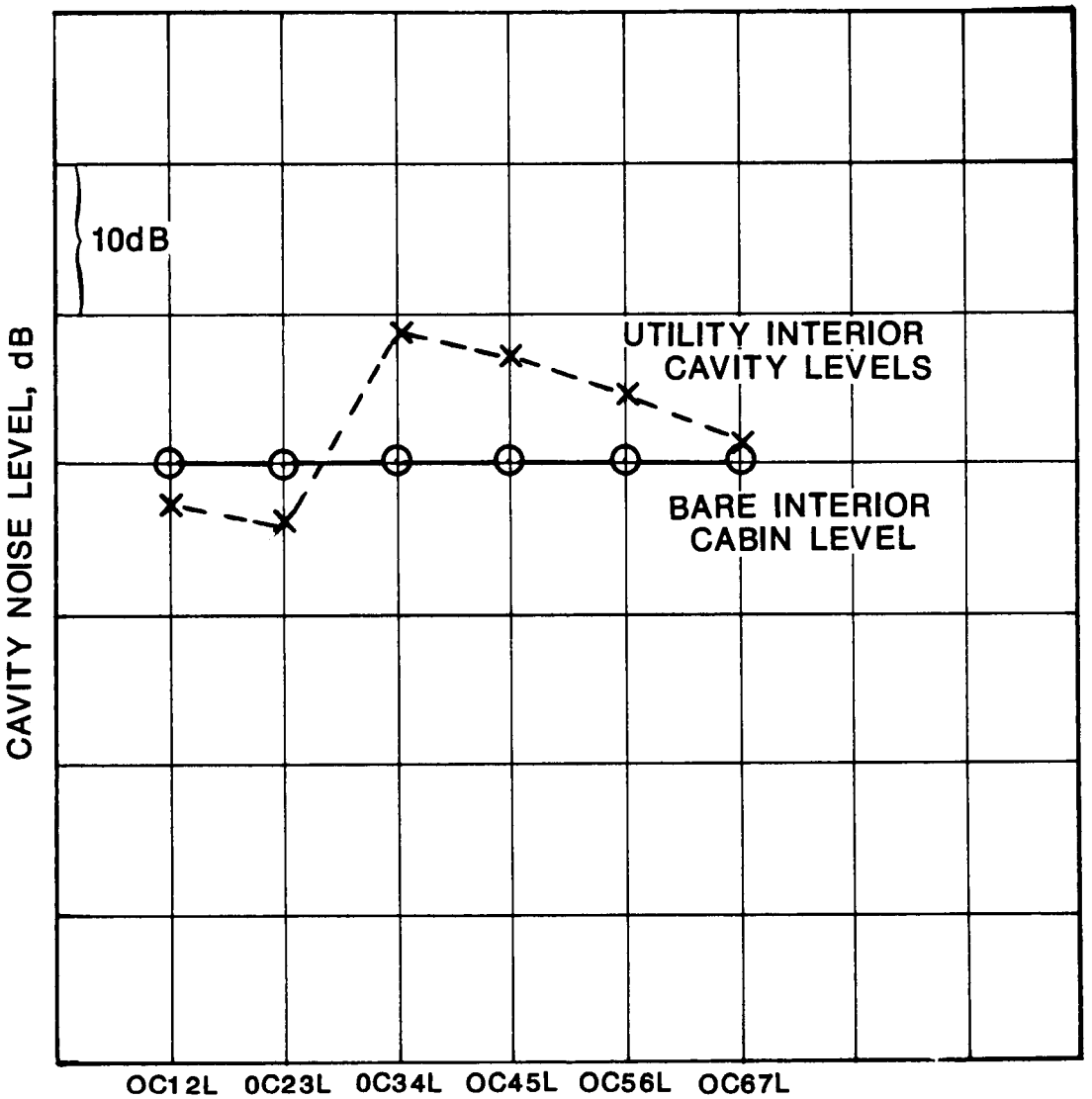

Figure 33. S-76 Overhead Cavity Noise Levels.

C-2

Predicted cabin acoustic levels for the bare and treated configurations are shown in Figure 34 as a function of frequency. The levels are scaled relative to the same arbitrary input power which does not correspond to actual input source levels for either an in-flight measurement or a ground test with shaker excitation. The predictions with the utility treatment are from 4-5 dB less in the lower frequency octave bands and from 9-10 dB less at 2 and 4 kHz. These differences are not as great as expected based on actual measurements on bare and treated aircraft and would suggest that a further review of the SEA model is needed.

Power Flow Description of Transmission Paths - The principal effect of the treatments in the utility interior is to block direct skin panel radiation into the cabin by the addition of trim panels. The VIP interior adds damping to panels and absorption to the cavity and cabin spaces to control the levels of these subsystems. An important consideration for the treated interiors is whether the treatments change fundamentally the mix of important contributors to the cabin noise environment or whether all are reduced in comparable fashion. Identifying possible flanking transmission paths that limit the actual effectiveness of the treatments is also important in assessing their performance.

Flanking transmission can occur due to gaps or holes in mounting the trim panels or through the isolation mounts that support them. The areas of these gaps and/or holes would need to be included in the SEA model in order to account for acoustic transmission through them. The predictions would serve to quantify the point where they are significant in increasing the cabin noise levels, thereby establishing a criteria for quality control in the installation of the treatment.

A similar assessment can be made with respect to the performance of the isolation mounts supporting the trim panels. Frame or skin panel vibration on the top of the mount is transmitted through to the trim panel where the resonant response of the trim results in a radiation into the cabin. The point attachment to the trim panel results in a nearfield vibration response that also radiates into the cabin. The significance of the contribution through the mount will indicate whether it is sufficiently soft in relation to the structures it connects.

Power flow contributions into the cabin are given in Table 2. Cavities are directly coupled to the cabin through leakage around and mass law transmission through the trim panels. Overhead cavities account for 53% of the total power flow into the cabin with the more important contributions coming from cavities closer to the excited frame section. The Table 2 data show that the distribution of contributions to the cabin noise level does not fundamentally differ from that for the bare aircraft.

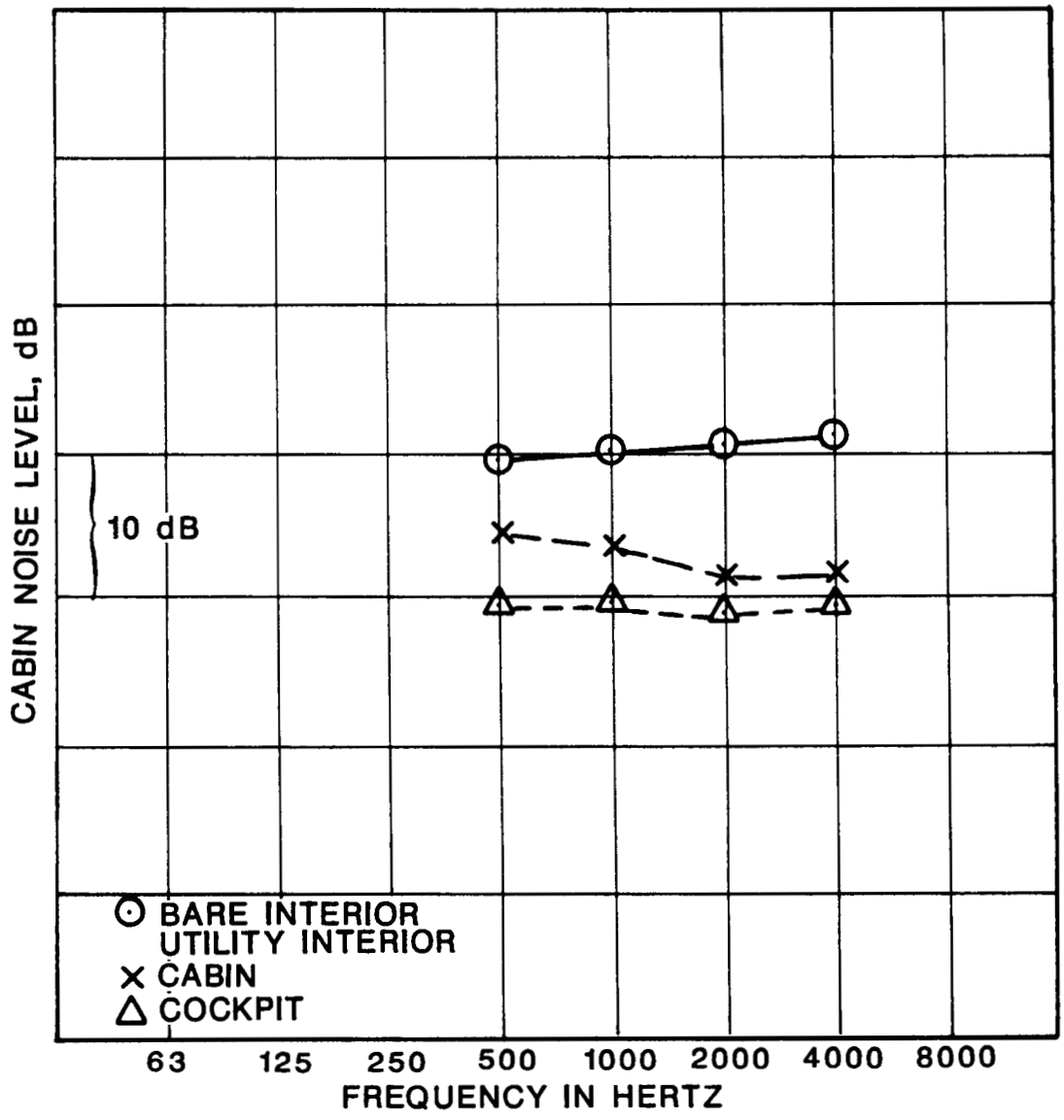

Figure 34. S-76 Cabin Noise Levels.

The aft side cavity is the single largest contributor to the cabin noise level. It receives essentially all of its power (98.6%) from the side skin panel. The power flow into the side panel from the side wall frame is 62% of its total power. This side wall frame is a primary structural member down the side of the cabin which connects to, and receives 100% of its power flow from, an overhead cross-frame just forward of the gearbox. Vibration transmission is strong along this important mechanical load path.

Cavities near the gearbox receive power from the overhead skin panels. Further from the gearbox, contributions from adjacent cavities closer to the gearbox grow in importance relative to skin panel radiation. The furthest forward cavity receives nearly all of its power from the adjacent "upstream" cavity.

The power flow contributions for a typical cavity acoustic space are shown in Table 5. The dominate contributor is the outer skin panel above the cavity, with important contributions from adjacent cavities that are closer to the source. Transmission from an adjacent cavity is related to mass law transmission through the web of the intervening frame or through openings in the web.

The power flow path from the forward overhead skin panel, OP67L, back to the source frame section is shown in Table 6. The transmission behavior in the underlying airframe structure is the same as in the untreated S-76. The path leads to adjacent frame members and along the main longitudinal frames to the source frame section.

*Shown as percentage of total power flow into the cabin for the particular configuration described.

Table 5. Power Flow Description for an Overhead Cavity (OC56L)

Power Inflow From:	Percent of Total Inflow
OP56L	69.2%
OC45L	30.0%
OC56M	0.7%

Table 6. Power Flow Path Description for the Utility Interior Cabin Overhead for LF14LO Vibratory Input

Power Inflow for OP67L, from:	Percent of Total Inflow
LF67LO	48.9%
CF6LO	23.3%
OP56L	15.7%
CF6LI	6.3%
Power Inflow for LF67LO, from:	
LF56LO	67.4%
CF6MO	13.7%
CF6LO	9.5%
CF6MI	6.5%
Power Inflow for LF67LO, from:	
LF45LO	100.0%
Power Inflow for LF45LO, from:	
LF14LO	98.6%

ISOLATION AS AN ALTERNATE NOISE CONTROL CONCEPT

Gearbox Isolation Mounts

The design of isolation mounts at the attachment location of the gearbox to the airframe offers the possibility of potentially significant reductions in the cabin noise environment. Mounts are a transmission type treatment which are used most effectively when located as close to the source as possible; a condition satisfied by gearbox isolation mounts. This section discusses the modeling of mount dynamics, accounting for the impedance characteristics of the gearbox and airframe structures at the location where they are attached through the mount.

An important presumption made in describing mount behavior is that motions or forces at the attachment points and in the different directions can be treated as being statistically independent or uncorrelated. This greatly simplifies impedance representations of gearbox and airframe behavior. The measured effects of source coherence which are described in the Phase II report [2], lend credibility to this presumption.

Individual motions at an attachment location involve a single pair of generalized force and velocity variables. The structural connection is presumed to occur at a point. The gearbox is modeled as the source and the airframe as the receiving structure into which power flows.

The source description of the gearbox is idealized in terms of an open circuit or free velocity, $V_{g,i}^{free}$, where the subscript i refers to the different attachment locations and directions of motion. Treating the gearbox as a linear time invariant system with internal sources at gear mesh locations, the free velocity is that which would occur at the gearbox attachment location when the internal sources are active and the gearbox has been detached from the airframe. This description is an idealization since a measurement under such conditions is an impossibility. It is convenient from a modeling point of view because the source description does not depend on the dynamics of the structure to which the gearbox is attached.

In the attached condition the force and velocity at the connection are related to the free velocity source levels according to:

$$V_{g,i} = Y_{g,i} F_i + V_{g,i}^{free} \tag{50}$$

Where $Y_{g,i}$ is the input mobility, i.e., the ratio of velocity to force, looking into the gearbox at the attachment location with the internal sources turned off. The airframe dynamics are also described by:

$$V_{a,i} = Y_{a,i} F_i \tag{51}$$

Without the mount $V_{g,i} = -V_{a,i}$ so that the velocity of the airframe is:

$$V_{a,i} = \frac{-Y_{a,i}}{Y_{a,i} + Y_{g,i}} V_{g,i}^{free} \tag{52}$$

The reduction of airframe motion at the attachment location which occurs as a result of the addition of an isolation mount is of particular interest. The mount connects on one side to the gearbox and on the other to the airframe. It is described by two force/velocity pairs of variables:

$$\begin{matrix} F_{g,i} \\ F_{a,i} \end{matrix} = \begin{matrix} Z_{11} & -Z_{12} \\ Z_{12} & -Z_{22} \end{matrix} \begin{matrix} -V_{g,i} \\ V_{a,i} \end{matrix} \tag{53}$$

Combining the above impedance matrix description of the mount with the descriptions for the gearbox and airframe an expression is obtained for the ratio of airframe attachment location velocities in the case with the mount, $V^m_{a,i}$, to that without the mount, $V_{a,i}$, as follows:

$$\frac{V^m_{a,i}}{V_{a,i}} = \frac{(Y_a + Y_g)\ Z_{12}}{(1 + Y_g Z_{11})(1 + Y_a Z_{22}) - Y_g Y_a Z_{12}^2} \tag{54}$$

When the mount behaves as a lightweight simple spring, then $Z_m = Z_{11} = Z_{22} = Z_{12}$ and the expression takes on the following simple form:

$$\frac{V^m_{a,i}}{V_{a,i}} = \frac{1}{1 + \frac{1}{Z_m (Y_a + Y_g)}} = \frac{1}{1 + \frac{Y_m}{Y_a + Y_g}} \tag{55}$$

Where Z_m is the stiffness reactance of the mount and Y_m is a mobility for the mount: $Y_m = 1/Z_m$.

When the mount is rigid compared to either the airframe or gearbox, i.e., when $Y_m << Y_a$ or $Y_m << Y_g$, then the mount has no effect in reducing the airframe vibration. This points out an important feature when stated as a criteria on mount stiffness in order to obtain significant reductions; namely, that the mount must be soft compared to the softer of either the airframe or gearbox.

For given airframe and gearbox structures the inclusion of a mount will result in a reduction in the power flow from the gearbox by the following amount:

$$\Delta\Pi = 10 \log_{10} \frac{1}{\left|1 + \frac{Y_m}{Y_a + Y_g}\right|^2} \quad \text{dB} \tag{56}$$

This is also the anticipated reduction in airframe response and cabin noise levels.

This evaluation depends on separate estimations of mount, airframe and gearbox impedance characteristics. Depending on frequency, the mount can often be modeled as a simple spring stiffness, including the effects of cross-sectional geometry. At higher frequencies transmission line models of mount impedances can be developed.

When many internal mount resonances are excited, an SEA model of the mount provides accurate statistical estimates of mean or average mount behavior. This applies also to the airframe structure where a statistical representation of attachment point impedance behavior depends on the motion type and details of the construction, for instance, whether the attachment is at a mid-point location along a frame member or at the intersection or junction of several such frame members.

The evaluation of power flow reduction in Equation (56) can be carried out separately from the SEA model of airframe vibration transmission and cabin noise. Experimental measurements of structural impedances for the airframe and gearbox with shakers and force gages can be combined with estimates of mount behavior as modeled analytically or measured experimentally. The estimated reductions in power flow apply directly to predictions of vibration transmission and cabin noise response levels from the SEA model.

Preliminary Design Definition

Physical constraints - Installation of compliant elements between the main gearbox and the S-76 airframe requires that certain analyses be performed to determine their effect on various aircraft systems, and safety. These include spatial envelope, failsafe design, and allowable static and transient maneuver motion between transmission and airframe. Physical size limitations and ease of retrofit must also be considered.

The spatial envelope considered is bordered by the height of the main longitudinal beams, and the flange width of the same, which are approximately 8 and 3 inches respectively. Given the elastomeric properties and loading information, a preliminary design can be developed. This appears in Figure 35. It basically consists of two "hat" style units configured end to end and through bolted to the transmission foot. This design provides the redundancy needed in case of elastomer failure, as well as high loading capabilities in the vertical direction needed to handle maximum maneuver loading. Safety considerations dictate the configuration of the encapsulation of the elastomer such that its failure precludes catastrophe. Static, transient maneuver and dynamic loadings define an envelope of practical designs. Maximum maneuver loading for this aircraft occur at the right front attachment location, where ~14000 lb. limit tension load vertical is encountered during symmetrical dive and pullout, with ~8000 lb. compression limit load at the left rear attachment in the vertical direction during a rolling pullout.

Dynamic 1 per rev and 4 per rev rotor forces must also be considered for fatigue analysis and change in airframe response from the non-isolated to the isolated configuration. Normal modes analysis was performed on the af/gearbox system in both conditions with spring rates of 20000 lb/in vertical, 110000 lb/in radial at each attachment, and twice more using 1.5 and 2 times these values. This was performed utilizing available finite element model for the S-76 to ensure that the vibratory response of the airframe was not detrimentally affected at these forcing frequencies. Hub loads measured at 4/rev during full scale wind tunnel testing are as high as ~900 lbs. vertical shearing force and 12000 in-lb yaw moment during 150 knot forward flight. A more detailed analysis of the fatigue characteristics of this installation will be performed for validation, using these figures as conservative estimates of actual loading.

Various mechanical components that have attachment on both the airframe and gearbox must be studied so that an increase in relative motion between the gearbox and airframe does not hinder their performance. These include fligh control rods, input power shafts and power takeoff items such as the tail takeoff from the main gearbox. The minimum stiffness requirement lies in the allowable values of error or misalignment for the control system and rotating shafting.

The controls system has mounting locations for control rod pivots on both the airframe and gearbox from the controls deck, on the outboard side of OP4-6M, and the collective and cyclic pitch actuators mounted on the upper housing of the main gearbox. Relative motion here induces error into the flight control system, which must be kept to less than 0.1 degree resultant pitch change, collective or cyclic. A NASTRAN static analysis of airframe/main gearbox installation with and without isolators installed was performed to approximate any added error that might be induced. Relative motion of grids adjacent to each end of each control rod with static and maneuver loading conditions applied is tracked, and resultant error calculated. Analysis of deflection between these components has shown that stiffnesses of 132000 lb/in vertical and 66000 lb/in radial at each attachment location provide control system error within allowable limits.

Rotating components connecting between the airframe and main gearbox include engine input power shafts and tail driveshaft. These components are mounted via flexible couplings designed to encounter a certain amount of misalignment under normal operating conditions, and provide either a limit isolator stiffness criteria or the need to handle more misalignment via redesign of coupling/shaft arrangements. The possibility of tandem installation is a feasible alternate approach

Shape and size effects - The shape, size, and encapsulement configuration of any given elastomer defines an isolators stiffness characteristics. Design equations for elastomeric springs along with properties of candidate elastomers are used for the final sizing of the units [Ref. 10]. Figure shows the preliminary design shape, with pertinent dimensions labeled.

For radial loading,

$$k_y = k_{1_y} + k_{2_y}$$

where k represents stiffness for each element. The top section, in bulk shear,

$$k_{1_y} = \frac{G\,A_L}{h_2}$$

and,

$$A_L = \pi\,[r_3^2 - r_1^2] + \pi r_1 h_2$$

therefore,

$$k_{1_y} = \frac{\pi\,G\,[(r_3^2 - r_1^2) + r_1 h_2}{h_2}$$

where, G = static shear modulus, Pa
A_L = Loaded area, m^2
h_2 = thickness, m

The lower body, radially loaded,

$$k_{2_y} = \frac{7.5\ \pi\ LG}{\ln\ (r_2/r_1)}\ K_1$$

where K1 is a form factor which depends on height to thickness ratio. This makes the total radial stiffness,

$$k_y = \pi G\ [\frac{(r_3^2 - r_1^2 + r_1 h_2)}{h_2} + \frac{7.5(h_1+h_2)}{\ln\ (r_2/r_1)}\ K_1]$$

For axial loading,

$$k_x = k_{1_x} + k_{2_x}$$

The top section is in shear and compression,

$$k_{1_x} = E\ [1 + \beta\ (\frac{A_L}{A_u})^2]\ \frac{A_L}{h_2}$$

where

$$A_L = \pi\ [(r_3^2 - r_1^2) + r_1 h_2]$$

$$A_u = \pi\ h_2 r_3$$

$$E = 3G$$

and A_u is the unloaded area, m^2.

The lower section is in pure shear,

$$k_{2_x} = \frac{2\pi(h_1+h_2)G}{\ln\ (r_2/r_1)}$$

Making the total axial stiffness,

$$k_x = G[3(1 + \beta\ (\frac{A_L}{A_u})^2)\ \frac{A_L}{h_2} + \frac{2\pi(h_1+h_2)}{\ln\ (r_2/r_1)}]$$

Predicted isolation characteristics - The transmissibility and isolation effectiveness of an installed isolator system can be predicted if the dynamics of each attachment location and direction is known. Using the method described, estimations of the possible benefits of vibration transmission through isolation mounts can be studied.

The structural characteristics of the gearbox and airframe are represented by compliance data obtained from frequency response measurements. Frequency response measurements were made on an S-76 gearbox (S/N A-081-00005) and a partially assembled S-76 airframe (A/C 244). Driving point frequency response measurements and cross frequency response measurements were taken at the four attachment locations of the gearbox and airframe in the vertical, lateral, and longitudinal directions (see Figures 40 through 44, typical). The data were generated using random excitation and were recorded on digital tape for further processing. A Hewlett-Packard 5420 two-channel Fourier analyzer was used to process the recorded data. The data were analyzed over four frequency ranges--500-2100 Hz, 2100-3700 Hz, 3700-5300 Hz, and 5300-6900 Hz. Each frequency response measurement was integrated twice and calibrated to produce compliance data with units of meters/Newton. In order to reduce the noise content in the data, the frequency response measurements were averaged to produce frequency spectra from 500-6900 Hz with a 25Hz frequency spacing.

Frequency response measurements were made on the gearbox at each of the four airframe attachment points in the three principal directions. The frequency response measurements are plotted in the form of compliance with units of meters/Newton. The attachment point numbering and sign convention for the gearbox are shown in Figure 37. Typical driving point measurements are shown in Figures 40 and 42.

The measurement locations and sign conventions used for the airframes are shown in Figure 38. Figures 41 and 43 show typical driving point frequency response measurements on the airframe at the gearbox attachment locations.

The isolator characteristics required for the model are the stiffness and damping of each isolating element. These characteristics can be obtained in three different ways. The simplest is to use stiffness and damping values which are constant or vary linearly with frequency. Another is to use experimentally measured values. The third way is to compute the isolator stiffness and damping values using the isolator geometry and actual material properties (modulus and loss factor). Experimental studies were performed on several isolator configurations. The tests were carried out in the isolation test rig shown in Photo 18. A typical isolator is shown in Photo 19 and the test results are shown in Figure 44. These experimental results were merged with the analytic prediction program to develop an overall methodology to predict isolation effectiveness.

ORIGINAL PAGE IS
OF POOR QUALITY

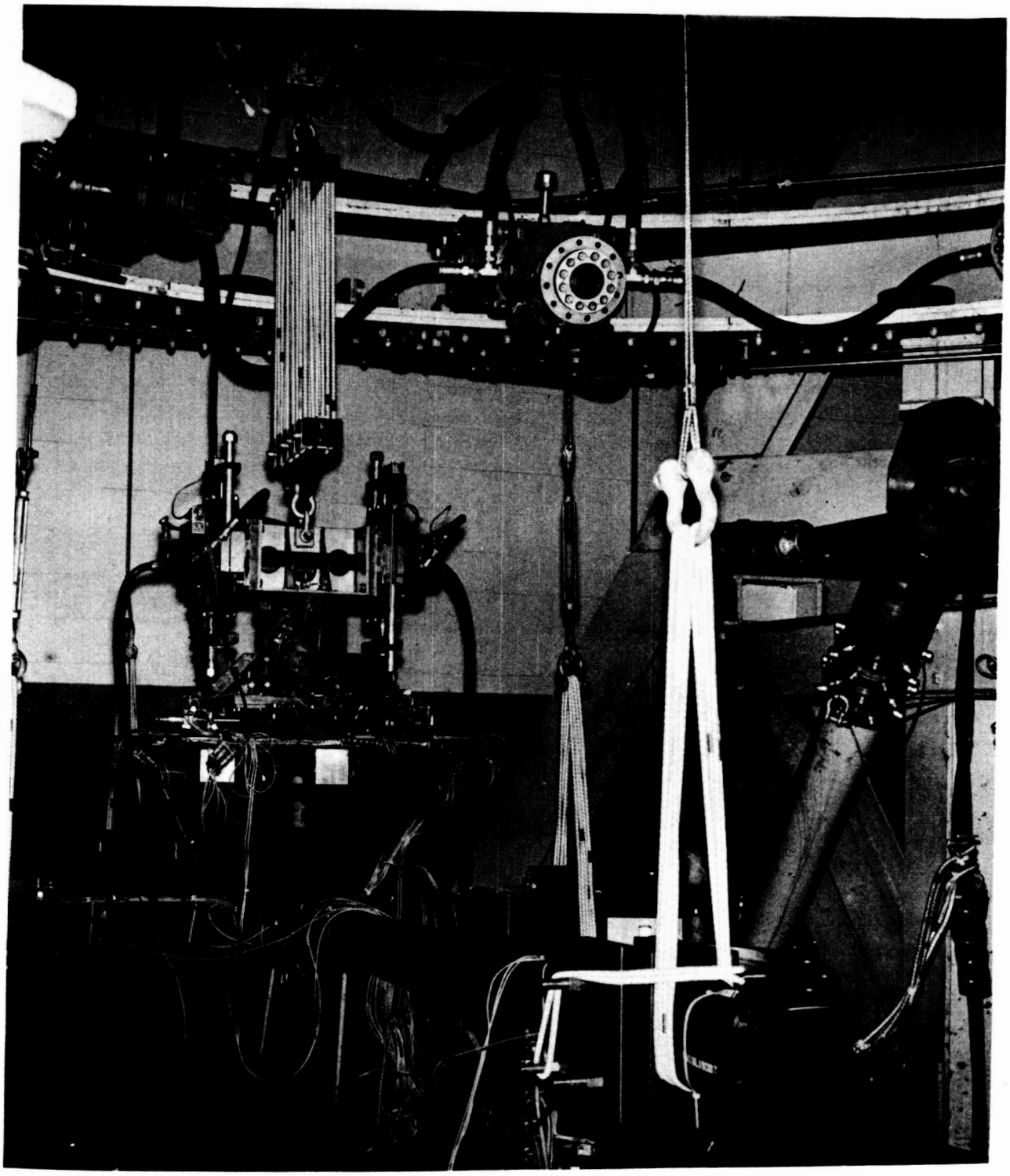

Photo 18. Isolation Test Rig.

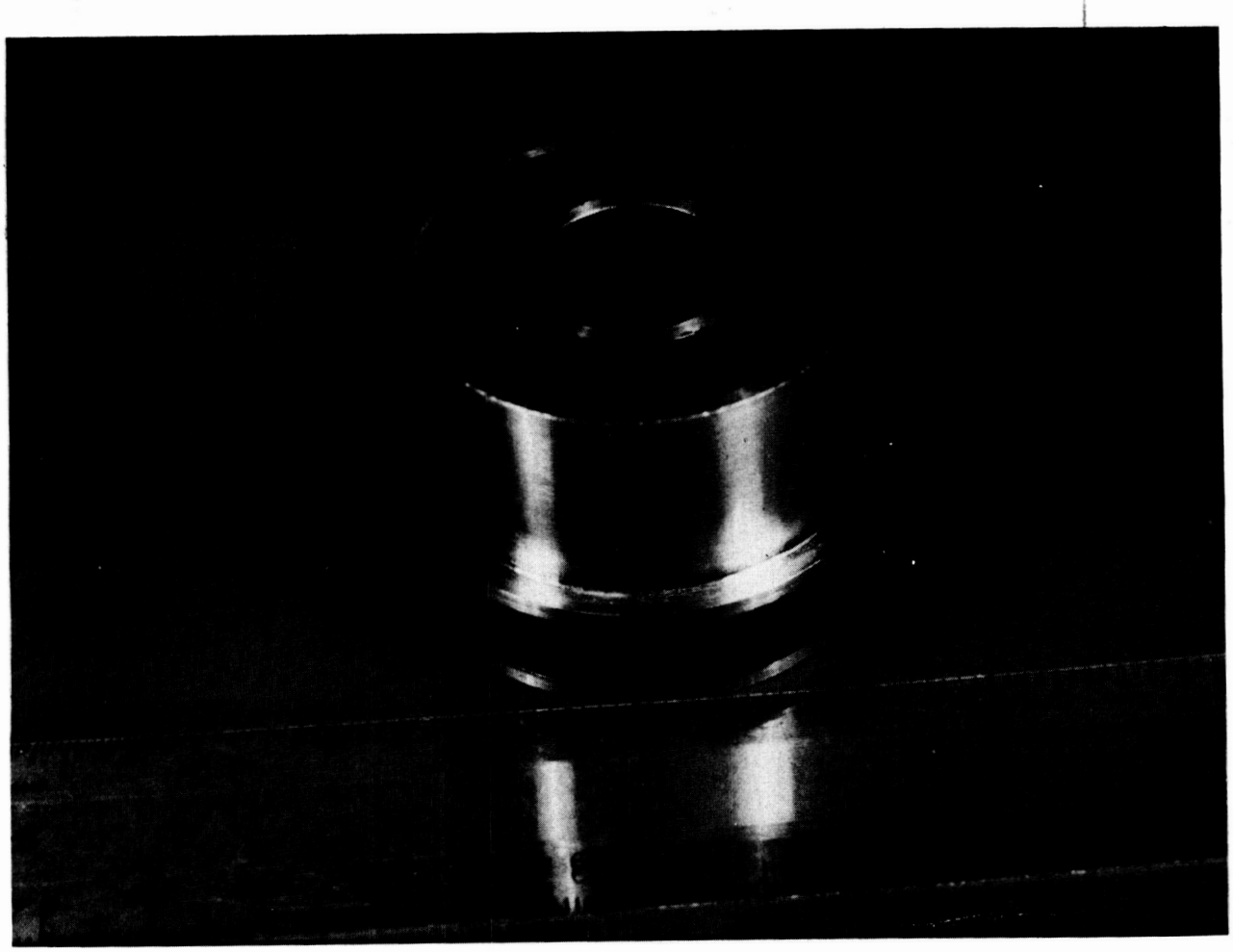

ORIGINAL PAGE IS
OF POOR QUALITY

Photo 19. Typical Isolator.

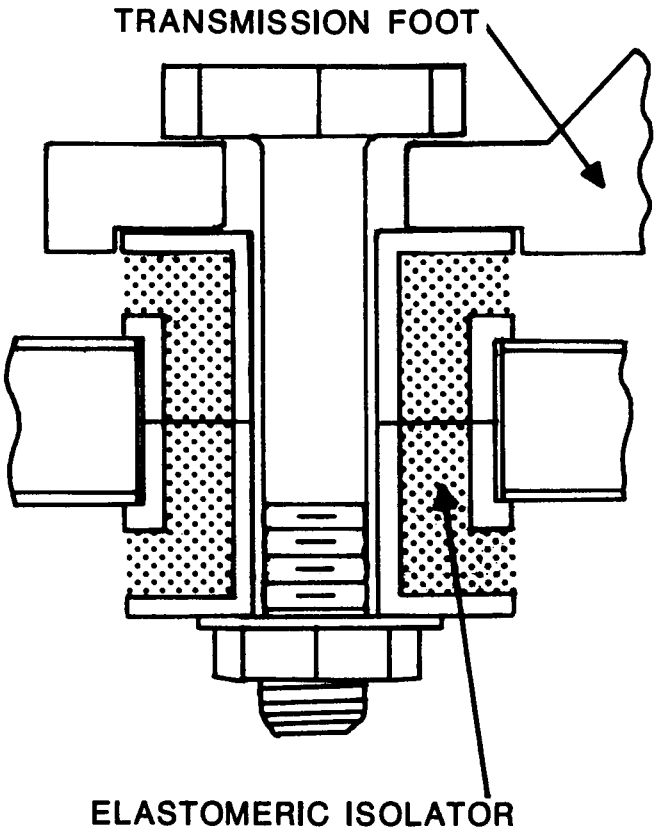

Figure 35. Typical Isolator Installation.

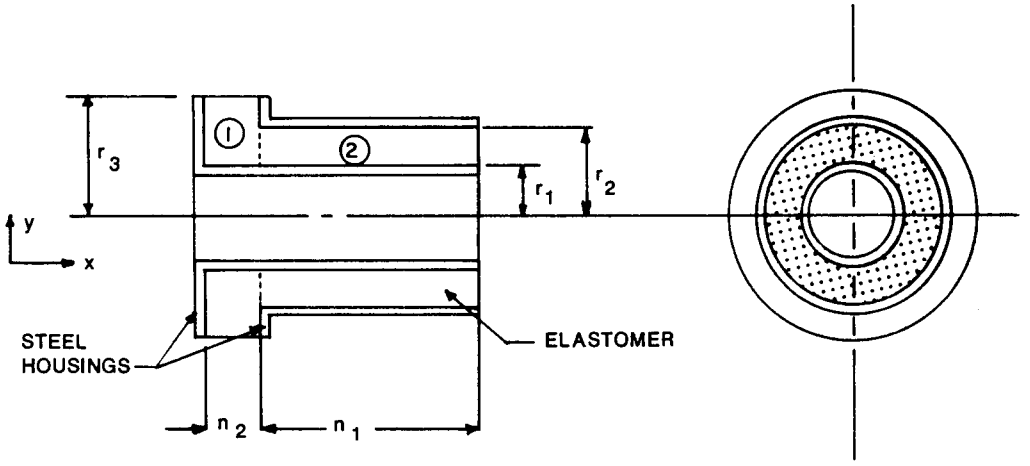

Figure 36. Single Isolator Geometry.

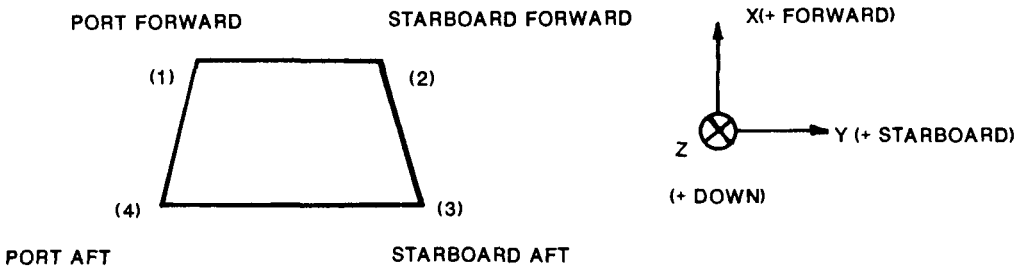

Figure 37. Gearbox Attachment Points and Sign Conventions.

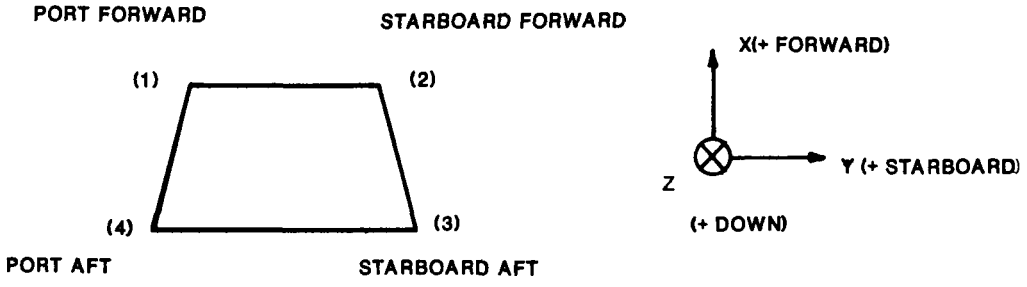

Figure 38. Airframe Attachment Points and Sign Conventions.

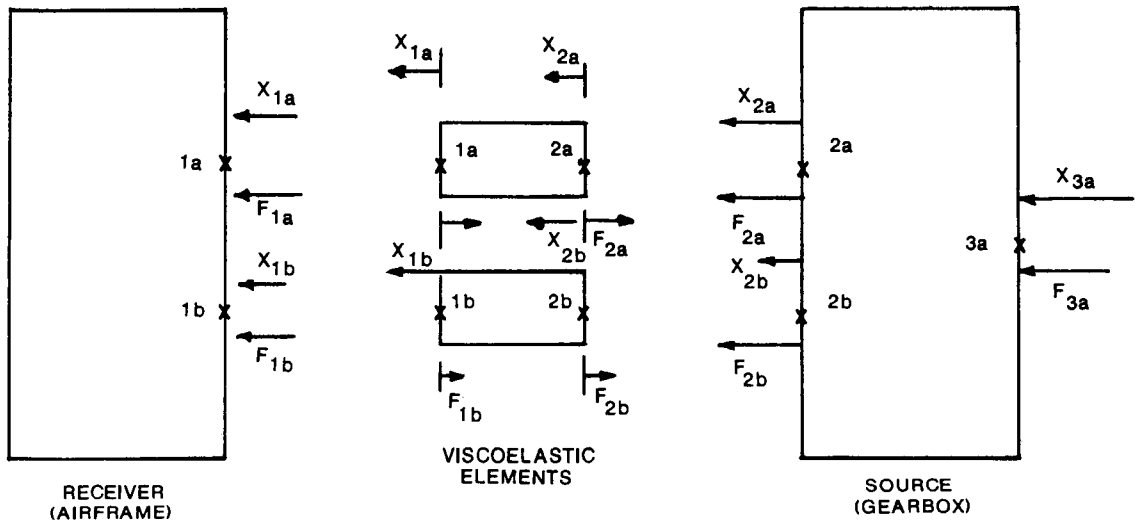

Figure 39. Block Diagram of Analytic Model.

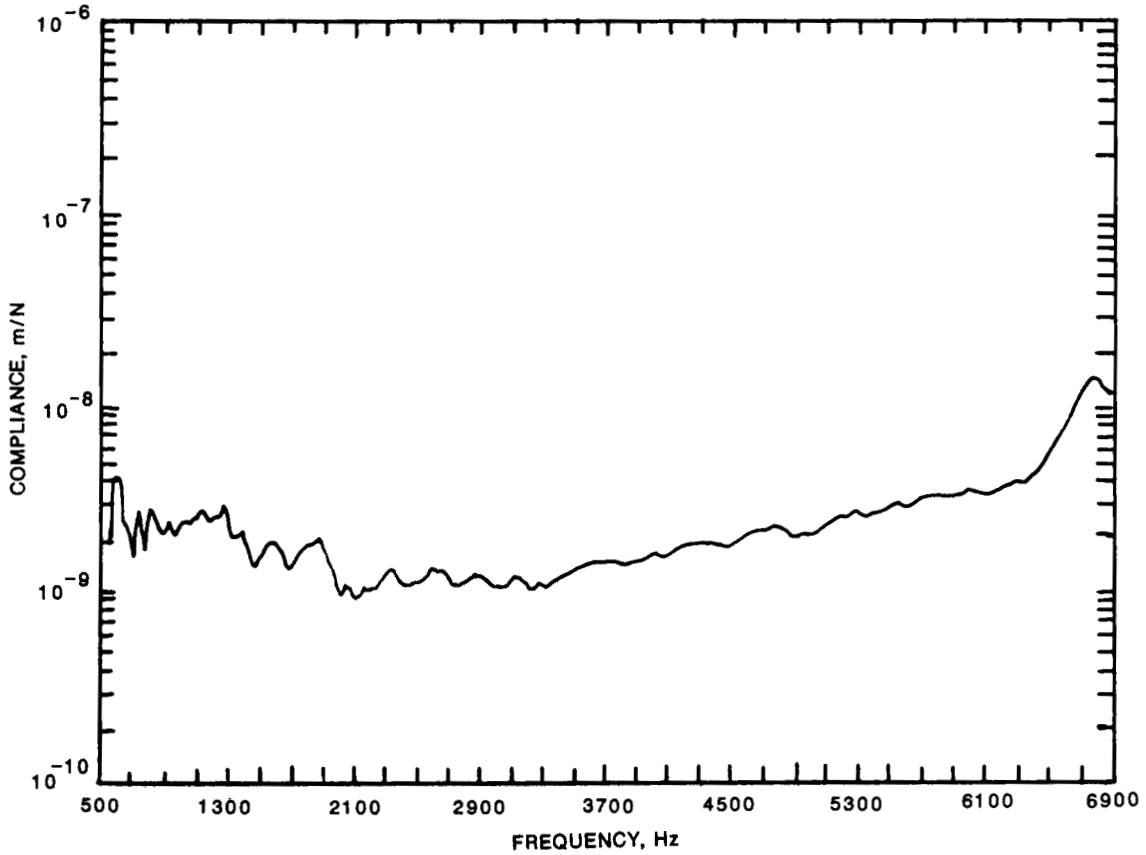

Figure 40. Main Gearbox Driving Point Frequency Response - Port Forward - Vertical.

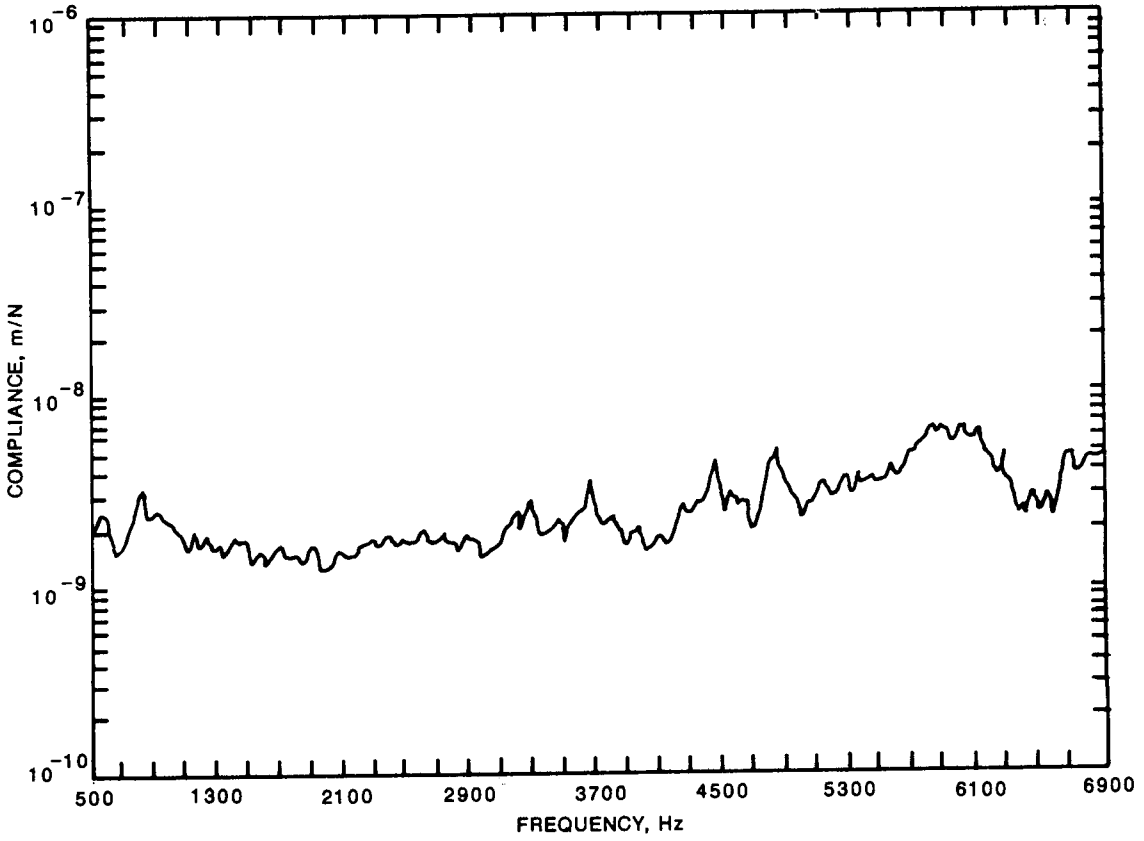

Figure 41. Airframe Driving Point Frequency Response - Port Forward - Vertical.

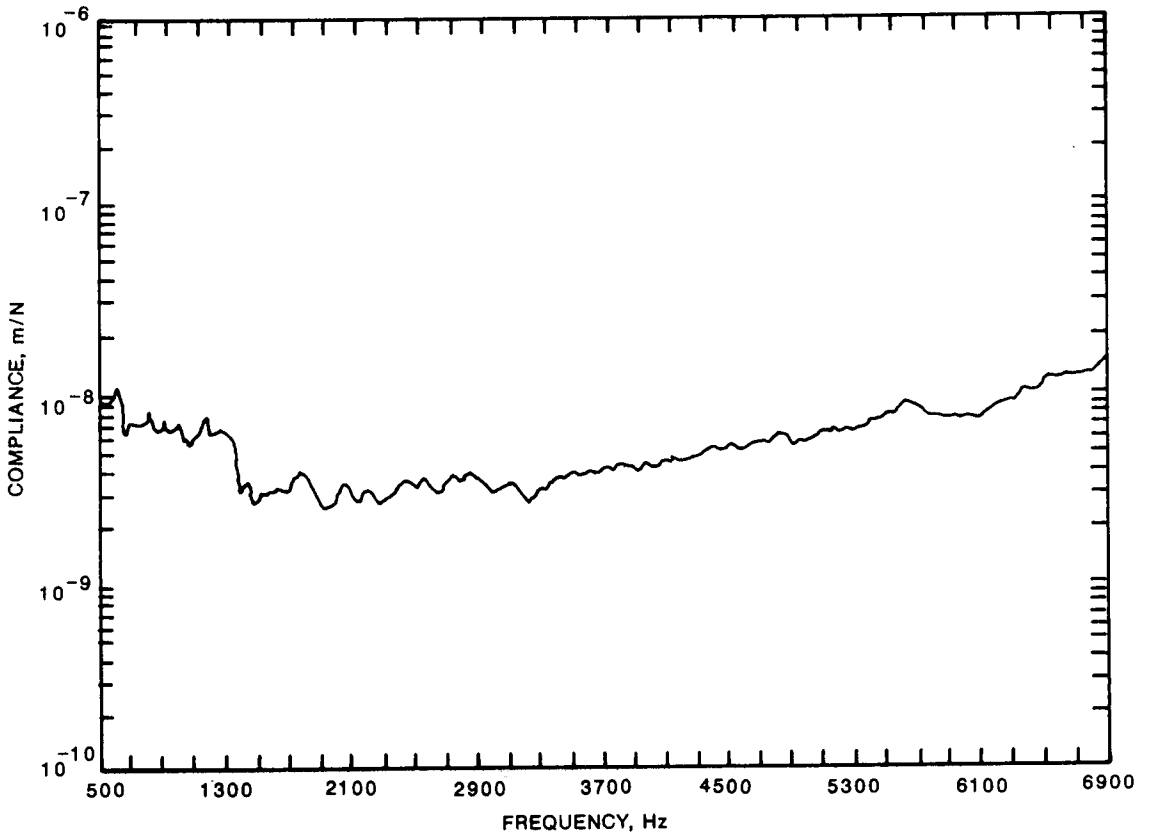

Figure 42. Main Gearbox Driving Point Frequency Response - Port Forward - Lateral.

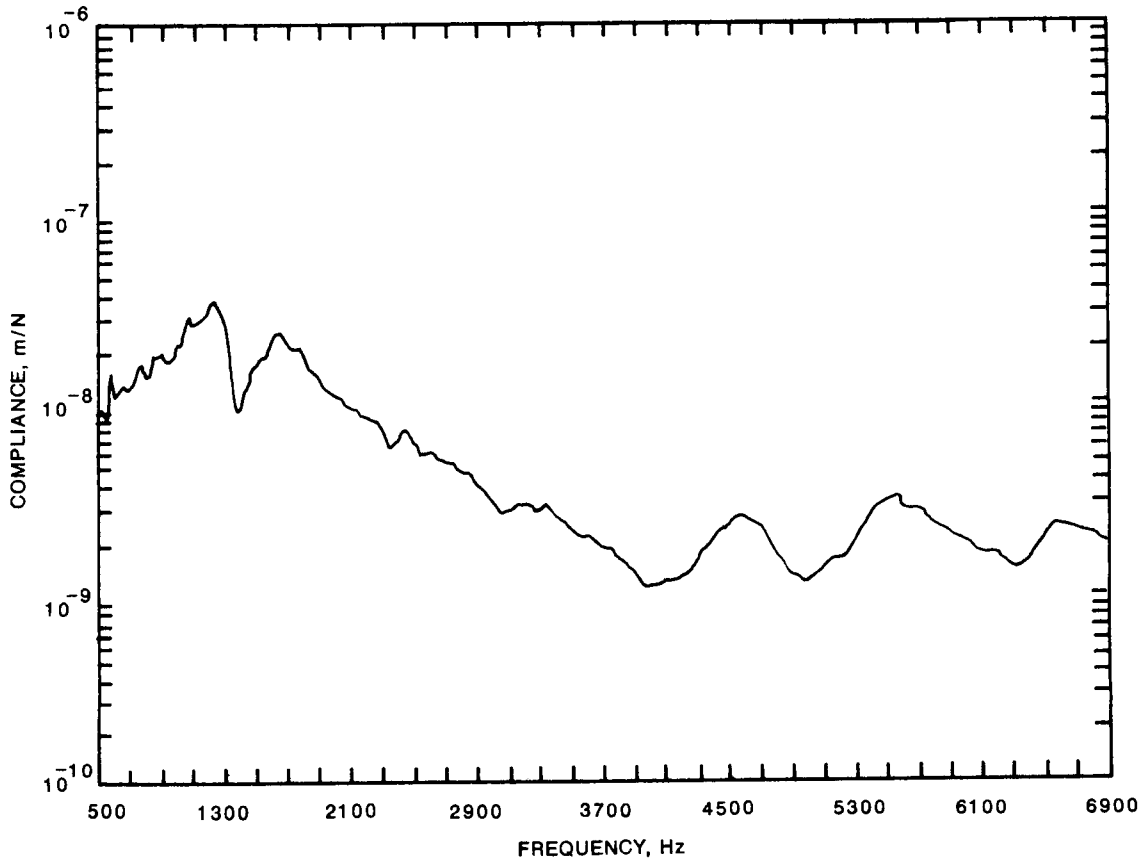

Figure 43. Airframe Driving Point Frequency Response - Port Forward - Lateral.

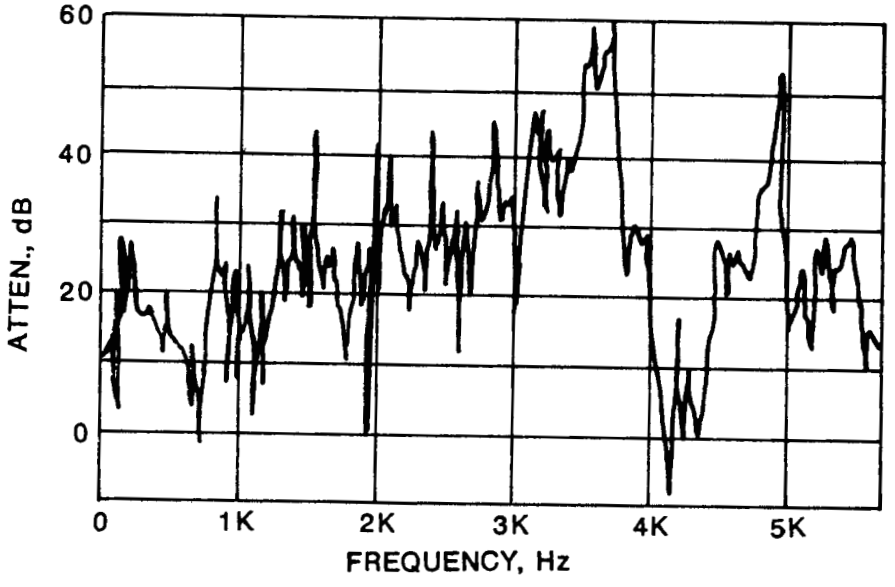

Figure 44. Isolator Bench Test Results.

Since the isolation system is subject to changes in temperature and experiences excitation over a broad frequency range, the use of isolator geometry and material properties was found to give the best representation of the isolator characteristics. The isolation model was exercised for many constant stiffness and damping values and for many isolator geometries.

The analytical model was used to predict the performance of many isolation systems. Each isolation system was composed of one or more identical isolators at each attachment point. Initially, the isolators at each attachment point were characterized by constant stiffness and damping values based on allowable gearbox displacements and desired levels of vibration reduction. Temperature and static preload levels were changed to investigate their effects on the vibration transmitted to the airframe. The variation of material properties over a wide temperature range is shown in Figure 45 over a range of frequencies. An output from the model is the relative displacement of the gearbox and airframe attachment points as a function of frequency. The ratio of the relative displacement of the gearbox (transmissibility) was calculated for each isolator configuration and was used as a basis for evaluating isolator designs.

Another measure used to evaluate isolation system performance was isolation effectiveness. Several isolator designs were evaluated in terms of isolation effectiveness in addition to transmissibility.

To investigate the temperature effects on the stiffness and damping of the isolators, transmissibility was predicted for the two isolator systems at temperatures of 80°C, and -25°C. These results are shown in Figure 46.

The effects of static preload on isolator stiffness and damping were likewise investigated. Static preload values chosen from the vertical in-flight isolator loads were 35kN and 70kN for forward and aft flight, respectively. Figure 47 shows the predicted transmissibility calculated for 0, 35, and 70 kN preloads on the two isolator systems at 80°C in the vertical direction.

Isolation effectiveness - Isolation effectiveness is defined as the ratio of the the receiver (airframe) displacement obtained when the receiver (airframe) is connected with a rigid link to the displacement obtained when an isolator is inserted between the source (gearbox) and receiver (airframe). Therefore, an isolation effectiveness value of one indicates a rigid connection with no isolation and higher values indicate better isolation. Isolation effectiveness is a more accurate indication of isolator performance than transmissibility because it takes into account the output characteristics of the source (gearbox). Isolation effectiveness equals the reciprocal of transmissibility only when the output of the source (gearbox) is independent of the attached load. The isolation effectiveness will become worse at structural resonance frequencies because the stiffness of the structure may be as low or lower than the isolator. Therefore, isolator performance at a resonance is not always dis-

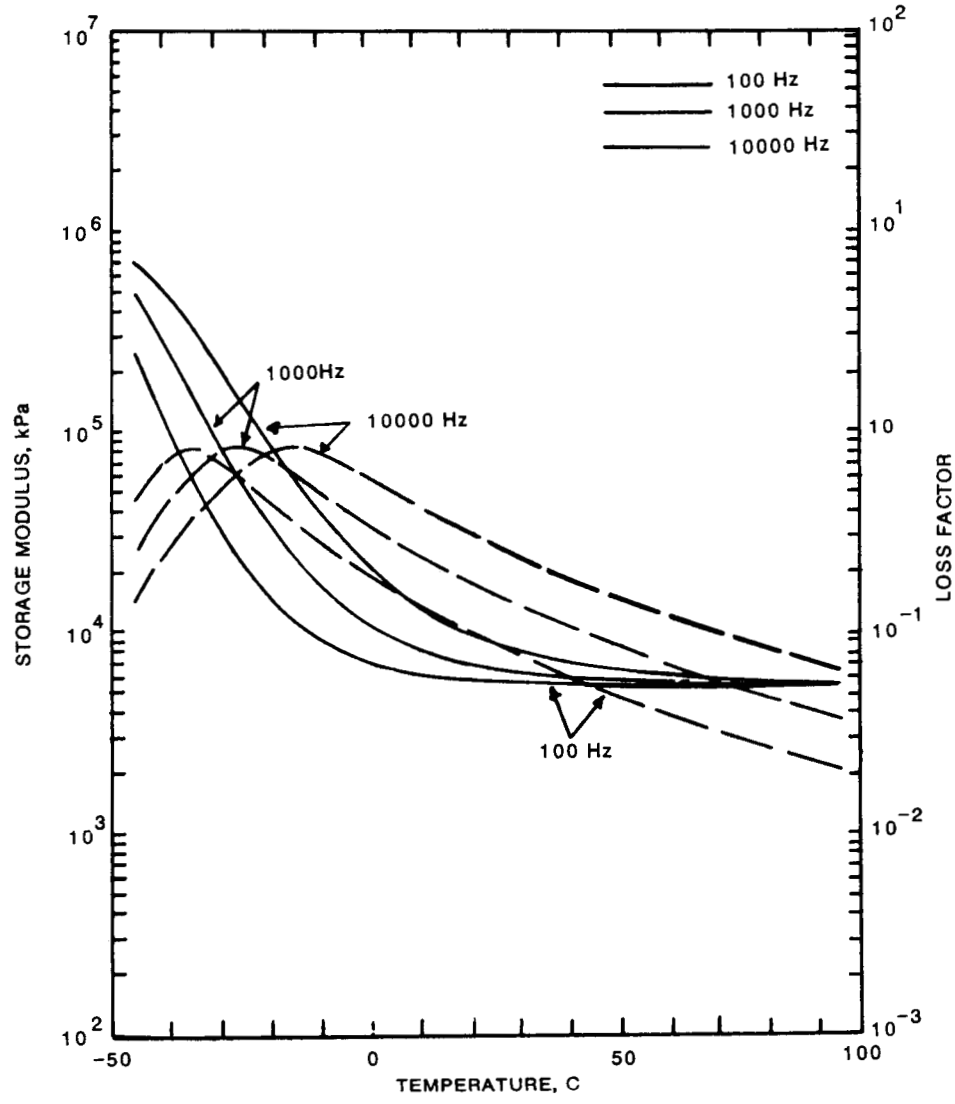

Figure 45. Variation of Material Properties at Constant Frequencies.

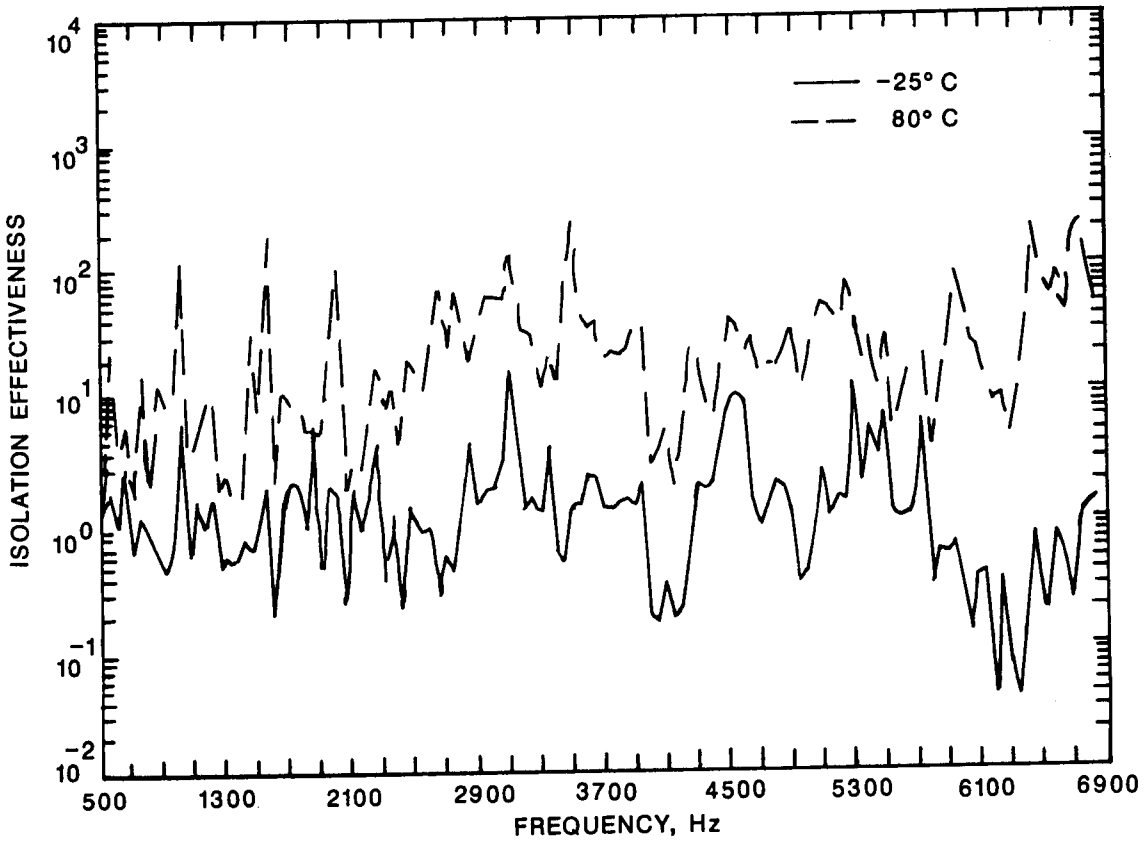

Figure 46. Influence of Temperature on the Predicted Isolation Effectiveness with Two Isolators in the Vertical Direction.

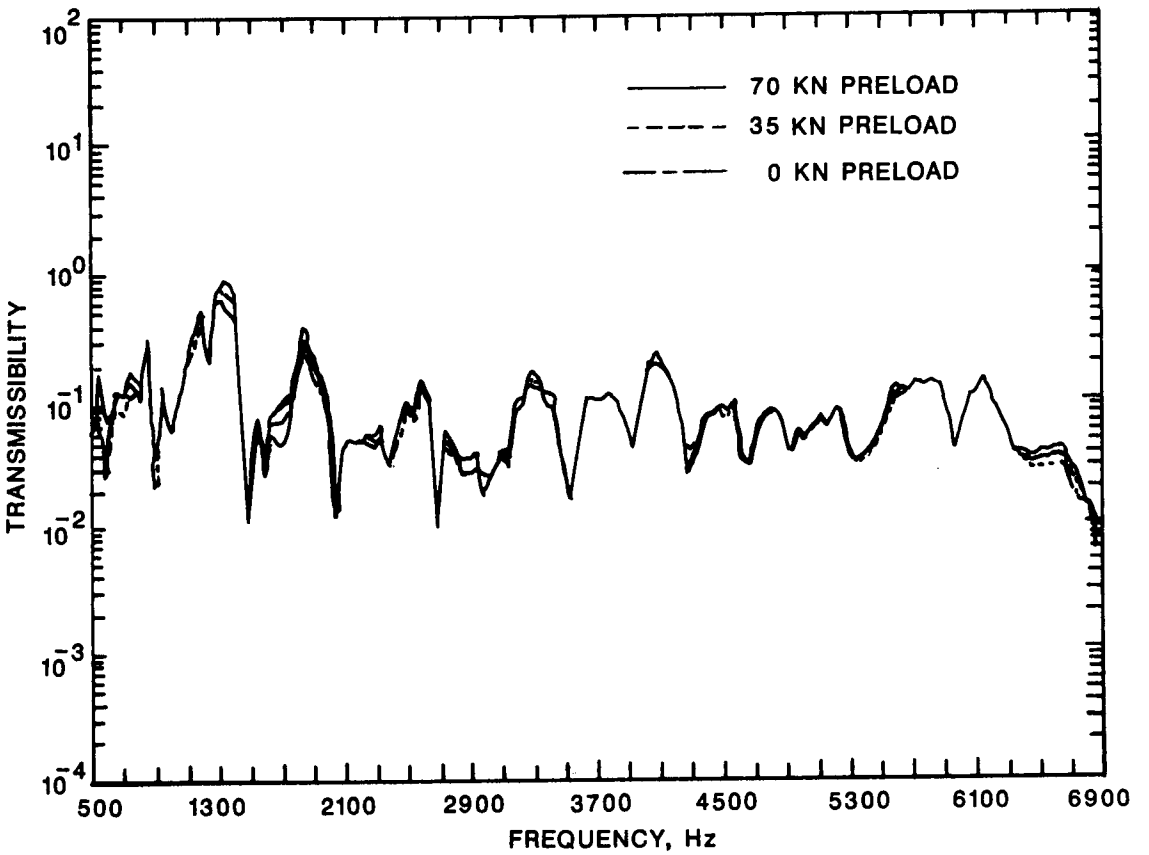

Figure 47. Influence of Preload on the Predicted Transmissibility with Two Isolators at 80°C in the Vertical Direction.

played by poor transmissibility but is always displayed by poor isolation effectiveness. The isolation effectiveness of the isolation system designs were calculated relative to a rigid connection of 10^{12} N/m. The predicted effectiveness of the two- and four-isolator designs are shown in Figures 48 and 49 for the vertical direction.

Plan For Validation

Isolation - The preliminary isolator design has been established in the Phase III effort. During Phase IV the detailed isolator design will be completed and full scale tests carried out. Final definition of the loads envelope and aircraft component deflections would be used to set the limits for isolator design. These parameters, together with a final spatial envelope will be input to the Isolator Design/Prediction Methodology procedures which have been developed by Sikorsky and validated by model scale tests of small scale isolators. A parametric evaluation of isolator effectiveness will then be made. The parameters will include stiffness in axial and radial directions, preload conditions, low frequency dynamic quasi-static load effects, material properties, geometry, and temperature.

A selected isolator set will be fabricated for bench testing and full scale evaluation. The bench test will involve a single unit in the half-scale dynamic airframe rig. These tests will involve several preload conditions and be repeated for several isolators to obtain representative results. These tests will provide the verification of the individual loading direction effects and isolation effectiveness in a controlled environment. The isolator design methodology will then be validated at full scale dimensions with representative preload conditions.

A full scale ground shake test on an S-76 aircraft will determine the isolator effectiveness as a group rather than individually. In this test the interaction of all eight isolators (2 at each attachment location between the main gearbox and airframe) will be evaluated. Rigid mount inserts of the same size as the isolators will be used as a baseline to compare with the isolated case. Measurements will be made at the isolator interface (on each side in all three directions at each attachment) and on the frames, panels, and in the cabin acoustic space. These measurements will be compared to the Statistical Energy Analysis (SEA) predictions for frame and panel energy levels. The beneficial influence which the isolation system has on cabin noise level reduction will be determined.

The following is an outline for the proposed plan:

2.5 Phase IV - Validation

2.5.1 Full Scale Validation of Isolator Analysis

2.5.1.1 Detailed Isolator Design

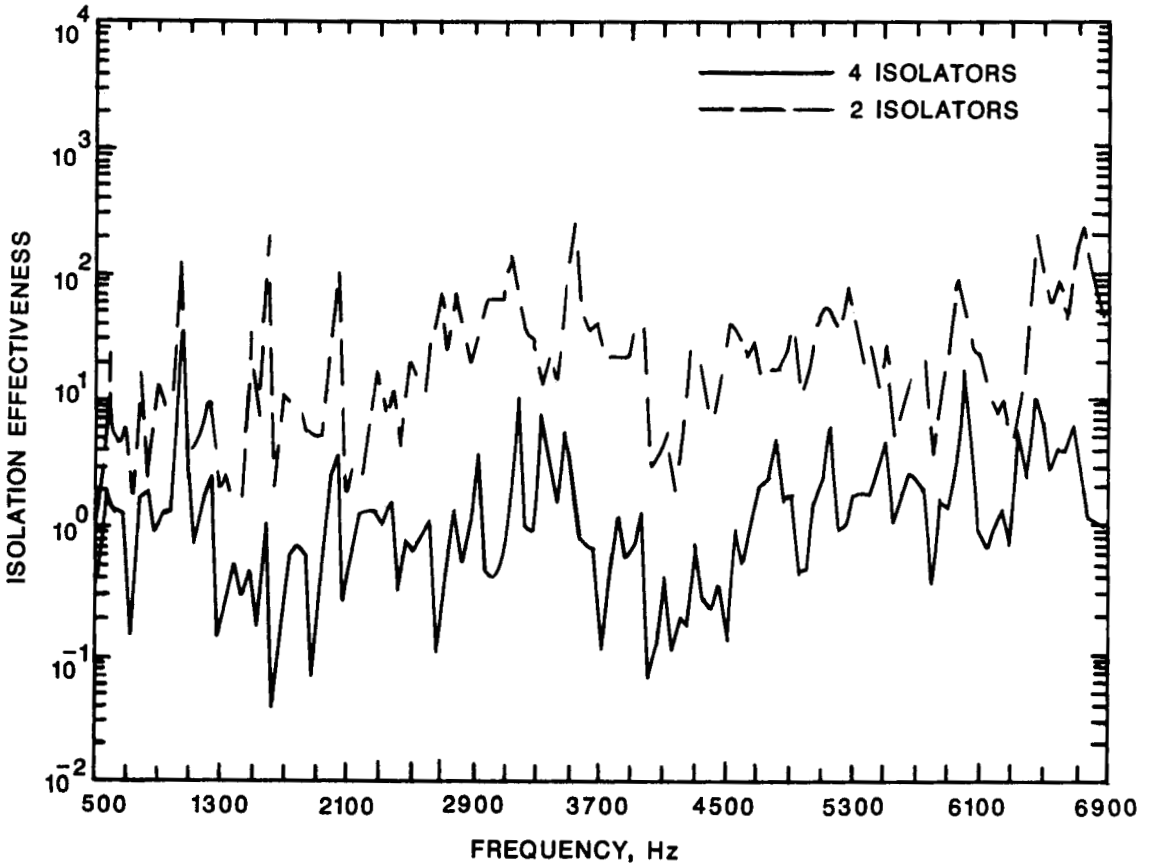

Figure 48. Predicted Isolation Effectiveness for Two vs. Four Isolators at 80°C in the Vertical Direction.

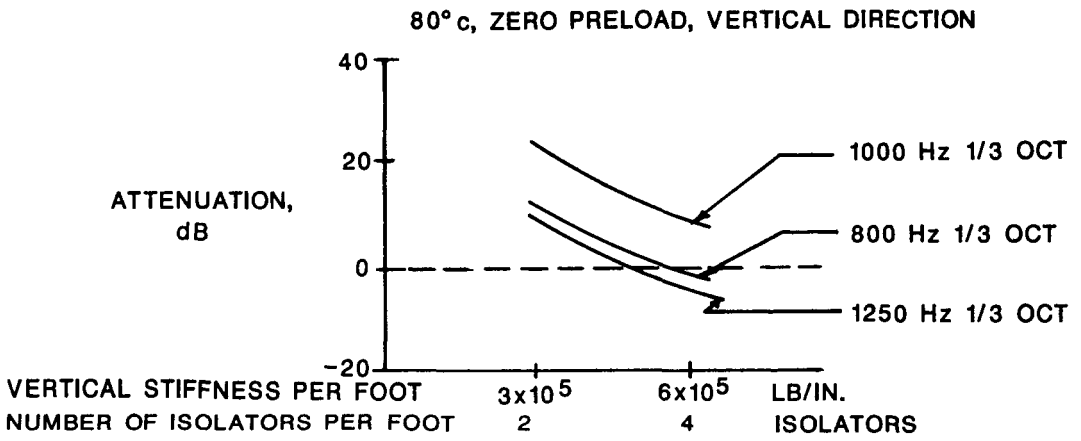

Figure 49. Predicted One-Third Octave Band Attenuation vs. Isolator Stiffness.

2.5.1.1.1 Verify loads envelope at airframe/gerabox interface (quasi-static maneuver conditions).

2.5.1.1.2 Verify allowable relative deflections for critical elements (e.g.: engine high speed shaft, swashplate controls, tail drive shaft).

2.5.1.1.3 Define allowable spatial envelope, and the structural impact, associated with isolator installation.

2.5.1.1.4 Conduct parametric evaluation of isolator effectiveness as a function of stiffness and material properties within the constraints of Items 2.5.1.1.1 through 2.5.1.1.3 above.

2.5.1.1.5 Develop the detail isolator drawings and fabricate a selected isolator set (10 units).

2.5.1.2 Unit Isolator Bench Test

2.5.1.2.1 Set up and instrument the half-scale dynamic airframe rig.

2.5.1.2.2 Install single isolator in the rig fixture and conduct isolation shake testing at acoustic frequencies at a given preload condition. Repeat tests at two additional preload conditions. Repeat tests for three additional isolator units to test for fabrication variations.

2.5.1.2.3 Analyze data from bench tests.

2.5.1.2.4 Compare bench test data with predicted isolator performance and validate overall prediction methodology at model scale.

2.5.1.3 Full Scale Ground Shake Test

2.5.1.3.1 Formalize the detailed test and measurement plan including any bench test benefits.

2.5.1.3.2 Fabricate inserts for rigid mount condition.

2.5.1.3.3 Install rigid mount inserts on an S-76 airframe at the four attachment locations between the main gearbox and airframe. Instrument the aircraft and conduct the baseline shake tests. Measure the vibration and acoustic levels.

2.5.1.3.4 Install isolators on an S-76 airframe at the four attachment locations between the main gearbox and airframe in place of the rigid mount. Instrument the aircraft and conduct shake tests with isolators. Measure the vibration and acoustic levels.

2.5.1.3.5 Reduce and analyze the full scale test data. Compare with predictions and make recommendations.

CONCLUDING COMMENTS

The application of SEA methodology to the prediction of helicopter interior noise [1, 2] generated many interesting views of how energy travels from source to receiver. This phase of the NASA program has looked at various ways to interrupt these varied energy paths. These include interior treatments, panel isolation, leakage control, damping, and source isolation. The influence each has on aircraft noise performance has been presented in this report and some of the key items are as follows:

- For the first time, a SEA model has been demonstrated for a complete aircraft including two different current interior configurations and one experimental.
- The coupling loss factor provides the proper information to conduct trade assessments between panel TL and leakage control.
- Predictions of interior treatment parametric variations are reasonable and consistent with experience.
- SEA predictions of existing designs are in good agreement with flight data.
- The modeling process and the predictions generated provide insight which will foster intrinsically better designs for future aircraft.
- The frequency response measurements made on the S-76 reveals that the airframe is stiffer than the gearbox and contains fewer resonances. Resonances in both structures are heavily damped.
- Adequate isolation can be provided at an operating temperature of 80°C using a two- or four-isolator design at each of the four gearbox-airframe attachment points.
- Additional isolation can be provided by making the isolators weaker and installing positive stops on the gearbox to limit its displacement while under peak in-flight loads.
- Stiffening the gearbox will improve the isolation system performance more than stiffening the airframe.

RECOMMENDATIONS

The benefits of modeling interior treatment types are demonstrated by the ability one has to do design studies and trade-offs. Since the SEA model contains information relative to both structureborne and airborne energy flow via various paths, a study conducted early in the design stage of a new aircraft is now possible. The effect of changing the frame/junction points and beam terminations could be assessed for their impact on acoustics.

Another area having strong potential is isolation. The dominant source of cabin noise has been shown to be the gear mesh forces generated in the main gearbox. These forces transmit through the gearbox housing to the airframe; subsequently radiating acoustic energy from those surfaces. The major path is structural and isolation interrupts that path. Thus a significant noise reduction is possible depending on the constraints of the overall helicopter performance, e.g.: swashplate control inputs, engine/gearbox and gearbox/tail take-off alignments, and spatial compactness. These items play a role in sizing an isolation system, and hence they tend to limit the acoustic reductions achievable. Even with these constraints it is apparent that important noise reductions are possible. It is recommended that the initial isolation study reported herein be completed and isolators fabricated and tested. A recommended program for Phase IV has been described and, pending the outcome, plans should be initiated for full scale flight testing of this concept.

REFERENCES

1. Yoerkie, C.A.; Moore, J.A.; and Manning, J.E.: Development of Rotorcraft Interior Noise Control Concepts - Phase I: Definition Study. NASA CR-166101, May 1983.

2. Yoerkie, C.A.; Gintoli, P.J.; and Moore, J.A.: Development of Rotorcraft Interior Noise Control Concepts - Phase II: Full Scale Testing. NASA CR-172594, February 1986.

3. Unger, E.E.; Ross, D.: Damping of Flexural Vibrations by Alternate Viscoelastic and Elastic Layers, Proceedings of the Fourth Annual Conference on Solid Mechanics, University of Texas, Austin, Sept. 1959.

4. Beranek, Leo L., ed.: Noise and Vibration Control. McGraw-Hill Book Co., 1971.

5. Cremer, L.; Heckl, M.; Ungar, E.E.: Structureborne Sound, Springer-Verlag, 1973.

6. Ungar, E.E.: Loss Factors of Viscoelastically Damped Beam Structures, Journal of the Acoustical Society of America, Vol. 34, pp. 1082-1084, 1962.

7. DeJong, R.D.: A Study of Pump and Piping Generated Ship Noise Using Statistical Energy Analysis. Cambridge Collaborative, Inc., Report to DTNSRDC, Annapolis, MD. Contract No. 00600-77-R-1417, 15 May 1978.

8. Swift, P.B.: The Vibrational Energy Transmission Through Connected Structures. Ph.D Thesis, The University of Adelaide, Australia, May 1977.

9. Blake, W.K.: The Radiation from Free-Free Beams in Air and in Water. Journal of Sound and Vibration, Vol. 33, No. 4, 1974, pp. 427-450.

10. Gobel, E. F. (A.M. Brichta, trans. and ed.): Rubber Springs Design, John Wiley & Sons, 1974.

11. McGary, Michael C.: A New Measurement Method for Separating Airborne and Structureborne Noise Radiated by Aircraft-Type Panels. NASA TP 2079, September 1982.

12. McGary, Michael C.: Noise Transmission Loss of Aircraft Panels Using Acoustic Intensity Methods. NASA TP 2046, August 1982.

APPENDIX A

Laboratory Experimentation

Test Chambers - Laboratory testing for varification of Panel TL type junctions were performed within the Acoustic Test Chambers at Sikorsky's Stratford plant. The Chambers consist of two rooms, side by side, with a test section of variable size joining the two (see Figure 2). One room is a reverberant type diffuser. The other room is an anechoic type with aborptive wedges on all inner surfaces. Both rooms are isolated from their surrounding support stucture as well as from each other. The dimensions of the chambers is of sufficient size to allow for measurements in the required range of 500 to 4000 Hz octave bands. The dimensions of the test section opening used in the below measurements is 4' x 4'. The test section can be closed for use of individual chambers.

Panel TL - TL of aircraft interior panels was determined using the two-room method in the test chambers. Typical panel buildups of the type used in this report were placed in the test section between chambers. Sound pressure levels were measured on both the incident side as well as the transmitted side. Sound intensity (Lit) was measured on the transmitted side directly using a two-microphone sound intensity analyzer. Intensity levels were derived on the incident side using

$$Lii = Lpi - 6$$

where Lii is the intensity level, incident side and Lpi is the pressure level, incident side and after checking of the phase error the transmission loss is calculated by

$$TL = Lii - (Lit + .16).$$

where Lit is the intensity level on the transmitted side. Typical responses of the panel layups used are shown in Figures 18 and 19.

Mass law confirms the ability of the chambers to determine TL as when compared to a panel of limp mass construction, such as a typical Utility type structural panel (Figure 18) the TL response is quite comparitive.

To verify trim panel response for transmission loss, SEA modeling techniques were used to recreate the chambers with an area junction of the size used in the actual chamber tests.

Panel Leakage

Leakage measurements of typical leakage area in a panel was performed in the two test chambers. An ABS plastic panel of the same general construction as those of the Utility type panels was placed in the test section. A slot of variable total area was cut into the panel to represent a typical leakage between two panels. The leakage area covered for 0.03 to 0.12 percent of total panel area with a comparison to a baseline panel with no slot (0.00% leakage). Noise levels were generated again in the reverberant chamber and an incident pressure level determined. Transmitted noise was measured in the anechoic chamber using ASTM 336 type methods and TL determined for each leakage condition.

In Figure 51 it can be seen that leakage around the trim panels has a strong effect on interior cabin levels. How energy flows through leakage area per frequency was measured experimentally and then compared to SEA predictions. Those predictions were based (as with the TL testing) on a model of the two chambers with a panel junction between the two and an additional junction directly from chamber to chamber of the specific leakage area. This again can be seen to compare quite well. There were some difficulties in matching up some of the lower frequencies (below the range of interest) which could possibly be due to the mehod used. It would have been preferred to generate the noise on the anechoic side and measured power directly in the reverberant chamber, but the chmaber characteristics made it impossible to generate levels required for the proper signal to noise ratio.

Cabin Absorption

Initially, an attempt was made to measure absorption in the individual components in the cabin and the total cabin absorption would be determined from that. Some of the measurements made can be seen in Figures 48 and 49. But, practical measurements of many of those components as they functioned in the aircraft proved impractical.

To determine the total absorption within the various cabin interior types it was decided that a direct measurement of the cabin as opposed to testing of the many various components would provide the mode accurate information. This method required only a space averaged sound pressure measurement with a known sound power source to derive the absorption. The other method required a very complicated series of absorption tests of the individual components making up the cabin interior.

A calibrated sound power source was placed in both a utility and executive type aircraft with interiors equivalent to those modeled and pressure measurements made. To determine the acoustic loss factor η, calculation of the cabin room constant R is required;

$$Lp = Lw + 10\log\left(\frac{Q\theta}{4\pi r^2} + \frac{4}{R} \right)$$

where Lp is the measured sound pressure in the cabin, Lw is the known sound power emitted from the source, Qθ is the directionality factor, and r is the distance from the source. By applying that value with the measured surface area St provides the average cabin absorption $\bar{\alpha}$ using

$$\bar{\alpha} = \frac{R}{St + R}$$

The absorption A in Sabins comes from

$$A = S\bar{\alpha}$$

and then applying the volume of the cabin V, the reverberation time T can be calculated

$$T = \frac{.161V}{A}$$

and finally the loss factor

$$\eta = \frac{2.2}{F\ T}$$

is calculated for each individual frequency F. This was applied directly to the cabin material model loss factor.

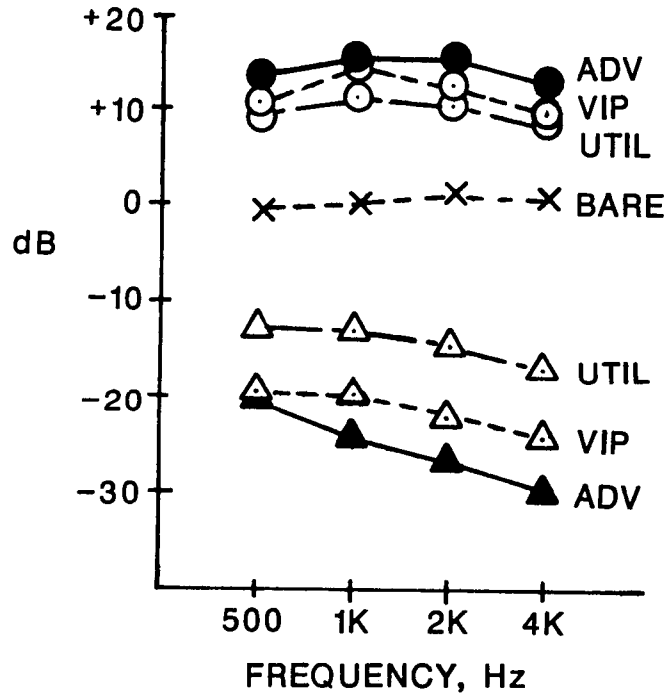

Figure 50. Relative Comparison of Bare Cabin Levels to the Utility, Executive and Advanced Overhead Cavities and Cabin Levels.

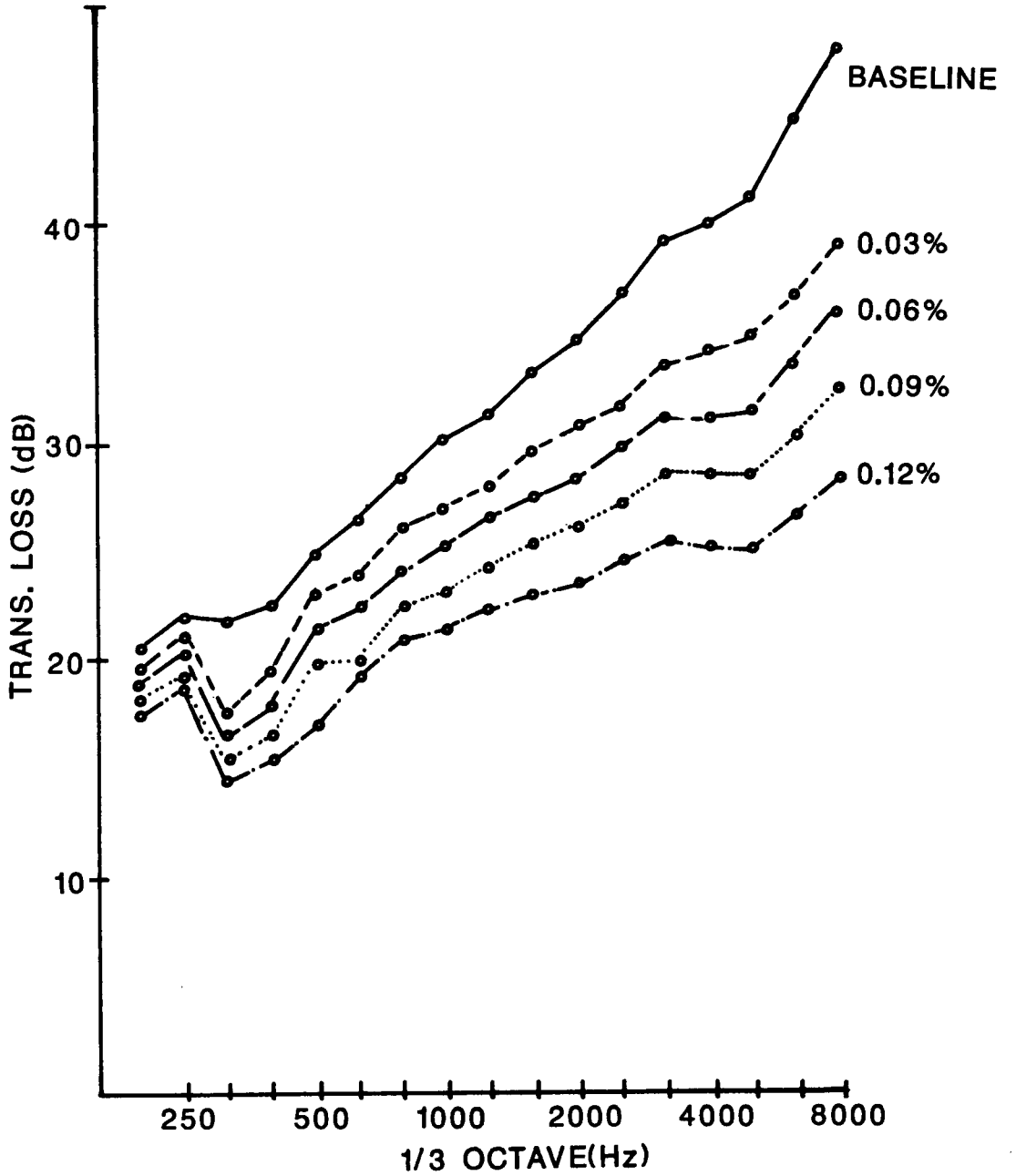

Figure 51. Effect of Increased Leakage Area on Panel TL.

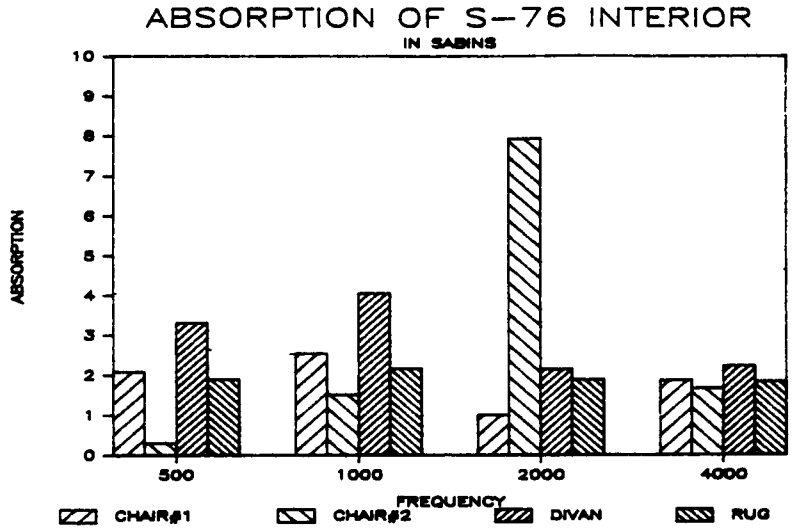

Figure 52. Absorption Provided by Several Typical Cabin Furnishings

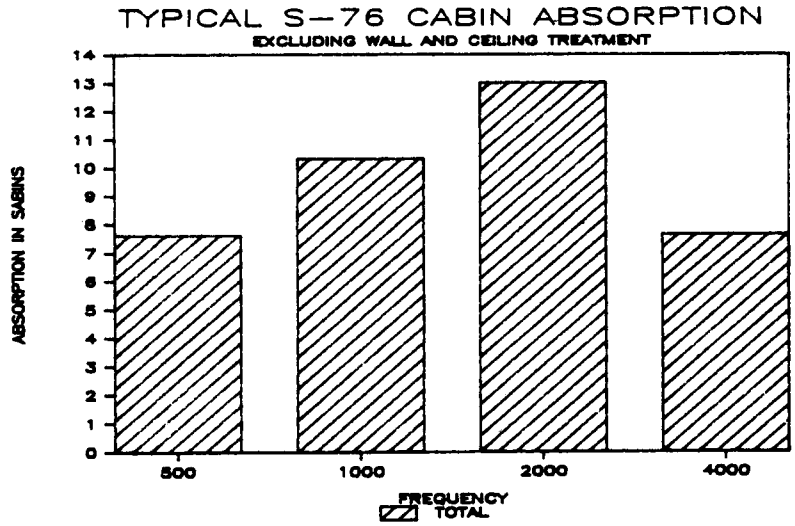

Figure 53. Typical Total Absorption of Cabin Furnishings.

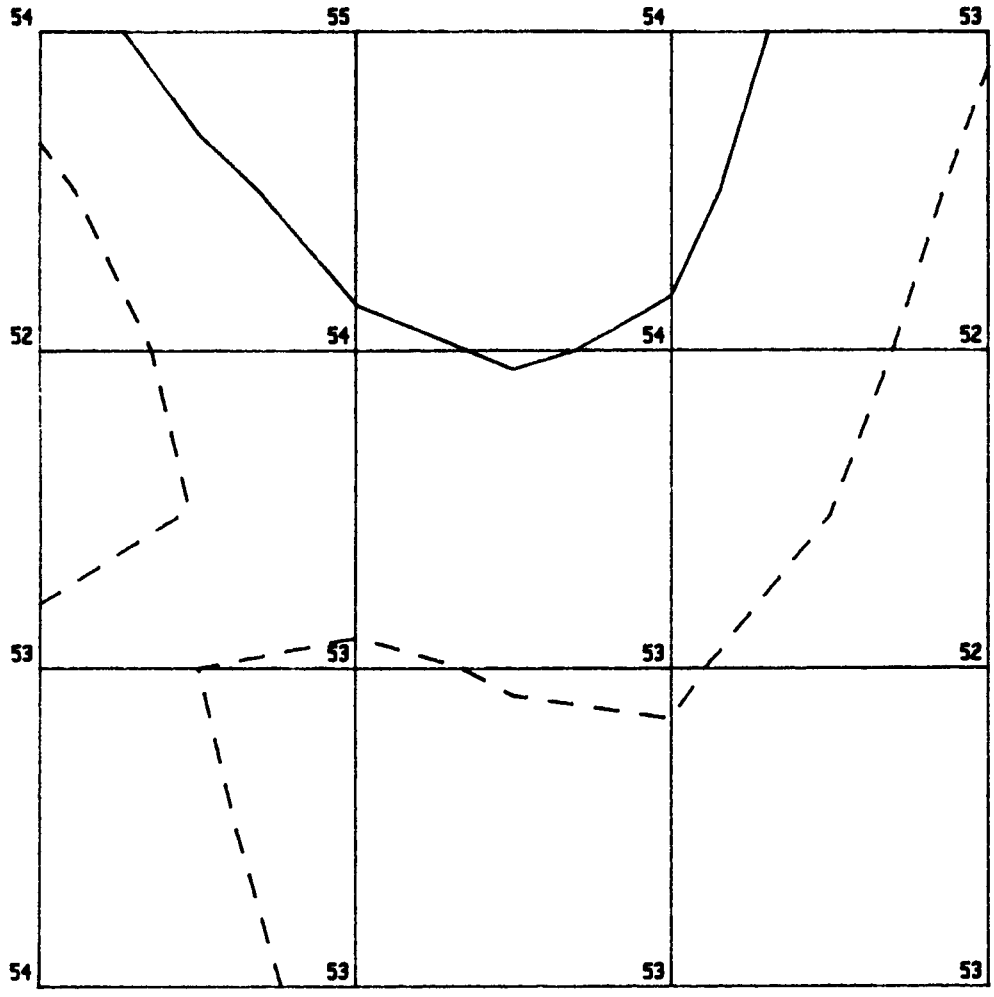

Figure 54a. Measured Intensity Contours for a Utility Type Panel at 0.5 kHz.

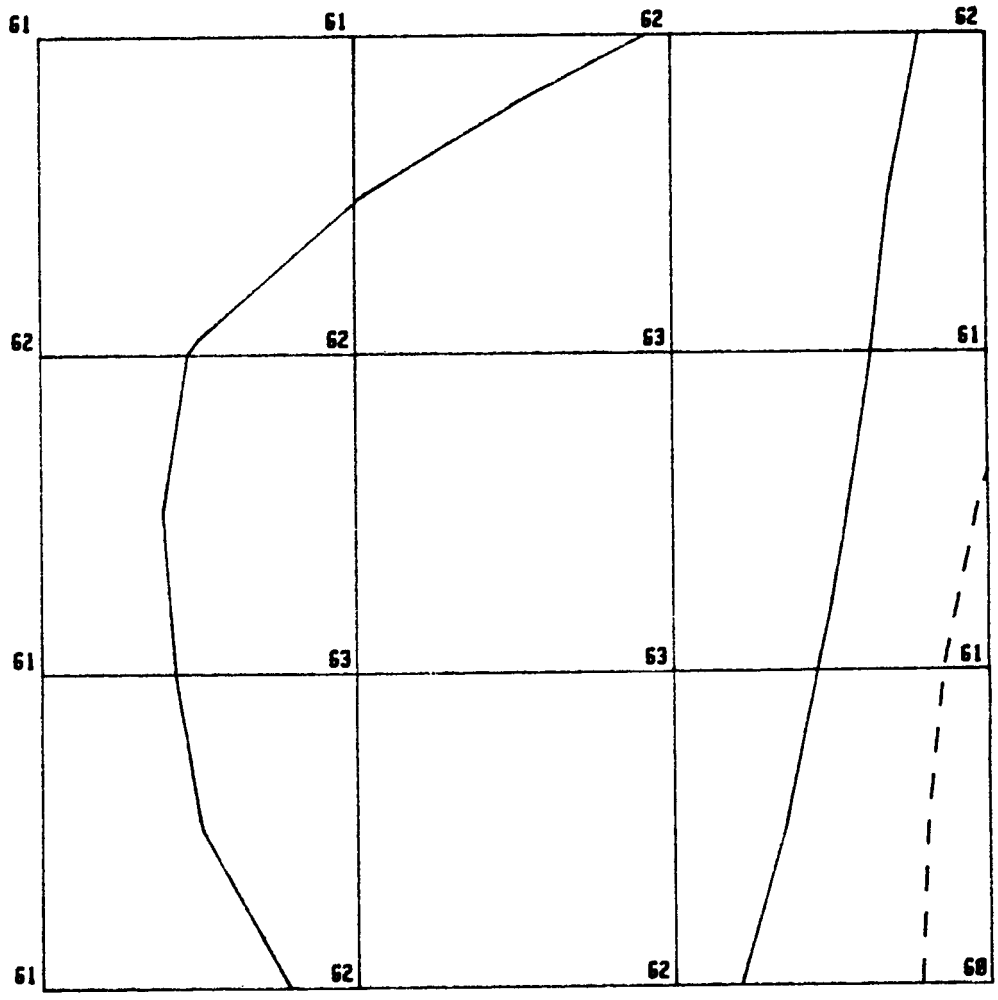

Figure 54b. Measured Intensity Contours for a Utility Type Panel at 1 kHz.

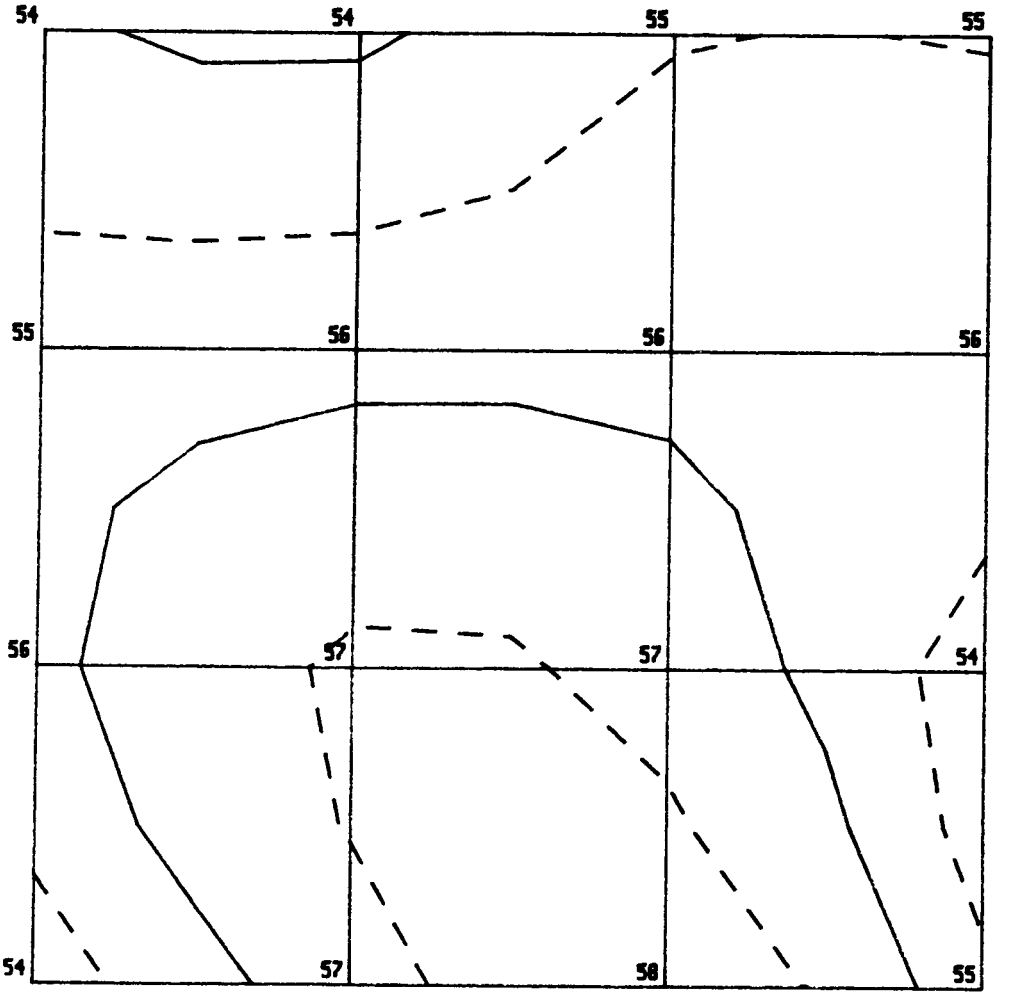

Figure 54c. Measured Intensity Contours for a Utility Type Panel at 2 kHz.

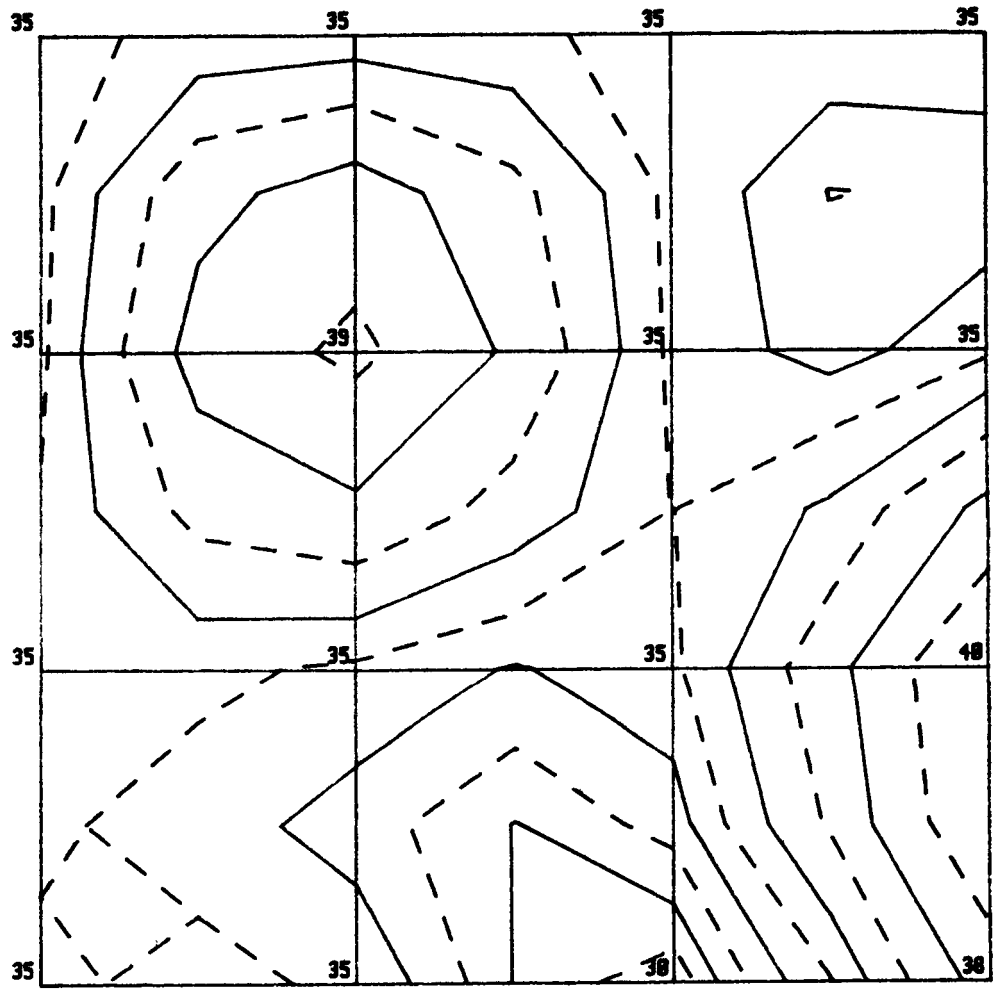

Figure 54d. Measured Intensity Contours for a Utility Type Panel at 4 kHz.

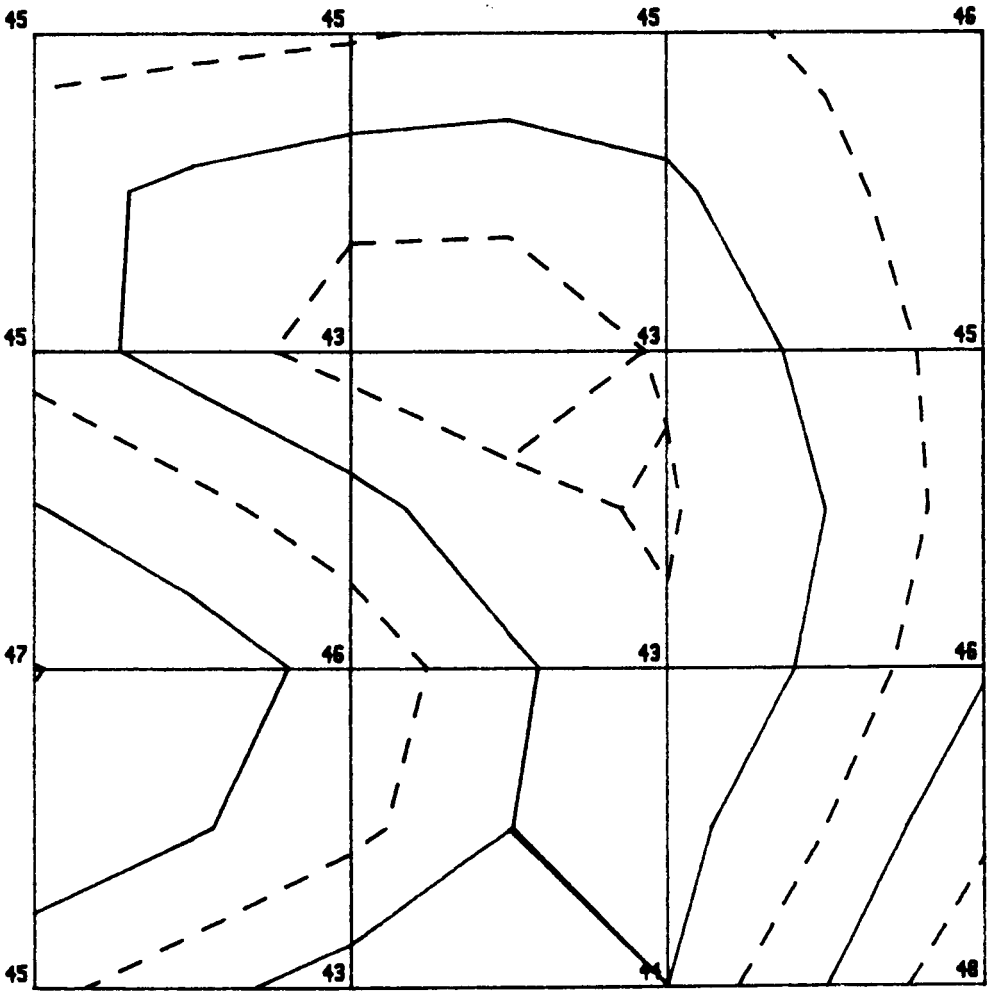

Figure 55a. Measured Intensity Contours for an Executive Type Panel at 0.5 kHz.

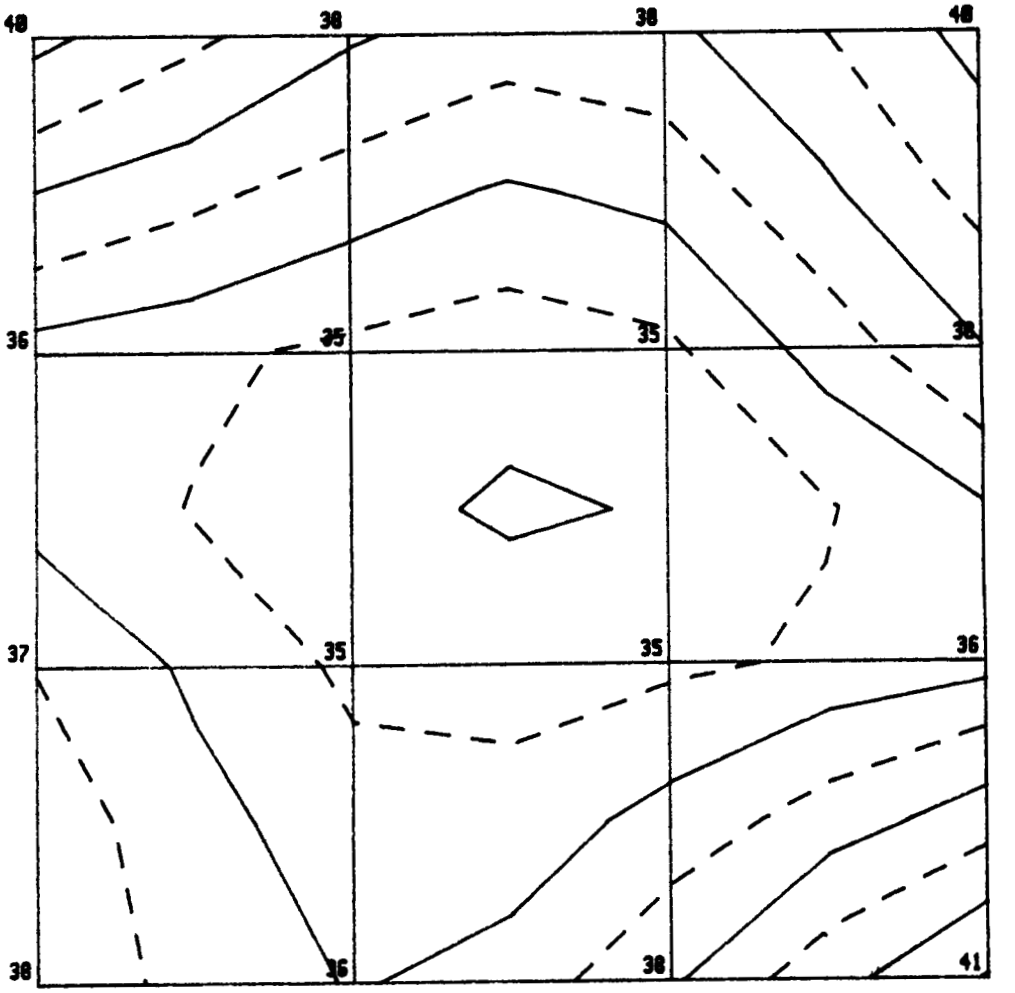

Figure 55b. Measured Intensity Contours for an Executive Type Panel at 1 kHz.

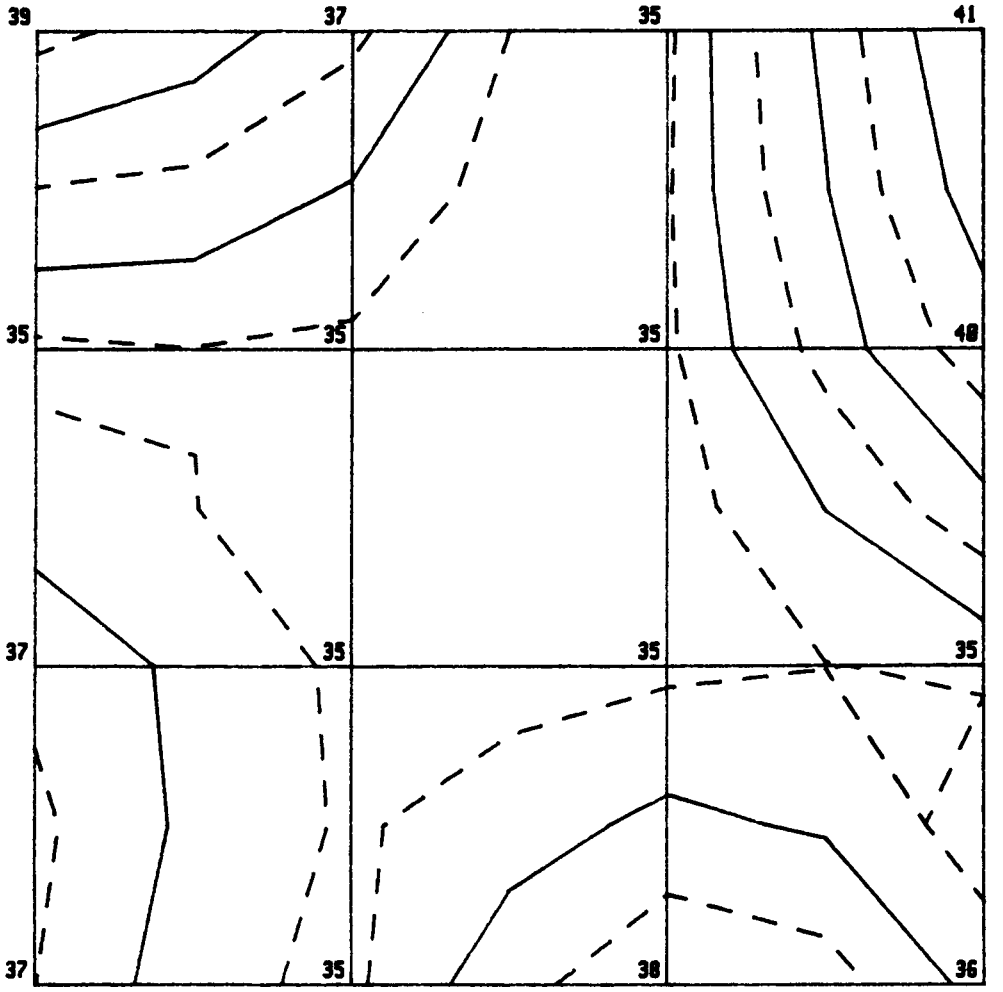

Figure 55c. Measured Intensity Contours for an Executive Type Panel at 2 kHz.

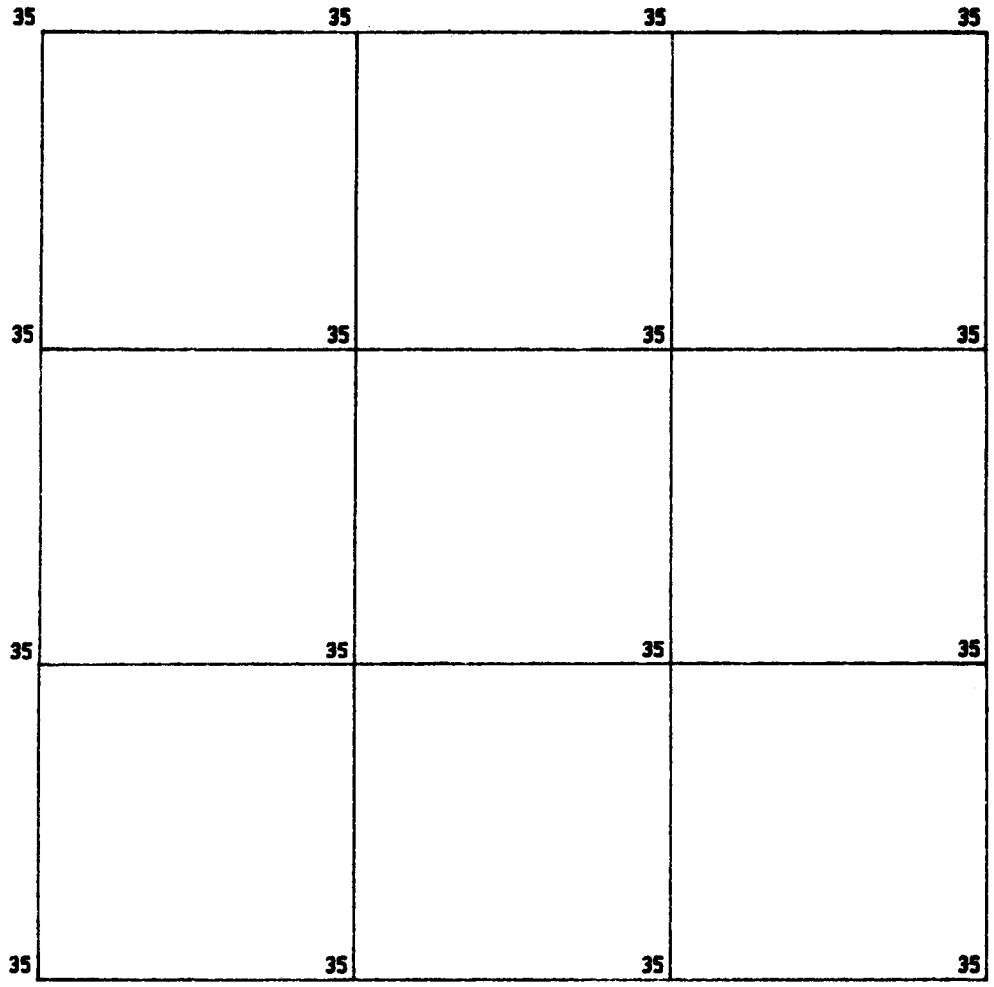

Figure 55d. Measured Intensity Contours for an Executive Type Panel at 4 kHz.

ORIGINAL PAGE IS
OF POOR QUALITY

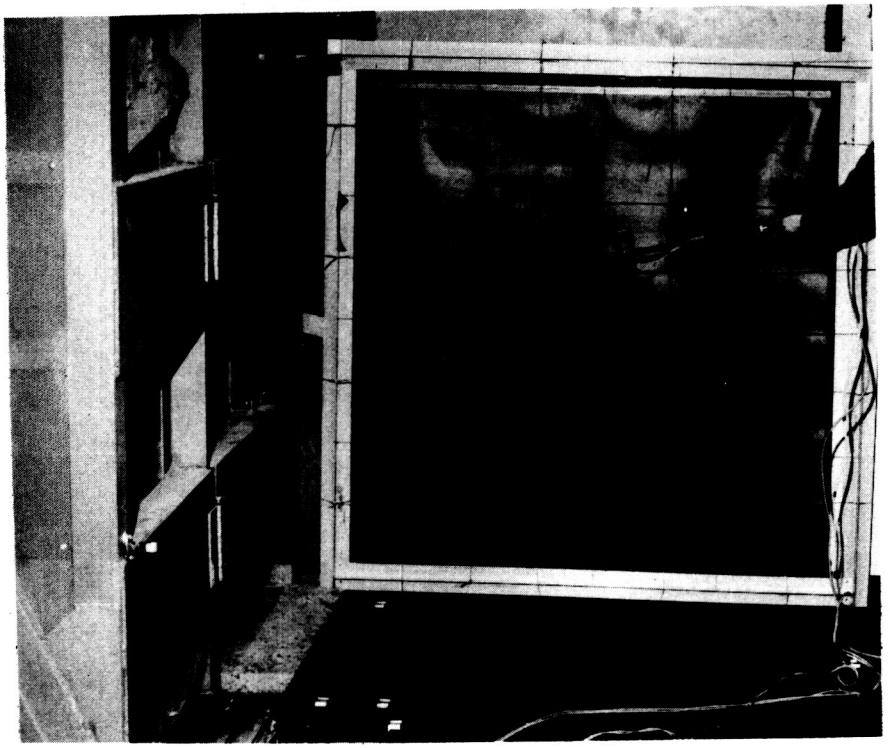

Photo 20. Typical Utility Type Panel Being Tested for TL in the Test Chambers from Anechoic Side, Sound Intensity Probe Shown

ORIGINAL PAGE IS
OF POOR QUALITY

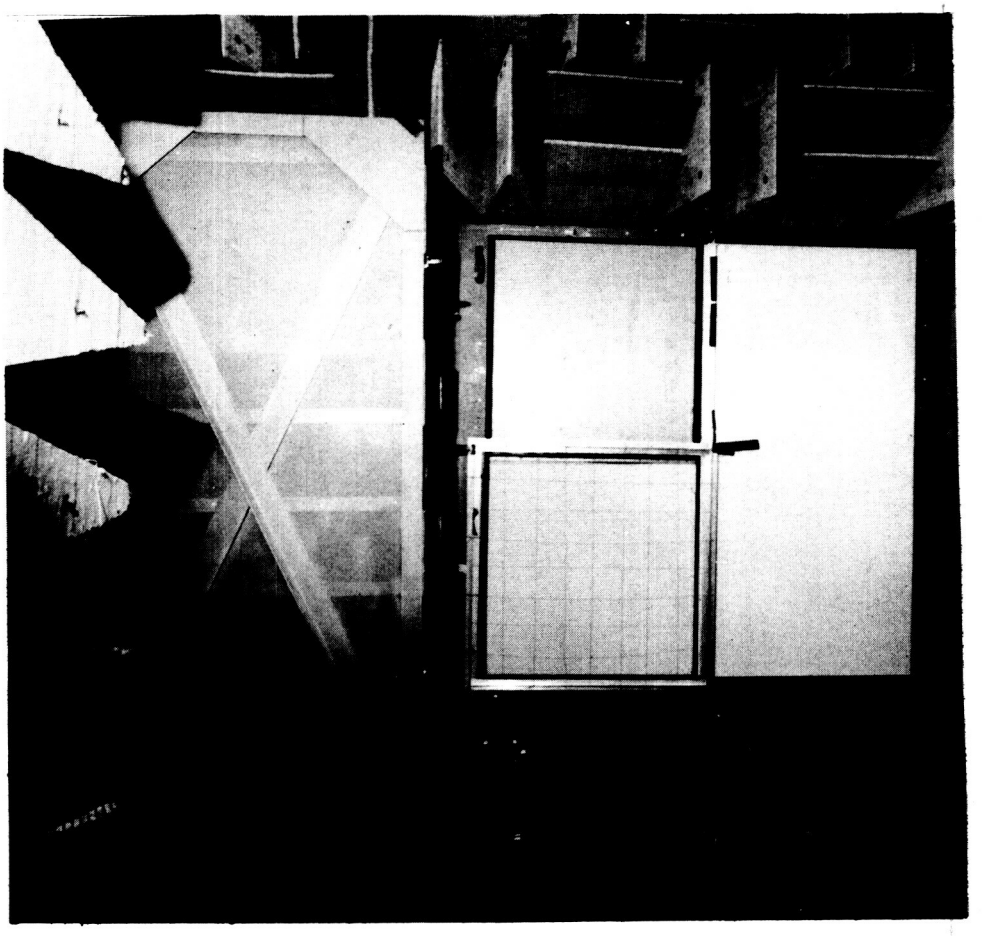

Photo 21. Typical View of Panel TL Testing - Anechoic Side

ORIGINAL PAGE IS
OF POOR QUALITY

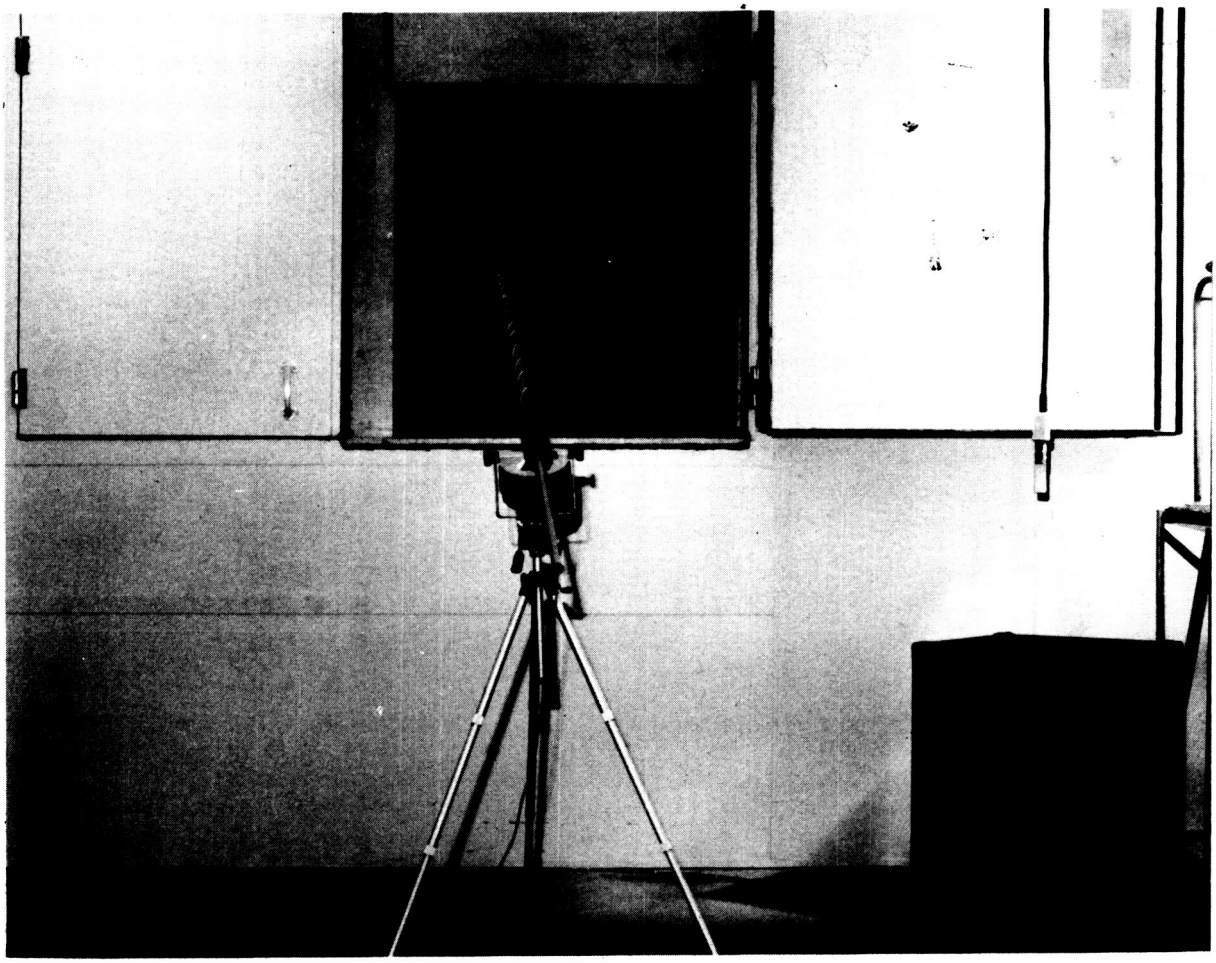

Photo 22. Typical View of Panel TL Testing - Reverberant Side

Standard Bibliographic Page

1. Report No. NASA CR-178172	2. Government Accession No.	3. Recipient's Catalog No.
4. Title and Subtitle Development of Rotorcraft Interior Noise Control Concepts, Phase III: Development of Noise Control Concepts		5. Report Date July 1987
		6. Performing Organization Code 78286
7. Author(s) C.A. Yoerkie, P.J. Gintoli, S.T. Ingraham and J.A. Moore		8. Performing Organization Report No. SER-510274
9. Performing Organization Name and Address Sikorsky Aircraft Division United Technologies Corporation Stratford, CT 06601-1381		10. Work Unit No. 505-61-51
		11. Contract or Grant No. NAS1-16932
12. Sponsoring Agency Name and Address National Aeronautics and Space Administration Langley Research Center Hampton, VA 23665		13. Type of Report and Period Covered Contractor Report Jan '85 - July '87
		14. Sponsoring Agency Code

15. Supplementary Notes
LaRC Technical Representative: William H. Mayes
Phase III Final Report

16. Abstract

The application of statistical energy analysis (SEA) to the modeling and design of helicopter cabin and cockpit interior noise control treatment is demonstrated. The interior configurations modeled are typical of utility, executive, and advanced type treatments. The utility and executive interior SEA models are developed directly from existing S-76 aircraft designs currently in production. The utility interior design priority is light weight with reasonable acoustic benefits; for the executive interior, emphasis is primarily on improving the acoustic environment while allowing for increased interior weight. The relative importance of panel transmission loss (TL), acoustic leakage, and absorption to the control of cabin noise is shown through SEA modeling parametric variation. The major cabin noise improvement below 1000 Hz comes from increased TL, while above 1000 Hz it's from reduced acoustic leakage and increased cabin and overhead absorption. Laboratory TL and aircraft flight noise data are shown to correlate very well with SEA predictions. Thus a viable technique for aircraft noise control design is established from which new interior design concepts can be evaluated with relative ease. A preliminary design was carried out for an acoustic isolation of the structureborne energy coming into the airframe from the main gearbox. This vibration isolation design shows significant reductions in cabin noise are possible. The Phase IV effort will refine this design and include fabrication and ground testing.

17. Key Words (Suggested by Authors(s)) Statistical Engergy Analysis Modeling, Helicopter, Transmission Isolation, Acoustics, Vibration, Cabin Noise, Structureborne Noise, Full Scale Vibro/ Acoustic Test		18. Distribution Statement Subject Category 71	
19. Security Classif.(of this report) Unclassified	20. Security Classif.(of this page) Unclassified	21. No. of Pages 148	22. Price

For sale by the National Technical Information Service, Springfield, Virginia 22161

NASA Langley Form 63 (June 1985)